CIVIL ENGINEERING STUDIES
Illinois Center for Transportation Series No. 21-033
UILU-ENG-2021-2033
ISSN: 0197-9191

Best Practice Operation of Reversible Express Lanes for the Kennedy Expressway

Prepared By
Abolfazl Mohammadian, PhD
Amir Bahador Parsa
Homa Taghipour, PhD
Amir Davatgari
Motahare Mohammadi

University of Illinois at Chicago

Research Report No. FHWA-ICT-21-028

A report of the findings of

ICT PROJECT R27-195
Best Practice Operation of Reversible Express Lanes for Kennedy Expressway

https://doi.org/10.36501/0197-9191/21-033

Illinois Center for Transportation

September 2021

TECHNICAL REPORT DOCUMENTATION PAGE

1. Report No.	2. Government Accession No.	3. Recipient's Catalog No.
FHWA-ICT-21-028	N/A	N/A

4. Title and Subtitle	5. Report Date
Best Practice Operation of Reversible Express Lanes for the Kennedy Expressway	September 2021
	6. Performing Organization Code N/A

7. Authors	8. Performing Organization Report No.
Abolfazl Mohammadian (https://orcid.org/0000-0003-3595-3664) Amir Bahador Parsa (https://orcid.org/0000-0001-8670-9894) Homa Taghipour (https://orcid.org/0000-0001-8450-5775) Amir Davatgari (https://orcid.org/0000-0003-0913-9706) Motahare Mohammadi (https://orcid.org/0000-0001-8744-4701)	ICT-21-033 UILU-2021-2033

9. Performing Organization Name and Address	10. Work Unit No.
Illinois Center for Transportation Department of Civil and Environmental Engineering University of Illinois at Urbana-Champaign 205 North Mathews Avenue, MC-250 Urbana, IL 61801	N/A
	11. Contract or Grant No. R27-195

12. Sponsoring Agency Name and Address	13. Type of Report and Period Covered
Illinois Department of Transportation (SPR) Bureau of Research 126 East Ash Street Springfield, IL 62704	Final Report 10/16/18–10/31/21
	14. Sponsoring Agency Code

15. Supplementary Notes

Conducted in cooperation with the U.S. Department of Transportation, Federal Highway Administration.

https://doi.org/10.36501/0197-9191/21-033

16. Abstract

Reversible lanes in Chicago's Kennedy Expressway are an available infrastructure that can significantly improve traffic performance; however, a special focus on congestion management is required to improve their operation. This research project aims to evaluate and improve the operation of reversible lanes in the Kennedy Expressway. The Kennedy Expressway is a nearly 18-mile-long freeway in Chicago, Illinois, that connects in the southeast to northwest direction between the West Loop and O'Hare International Airport. There are two approximately 8-mile reversible lanes in the Kennedy Expressway's median, where I-94 merges into I-90, and there are three entrance gates in each direction of this corridor. The purpose of the reversible lanes is to help the congested direction of the Kennedy Expressway increase its traffic flow and decrease the delay in the whole corridor. Currently, experts in a control location switch the direction of the reversible lanes two to three times per day by observing real-time traffic conditions captured by a traffic surveillance camera. In general, inbound gates are opened and outbound gates are closed around midnight because morning traffic is usually heavier toward the central city neighborhoods. In contrast, evening peak-hour traffic is usually heavier toward the outbound direction, so the direction of the reversible lanes is switched from inbound to outbound around noon. This study evaluates the Kennedy Expressway's current reversing operation. Different indices are generated for the corridor to measure the reversible lanes' performance, and a data-driven approach is selected to find the best time to start the operation. Subsequently, real-time and offline instruction for the operation of the reversible lanes is provided through employing deep learning and statistical techniques. In addition, an offline timetable is also provided through an optimization technique. Eventually, integration of the data-driven and optimization techniques results in the best practice operation of the reversible lanes.

17. Key Words	18. Distribution Statement
Reversible Lanes, Data-driven Techniques, Corridor Operation Management, Machine Learning	No restrictions. This document is available through the National Technical Information Service, Springfield, VA 22161.

19. Security Classif. (of this report)	20. Security Classif. (of this page)	21. No. of Pages	22. Price
Unclassified	Unclassified	53 + appendices	N/A

ACKNOWLEDGMENT, DISCLAIMER, MANUFACTURERS' NAMES

This publication is based on the results of **R27-195: Best Practice Operation of Reversible Express Lanes for Kennedy Expressway**. R27-195 was conducted in cooperation with the Illinois Center for Transportation; the Illinois Department of Transportation; and the U.S. Department of Transportation, Federal Highway Administration.

Members of the Technical Review Panel (TRP) were the following:

- Matthew Daeda, TRP Chair, Illinois Department of Transportation
- Dean Mentjes, Federal Highway Administration
- Richard Reichenbach, Illinois Department of Transportation
- Jeff Galas, Illinois Department of Transportation
- Megan Swanson, Illinois Department of Transportation

TABLE OF CONTENTS

LIST OF FIGURES

LIST OF TABLES

CHAPTER 1: INTRODUCTION

This research aims to evaluate and improve the operation of reversible lanes in the Kennedy Expressway. The Kennedy Expressway is a nearly 18-mile-long freeway in Chicago, Illinois, that connects in the southeast to northwest direction between the West Loop and O'Hare International Airport. There are two approximately 8-mile reversible lanes in the Kennedy Expressway's median, where I-94 merges into I-90 (i.e., from the Kennedy Expressway/Edens Expressway junction until just north of the Loop). There are three entrance gates in each direction of this corridor. In the inbound direction (i.e., toward the southeast), there are two entrance gates at the beginning of the reversible lanes coming from the Edens and West leg, and there is one gate in the middle of the corridor directing the traffic flow from the slip ramp into the reversible lanes. Similarly, in the outbound direction (i.e., toward the northwest), there are two entrance gates at the beginning of the reversible lanes coming from the Ontario and mainline leg, and there is one gate in the middle of the corridor directing the traffic flow from the slip ramp into the reversible lanes. The purpose of the reversible lanes is to help the congested direction of the Kennedy Expressway increase its traffic flow.

Currently, experts in a control location switch the direction of the reversible lanes two to three times per day by observing real-time traffic conditions captured by a traffic surveillance camera. In general, inbound gates are opened and outbound gates are closed around midnight because morning traffic is usually heavier toward the central city neighborhoods. In contrast, evening peak-hour traffic is usually heavier toward the outbound direction, so the direction of the reversible lanes is switched from inbound to outbound around noon.

Figure 1 presents the corridor of reversible lanes in the Kennedy Expressway and its entrance gates. The three inbound gates are shown in orange, and the three outbound gates are shown in green. Therefore, the order of the reversing operation can be defined as follows:

- Switching the direction of the reversible lanes toward the inbound direction (usually around midnight):
    1. Close outbound Ontario Street (OO)
    2. Close outbound Mainline leg (OM)
    3. Close outbound Slip ramp (OS)
    4. Open inbound Slip ramp (IS)
    5. Open inbound West leg (IW)
    6. Open inbound Edens Expressway (IE)
- Switching the direction of the reversible lanes toward the outbound direction (usually around noon):

1. Close inbound Edens Expressway (IE)
2. Close inbound West leg (IW)
3. Close inbound Slip ramp (IS)
4. Open outbound Slip ramp (OS)
5. Open outbound Mainline leg (OM)
6. Open outbound Ontario Street (OO)

After a comprehensive review of related studies, the available sources of data are cleaned and preprocessed in this study. Then, the current reversing operation is evaluated. Finally, two approaches are proposed to improve the operation and traffic-flow performance of the Kennedy Expressway's reversible lanes.

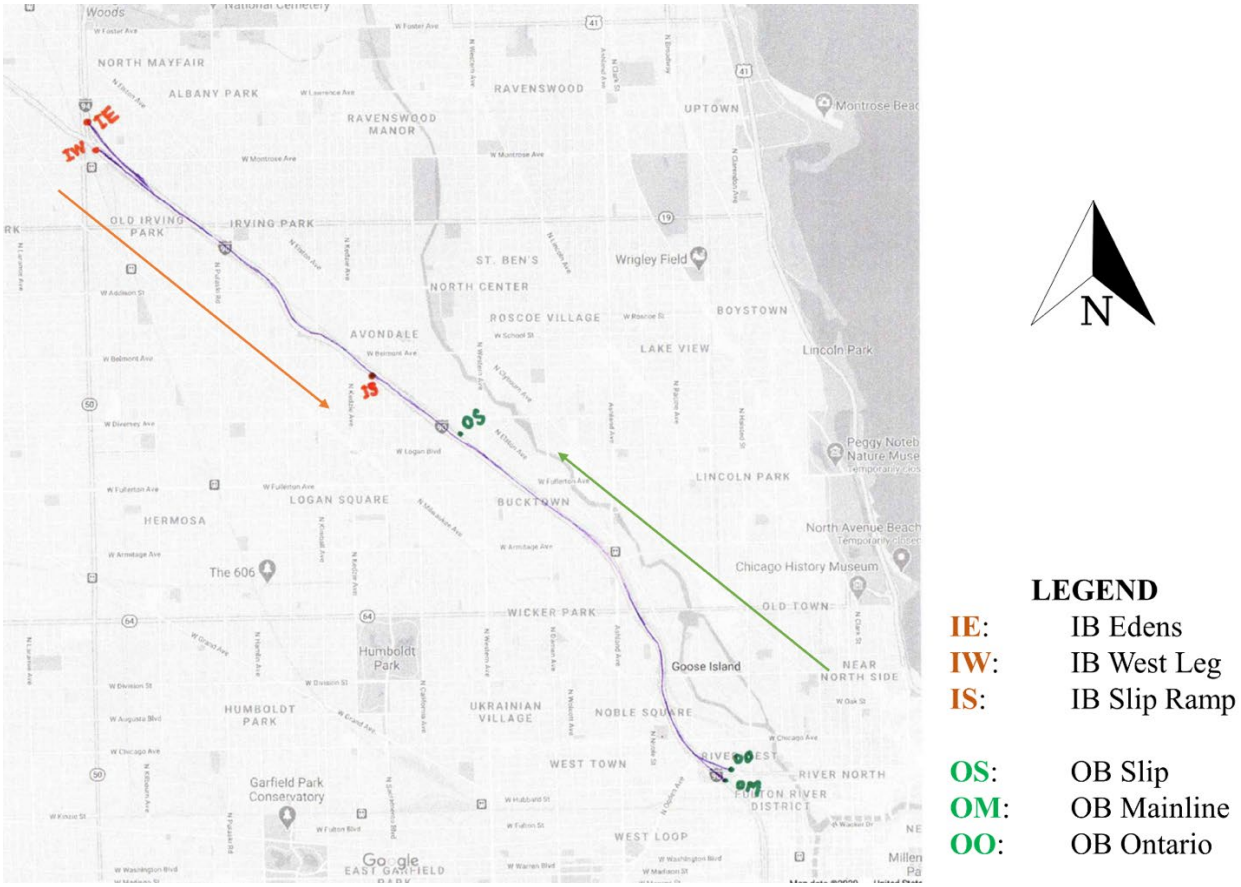

Figure 1. Illustration. Kennedy Expressway reversible lanes.

CHAPTER 2: LITERATURE REVIEW

The operation of reversible express lanes is a transportation system management technique that ensures a higher utilization of existing expressway assets while minimizing the need for expensive alternatives like widening roadway facilities. Reversible lanes allow transportation agencies to make better use of underutilized roadways by aligning the capacity with traffic demand. The reversible lane system designates traffic flow in one direction during some periods and reverses it to the opposing direction during other periods. The direction of traffic flow can be adjusted at different times to adapt to changing traffic conditions. These conditions are commonly based on demand associated with frequent and predictable unbalanced peak-period travel times on corridors that accommodate predominantly commuter traffic. The basic principle is to configure the reversible lanes of the expressway to provide the additional directional capacity to match the anticipated periodic and unbalanced directional traffic demand.

Reversible lanes have been used throughout the world for more than 70 years on different kinds of roadway types, including freeways, arterial roadways, bridges, and tunnels. Different methods of control have been applied to address the following classification of needs regarding reversible lanes: increasing capacity of unbalanced directional traffic during peak hours, emergency evacuations, roadway construction works, and other major events (Wolshon and Lambert 2006).

PEAK-HOUR TRAFFIC

Reversible lanes that are used for increasing capacity during peak-hour traffic are mostly on arterial roadways and freeways. These kinds of reversible lanes usually increase the capacity of the way toward the Central Business District or downtown of cities during the morning rush hour and increase the outbound capacity in the opposite direction during the evening rush hour. The efficiency of these kinds of reversible lanes is higher for the routes that have restricted access to the local area and have a high percentage of pass-through flow (Wolshon and Lambert 2006).

EMERGENCY EVACUATION TRAFFIC

Another important usage of reversible lanes is for emergency evacuation of traffic. During a natural disaster such as Hurricane Floyd in 1999 or man-made dangers, including several nuclear, biological, chemical, and terrorist threats, reversible lanes could play a pivotal role in leading a large flow of traffic away from the city. An important benefit of reversible lanes on freeways is that their access to the local lanes and area is relatively restricted, and they can reduce the need for a lot of man power or control elements for the reversal process. In contrast, a major shortcoming of these reversal lanes on freeways is that the speed in freeways is much higher than other road types, which can cause serious safety issues during the direction-changing period. In fact, reversible lanes on freeways require a precise and adequate protection plan for clearing the route from vehicles before changing the direction of the lanes (Wolshon and Lambert 2006).

ROADWAY CONSTRUCTION TRAFFIC

Another practical and effective usage of reversible lanes is when there is roadway construction in a path that increases the traffic congestion in one direction. So, setting the direction of the reversible lanes to align with that direction could maintain the capacity within the restricted way of work zones, especially on bridges and within tunnels (Wolshon and Lambert 2006).

EVENT TRAFFIC

In general, important events do not occur frequently and are held annually or seasonally. So, the constitution of new infrastructure such as additional lanes or complex control tools to manage the increased traffic demand is not reasonable. Using a reversible lane system as a temporary traffic control system is one of the most suitable solutions to manage inbound and outbound traffic before and after an event, respectively. For urban areas in which various events are held during the year, however, a precise schedule for changing the reversible lanes' direction is required (Wolshon and Lambert 2006).

The main objective of the four categories is to take advantage of the underutilized lanes or shoulders so that it increases the capacity in the direction with higher demand while it decreases the capacity in the opposite direction. A major advantage of the reversible lane system is that it could increase the capacity of roads significantly with a small amount of initial capital costs. In contrast, decreasing the flexibility and capacity of the uncongested direction could be a major disadvantage of reversible lanes. This system could also be costly in the long term if the required maintenance is not taken into account, and it also would be dangerous if it causes confusion due to an inadequate number of informative signs.

Although the implementation of reversible lanes has a long history and they have been used throughout the world continuously, there are few studies and research carried out regarding their performance. Furthermore, the number of studies and publications on guidelines and standards of reversible lanes' planning, design, operation, and management are so few that most reversible lanes are operated and managed based on experience, professional judgment, and empirical observation (Frejo et al. 2015).

Although the concept of reversible lanes is simple, it could be complicated to design and manage them in such a way that traffic flow in both directions gets to maximum efficiency. Stenneth (2016) suggested that analysis of historical traffic data along with real-time traffic data from loop detectors could lead to a dynamic management plan to control the traffic flow of opposite directions to consequently reduce the congestion efficiently. There are several examples of dynamic traffic control plans in the literature as a solution to reduce congestion such as using ramp metering, variable speed limits, and other traffic control measures. However, dynamic traffic control has rarely been reported to be applied to control the reversible lane system (Frejo et al. 2015). Currently, the direction of reversible lanes in most cases is switched manually by traffic operators looking at cameras.

In a study conducted over the Centenario Bridge of the SE-30 freeway in Seville, Spain, an extension of the METANET macroscopic second-order traffic-flow model has been proposed that would be able

to reproduce traffic congestion regarding reversible lanes (Frejo et al. 2015). One control algorithm for the dynamic operation of reversible lanes would evaluate the cost function and conduct discrete optimization to determine the best sequence of system management actions. This has some benefits, including the possibility of considering constraints and reducing the number of direction shifts for reversible lanes.

Real-time manual control is deemed to perform better than fixed control. In fixed control, the direction of reversible lanes is changed based on predefined peak-hour intervals. In real-time manual control, however, the direction of reversible lanes is defined based on real-time data with respect to the length of congestion. Once the length of congestion is defined, the direction of reversible lanes will be delineated regarding the following three cases (Frejo et al. 2015):

1) *Congestion lengths are zero in both directions*. In this case, because the direction of reversible lanes is not critical, it would be reasonable to maintain the current condition and not change the direction unless the volume in the direction using the reversible lanes becomes much lower than the other direction.

2) *Congestion length becomes bigger than zero and smaller than the maximum congestion length in one or both directions*. In this case, the congestion length of both directions should balance in such a way that switching between directions should not happen frequently, especially for long paths, which requires an adequate amount of time to be cleared before switching.

3) *Congestion lengths are equal to or bigger than their relative maximum values in both directions*. This condition would be overcritical, and the strategy to deal with this condition depends on the responsible authority. Please note it would be suboptimal to keep reversible lanes closed (to allow the remaining vehicles of the current direction to leave the reversible lanes) repeatedly for both directions, so the direction of reversible lanes should be switched infrequently.

The direction of reversible lanes could be managed by using a logic-based controller that changes the state of the reversible lanes based on simple feedback. This kind of controller can be easily used in practice without the need for any online optimization. The feedback of the controller will be made based on the length of congestion, and this length could be measured based on the average speed of each direction (Frejo et al. 2015).

Sometimes, comprehensive traffic data is not available, so having an accurate estimate of traffic on the reversible lanes is critical to evaluate their performance, especially for traffic simulation models. For instance, there are different theories for estimating the capacity of a reversed lane compared to normal lanes when data for both is not available. Some theories estimate the capacity of a reversible lane to be equal to that of a normal lane, while in others, reversible lane capacity is half of this value (Lambert and Wolshon 2010). Lambert and Wolshon (2010) measured and evaluated the speed and flow of the reversible lanes by considering different operation conditions and locations. They showed the similarity of the flow characteristics of reversible lanes compared to normal lanes of the corridor under a variety of traffic volumes, times of day, and locations.

In a study in 2019, Kotagi and Asaithambi evaluated the performance of reversible lanes by using a microscopic simulation model. They studied the impact of reversible lane operation on the capacity of roads by considering different compositions of vehicles based on the traffic history of urban arterials in Indian cities. The findings of this study showed that implementing reversible lanes during peak hours could improve road capacity (Kotagi and Asaithambi 2019). In another study, Zhao et al. (2014) used a lane-based optimization model to maximize the operational performance of an arterial with reversible lanes.

Liu (2020) introduced a bi-level method based on short-term traffic-flow prediction to control dynamic reversible lanes. To achieve the best results, historical, real-time, and predicted data were utilized to develop models in this study. To predict the short-term traffic flow, the advanced bi-directional long short-term memory (Abi-LSTM) model is employed. Also, a bi-level optimization method is employed for the control algorithm in order to maximize the traffic flow in both corridor directions. Then, using a simulation technique, the effect of dynamic controlling of the reversible lane is tested. This study showed that dynamic real-time traffic management improved performance compared to traditional static traffic management.

In smart cities with vehicle-to-infrastructure connectivity, reversible lanes could work as a part of the sustainable transportation system, because automated vehicles could be informed about lane configuration changes. In a study in the Netherlands (Conceição, Correia, and Tavares 2020), a network design problem with reversible lanes is introduced using mixed-integer nonlinear mathematical programming. In this modeling approach, both traffic assignment and decisions about the reversible lanes are considered. This study showed the effect of reversible lanes on the reduction of road congestion, total travel time, and delays by 36%, 9%, and 22%, respectively.

In a case study in Germany, Waleczek et al. (2016) investigated a highly congested corridor with considerable peak-hour fluctuations. In this research, traffic flow, travel time, and road safety are factors affected by reversible lanes. Using reversible lanes could increase capacity of the road around 15% and significantly decrease travel times. The study also showed that only 10% of the reported traffic incidents and none of the severe traffic incidents could be linked to the reversible lane system.

The most notable example of reversible lanes in Illinois is on the Kennedy Expressway. The reversible lanes lie in the median of the highway from north of the Loop (at Ohio Street) to the Kennedy Expressway/Edens Expressway junction, a distance of approximately 8 miles. These reversible lanes allow two lanes of traffic to flow toward or away from the city, depending on the time of day. The lanes are controlled by computers and are verified by humans at a separate control center. So, a comprehensive algorithm that can dynamically manage the direction of Kennedy Expressway's reversible lanes with respect to real-time data is essential to reduce traffic congestion efficiently.

CHAPTER 3: STUDY FRAMEWORK

Currently, operators typically use their experience and observation to switch the direction of reversible lanes. Therefore, the main goal of this study is to find the best online and offline approaches to start the reversing operation so that the corridor passes traffic more efficiently. To this end, after cleaning and preprocessing the available data sources, a comprehensive analysis was done on the traffic pattern under the influence of the current operating schedule. Then, different indices were generated for the corridor to measure the performance of reversible lanes, and a data-driven approach was selected to find the best time to start the operation. This approach uses data-driven techniques to model the impact of the reversing operation on corridor indices and then provides real-time and offline instruction for the operation based on the model's result. Therefore, integration of the real-time and offline techniques results in the best practice operation of reversible lanes. Figure 2 displays the framework of this study.

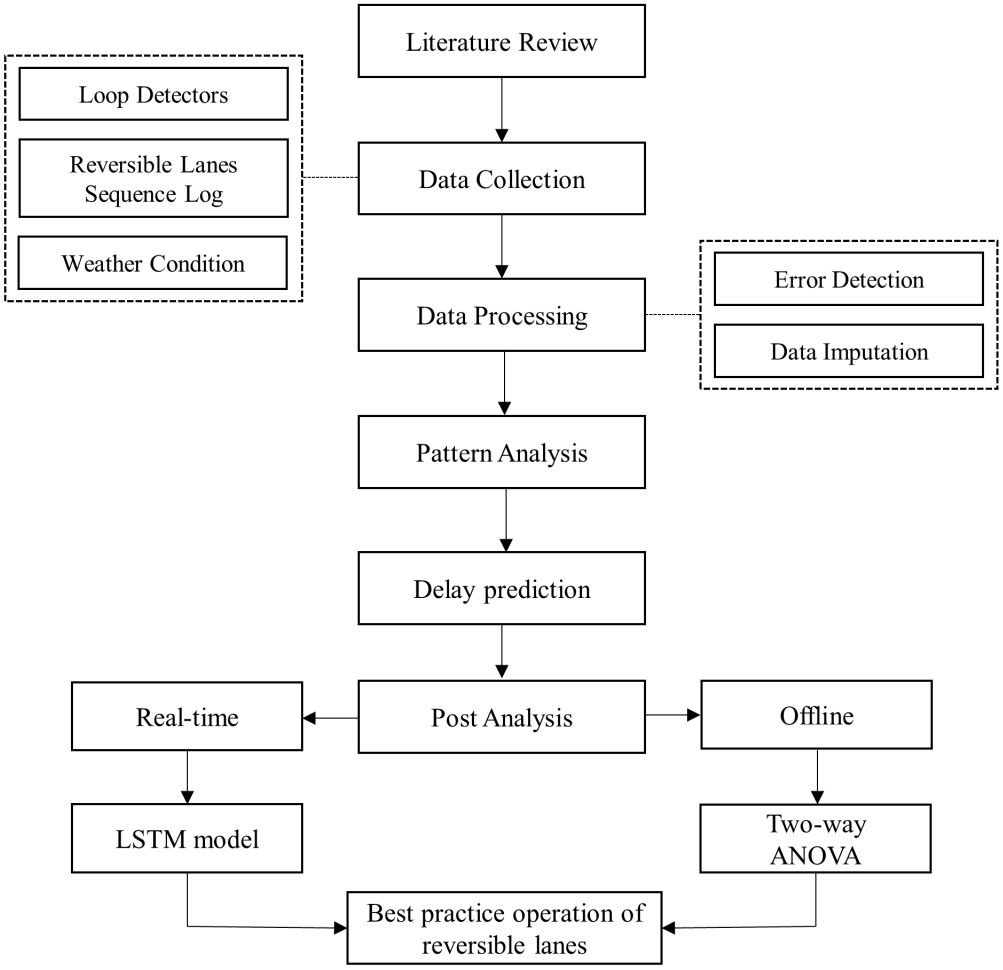

Figure 2. Chart. Study framework.

CHAPTER 4: DATA

Two main sources of data—loop detector and reversible lanes sequence log—are employed in this study to evaluate and improve the operation of reversible lanes in the Kennedy Expressway. In addition to these data sources, weather condition is also used in this study to improve the accuracy.

LOOP-DETECTOR DATA

The data collected by inductive loop detectors is the main source of traffic data used in this study. The nine loop detectors on the reversible lanes lie between Montrose and Ohio Streets. These loop detectors collect traffic data of reversible lanes for both directions so that when the direction of the reversible lanes is toward the northwest (i.e., outbound), the loop detector at Ohio Street is the first loop detector for that direction. This loop detector is the last loop detector when the direction of the reversible lanes is toward the southeast (i.e., inbound). Regarding the mainline of the Kennedy Expressway, there are 17 loop detectors in each direction of the expressway. Table 1 shows all loop detectors of the studied corridor, including the reversible lanes' loop detectors and Kennedy Expressway's mainline, for both directions.

Table 1. List of Loop Detectors of the Studied Corridor

Row	Detector ID	Street Name	Link Direction	Route Designator
1	2200	MONTROSE	East	REVERSIBLES
2	2201	KEELER	East	REVERSIBLES
3	2202	ADDISON	East	REVERSIBLES
4	2203	SACRAMENTO	East	REVERSIBLES
5	2204	DIVERSEY	East	REVERSIBLES
6	2205	WESTERN	East	REVERSIBLES
7	2206	ARMITAGE	East	REVERSIBLES
8	2207	DIVISION	East	REVERSIBLES
9	2208	OHIO	East	REVERSIBLES
10	2301	OHIO	West	REVERSIBLES
11	2302	DIVISION	West	REVERSIBLES
12	2303	ARMITAGE	West	REVERSIBLES
13	2304	WESTERN	West	REVERSIBLES
14	2305	DIVERSEY	West	REVERSIBLES
15	2306	SACRAMENTO	West	REVERSIBLES
16	2307	ADDISON	West	REVERSIBLES
17	2308	KEELER	West	REVERSIBLES
18	2309	MONTROSE	West	REVERSIBLES
19	2021	MONTROSE	East	KENNEDY
20	2022	KEELER	East	KENNEDY
21	2023	PULASKI	East	KENNEDY
22	2024	ADDISON	East	KENNEDY
23	2025	KIMBALL	East	KENNEDY
24	2026	KEDZIE	East	KENNEDY
25	2027	SACRAMENTO	East	KENNEDY
26	2028	DIVERSEY	East	KENNEDY
27	2029	WESTERN	East	KENNEDY

Row	Detector ID	Street Name	Link Direction	Route Designator
28	2030	DAMEN	East	KENNEDY
29	2031	ARMITAGE	East	KENNEDY
30	2032	NORTH	East	KENNEDY
31	2033	DIVISION	East	KENNEDY
32	2034	OGDEN	East	KENNEDY
33	2035	OHIO	East	KENNEDY
34	2036	GREEN	East	KENNEDY
35	2037	LAKE	East	KENNEDY
36	2101	J BYRNE INTRCHGE	West	KENNEDY
37	2102	ADAMS	West	KENNEDY
38	2103	MONROE	West	KENNEDY
39	2105	WASHINGTON	West	KENNEDY
40	2107	LAKE	West	KENNEDY
41	2108	GREEN	West	KENNEDY
42	2114	DAMEN	West	KENNEDY
43	2115	WESTERN	West	KENNEDY
44	2116	DIVERSEY	West	KENNEDY
45	2117	SACRAMENTO	West	KENNEDY
46	2118	KEDZIE	West	KENNEDY
47	2119	KIMBALL	West	KENNEDY
48	2120	ADDISON	West	KENNEDY
49	2121	PULASKI	West	KENNEDY
50	2122	KEELER	West	KENNEDY
51	2123	MONTROSE	West	KENNEDY
52	2124	CICERO	West	KENNEDY

The loop detectors' traffic data is collected by the Gateway Traveler Information System and provided by the Illinois Department of Transportation. Each loop detector can collect the number of vehicles, occupancy, and average speed every 20 seconds per lane of the highway. One important issue of this large traffic data is that it includes missing and erroneous records, which might be caused by malfunctioning detectors, deteriorating pavement, or other reasons.

To take advantage of the large traffic data set collected by the loop detectors, this data set needs to be cleaned and preprocessed. Therefore, using the methods provided in the literature, two types of thresholds—single and combined—are applied to the data set as part of the data-cleaning procedure.

Single Threshold

In the single threshold approach, several thresholds are applied for each traffic variable—count, occupancy, and speed—to eliminate erroneous data. Based on the characteristics of the selected highway, the following thresholds are set:

1. Count: If the number of passing vehicles exceeds a value of 3,000 vehicles per hour per lane (i.e., 17 vehicles per 20 seconds per lane), it is labeled an erroneous data point.

2. Occupancy: If the recorded value for the occupancy exceeds 90%, meaning that more than 90% of the time the loop detector was occupied by vehicles, it is assumed to be incorrect data.

3. Speed: If loop detectors record any average speed above 80 mph, this record is considered an outlier.

Combined Threshold

Three combined thresholds are taken into account to eliminate erroneous data points, as follows:

1. Only one zero variable out of three: If only one of the three variables (count, occupancy, and speed) is equal to zero, whereas the other two variables are non-zero, then that record is considered an erroneous record.

2. Only one non-zero variable out of three: If two of the variables are zero while the other is non-zero, then this record is labeled an erroneous data point.

3. All zero variables: A record is considered an error if all three variables (count, occupancy, and speed) are zero. This threshold filters out the data points that could incorrectly impact the average speed of corridors.

Data Imputation

Because missing and erroneous data points could negatively affect the results of prediction models, these points should either be eliminated from the data set or imputed by new data points through one of the following techniques:

1. Temporal Estimation: Temporal estimation is used whenever there is a missing or erroneous data point and there are valid available data points in the previous and next time intervals. In this case, the average value of the previous and next time intervals is used for imputing the missing or erroneous data point, especially when the time intervals are short (i.e., 20 seconds).

2. Spatial Estimation: Spatial estimation is used whenever there is a missing or erroneous data point and there are valid available data points in the previous and next loop detectors at the same time. This method is appropriate whenever loop detectors are close to each other or using temporal estimation is not applicable.

3. Historical Estimation: Historical estimation is used whenever traffic condition is recurrent in a location in which there is a missing or erroneous data point. In this case, erroneous data points are imputed using reported data points from the same location, time of day, and day of week in past records. After applying data cleaning and missing imputation techniques, the data of loop detectors is used for years 2017 and 2019. Besides the sanity checks applied on 2017 and 2019 loop detector data, the research team realized there were time shifts in the 2019 loop detector data. Daily traffic pattern and knowing the exact time of the reversing operation helped the research team to find the shifting pattern, which is shown in Table 2.

Table 2. Mismatch Correction of 2019 Loop Detector Data

Month	Correction to be applied on the timestamp of loop detectors
1	Subtract 6 hours
2	Subtract 12 hours
3	Subtract 6 hours
4	By 7th: Subtract 6 hours — After 7th: As is
5	As is
6	By 12th: As is — After 12th: Subtract 5 hours
7	Subtract 5 hours
8	Subtract 5 hours
9	Subtract 5 hours
10	Subtract 5 hours
11	By 2nd: Subtract 5 hours — After 2nd: Subtract 6 hours
12	Subtract 6 hours

REVERSIBLE LANES SEQUENCE LOG

To switch the direction of the reversible lanes, three gates are closed in one direction and three gates are opened in another direction. The reversible lanes sequence log is a sheet in which all information on the reversing operation such as date, "in position" time, "do it now" time, "operation completed" time, and operator are provided. Figure 3 presents a sample of the reversible lanes sequence log.

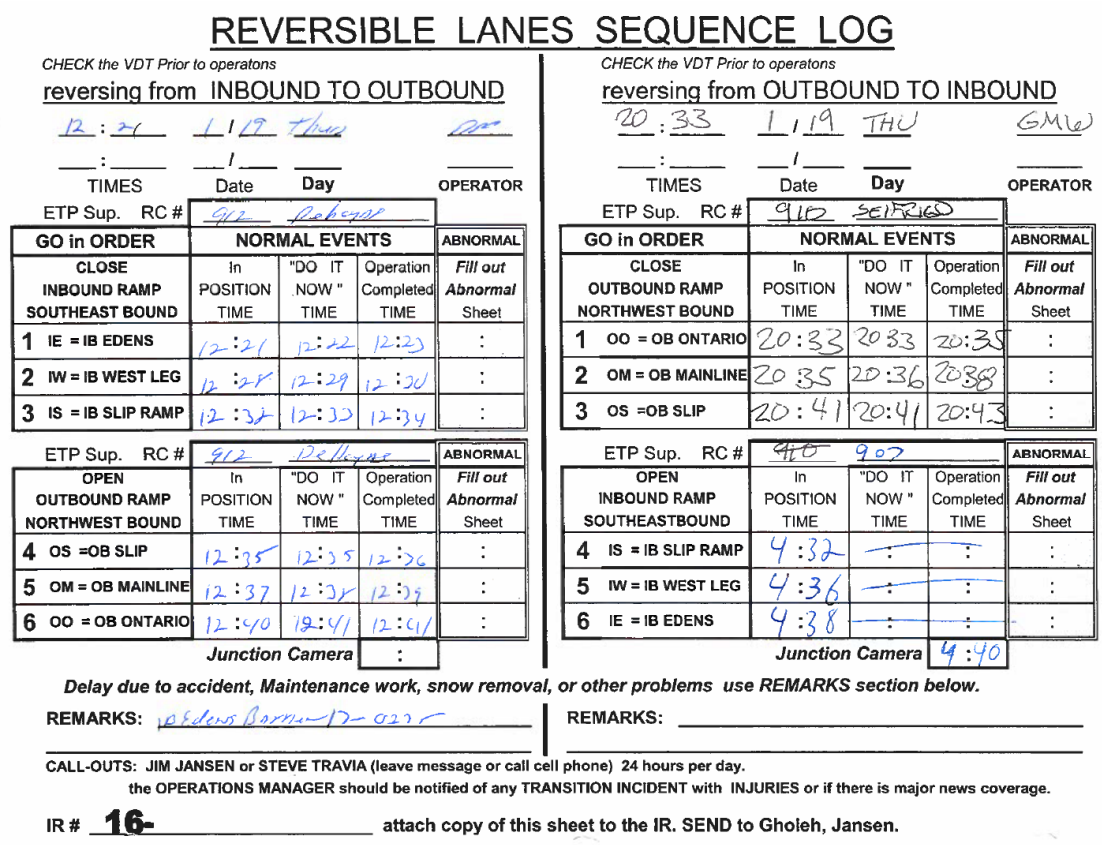

REVERSIBLE LANES SEQUENCE LOG

CHECK the VDT Prior to operatons
reversing from INBOUND TO OUTBOUND

12 : 2[illegible] | 1/19 | Thu | [illegible]
TIMES | Date | Day | OPERATOR

ETP Sup. RC # 912 [illegible]

GO in ORDER	NORMAL EVENTS			ABNORMAL
CLOSE INBOUND RAMP SOUTHEAST BOUND	In POSITION TIME	"DO IT NOW" TIME	Operation Completed TIME	Fill out Abnormal Sheet
1 IE = IB EDENS	12:21	12:22	12:23	:
2 IW = IB WEST LEG	12:28	12:29	12:30	:
3 IS = IB SLIP RAMP	12:32	12:33	12:34	:

ETP Sup. RC # 912 [illegible]

OPEN OUTBOUND RAMP NORTHWEST BOUND	In POSITION TIME	"DO IT NOW" TIME	Operation Completed TIME	ABNORMAL Fill out Abnormal Sheet
4 OS =OB SLIP	12:35	12:35	12:36	:
5 OM = OB MAINLINE	12:37	12:38	12:39	:
6 OO = OB ONTARIO	12:40	12:41	12:41	:
Junction Camera				:

CHECK the VDT Prior to operatons
reversing from OUTBOUND TO INBOUND

20:33 | 1/19 | THU | GMW
TIMES | Date | Day | OPERATOR

ETP Sup. RC # 910 SEIRIG

GO in ORDER	NORMAL EVENTS			ABNORMAL
CLOSE OUTBOUND RAMP NORTHWEST BOUND	In POSITION TIME	"DO IT NOW" TIME	Operation Completed TIME	Fill out Abnormal Sheet
1 OO = OB ONTARIO	20:33	20:33	20:35	:
2 OM = OB MAINLINE	20:35	20:36	20:38	:
3 OS =OB SLIP	20:41	20:41	20:43	:

ETP Sup. RC # 910 902

OPEN INBOUND RAMP SOUTHEASTBOUND	In POSITION TIME	"DO IT NOW" TIME	Operation Completed TIME	ABNORMAL Fill out Abnormal Sheet
4 IS = IB SLIP RAMP	4:32	:	:	:
5 IW = IB WEST LEG	4:36	:	:	:
6 IE = IB EDENS	4:38	:	:	:
Junction Camera			4:40	

Delay due to accident, Maintenance work, snow removal, or other problems use REMARKS section below.

REMARKS: Edens Barrier 12-022[illegible]

REMARKS:

CALL-OUTS: JIM JANSEN or STEVE TRAVIA (leave message or call cell phone) 24 hours per day.
the OPERATIONS MANAGER should be notified of any TRANSITION INCIDENT with INJURIES or if there is major news coverage.

IR # 16- attach copy of this sheet to the IR. SEND to Gholeh, Jansen.

Figure 3. Photo. Reversible lanes sequence log.

The direction of the reversible lanes is usually changed twice on weekdays and three times on weekends. Having compared traffic conditions, switching the direction of the reversible lanes around noon (i.e., changing the direction toward northwest) is critical because both inbound and outbound lanes of the Kennedy Expressway are almost congested. In contrast, changing the direction of the reversible lanes toward the southeast usually happens sometime before midnight to give more capacity to the inbound direction for the morning traffic toward the central part of the city. Therefore, switching the reversible lanes' direction toward the southeast usually happens when the traffic condition of both directions is not critical. Figure 4 and Figure 5 show operation duration and operation start time, respectively, for both reversing directions (i.e., toward northwest and southeast).

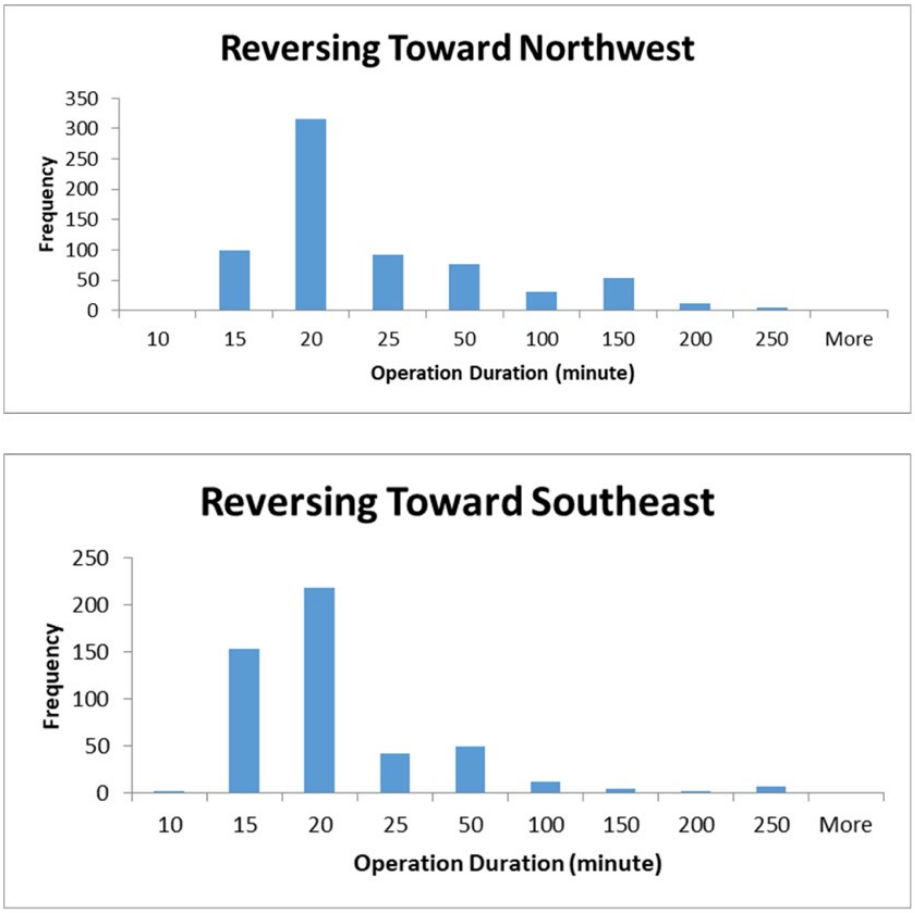

Figure 4. Graph. Operation duration.

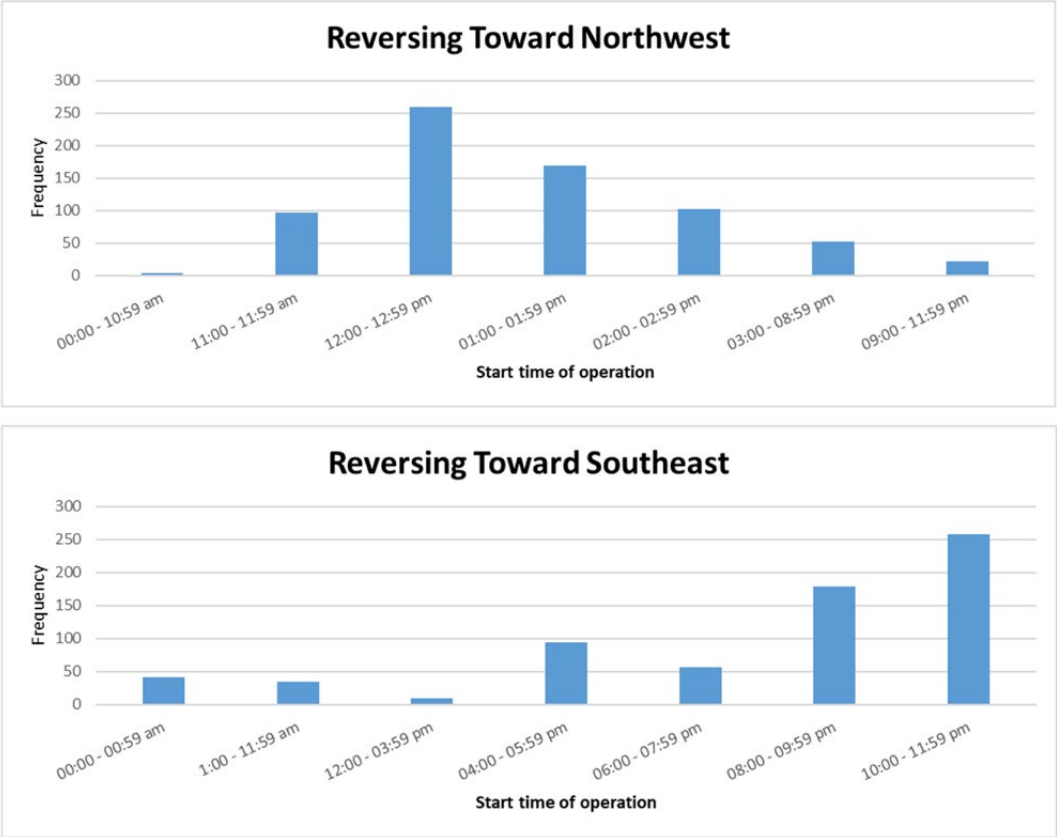

Figure 5. Graph. Operation start time.

WEATHER CONDITION

An important source of data used in this study is weather condition, which is collected hourly by the National Weather Service from airport stations. In this study, weather condition data from O'Hare International Airport is used because it is the closest airport to the Kennedy Expressway. The weather conditions reported in this data set consist of 94 states, which show all possible conditions for the weather; these 94 states are categorized into four main groups, from fair to severe. Some examples of weather conditions in these four groups are as follows:

1. Category 1 contains weather conditions such as "fair" and "partly cloudy."
2. Category 2 is comprised of weather conditions such as "fair with light haze" and "light haze dust and windy."
3. Category 3 includes unfavorable weather conditions such as "light drizzle" and "light rain fog."
4. Category 4 is the most severe category and includes weather conditions like "snow fog" and "thunderstorm heavy rain fog."

OPERATION ANALYSIS

After cleaning the two data sources (loop detector and reversible lanes sequence log), the data are combined to check and evaluate the current operation of the reversible lanes. To this end, first, it is needed to observe how the reversing operation impacts the traffic variables in each direction. Using a boxplot, Figure 6 presents the impacts of the reversing operation (i.e., in this example closing inbound gates and opening the westbound gates) on vehicle count and speed for one of the loop detectors on the inbound mainline (Figure 6-A) and one of the loop detectors on the outbound mainline (Figure 6-B). In the x-axis of Figure 6, "B" represents 15 minutes before the operation, "A15" means from the operation time to 15 minutes later, "A30" means from 15 to 30 minutes after the operation time, "A45" means from 30 to 45 minutes after the operation time, and "A60" means from 45 to 60 minutes after the operation time.

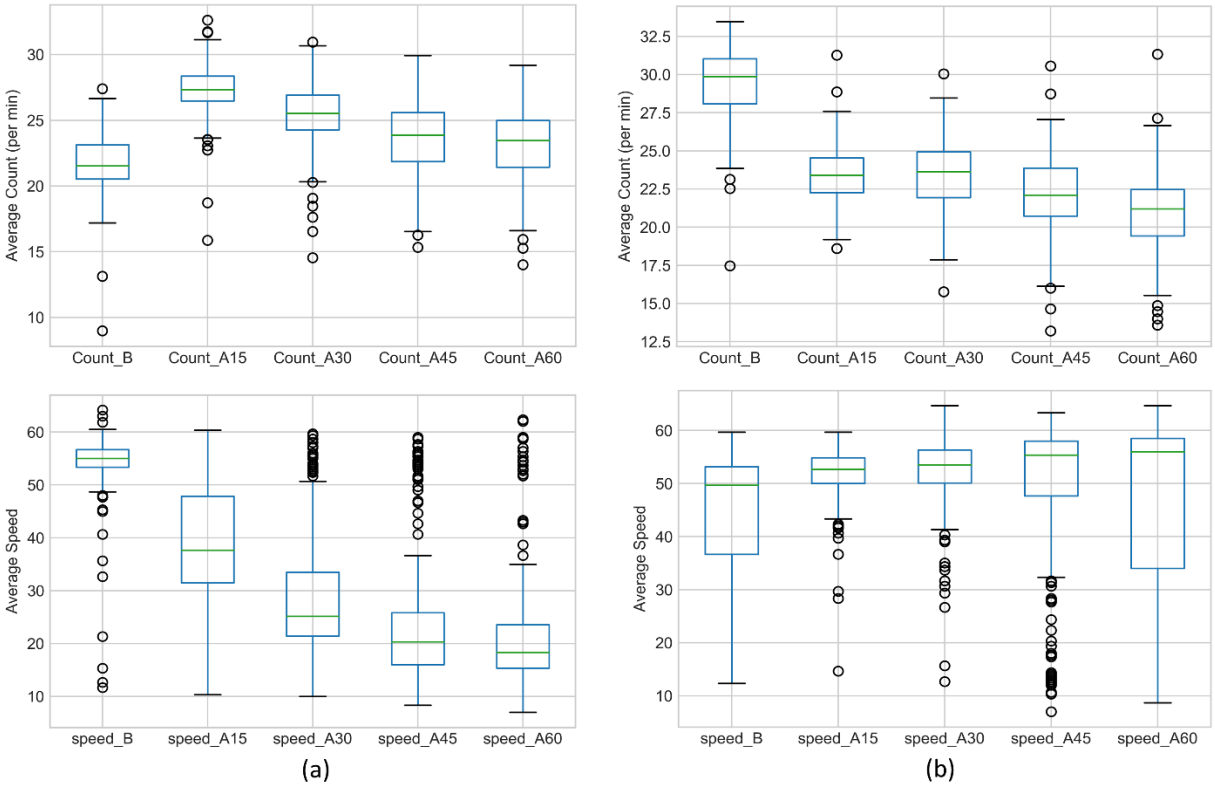

Figure 6. Graph. Impact of inbound to outbound operation on traffic variables collected by a loop detector on the (a) inbound and (b) outbound mainline.

As shown in Figure 6-A, 15 minutes before operation (i.e., switching the direction of the reversible lanes from inbound to eastbound) there are fewer vehicles with higher speeds passing through the inbound direction than after the operation. This is because after closing the gates in the inbound direction, all vehicles should only use the mainline in this direction, which results in congestion and lower speeds. However, this impact plateaus in sequential intervals till 1 hour after the reversing operation. In contrast, because two reversible lanes help the outbound mainline pass traffic after the reversing operation, vehicle count and speed decrease and increase, respectively, in the outbound

mainline (Figure 6-B). To better observe the impact of operation on all loop detectors in both directions, please refer to Appendix A.

To better observe how reversing the operation can impact the traffic variables' trends, Figure 7 and Figure 8 display traffic flow, speed, and occupancy trends within a 4-hour time span in which the switching direction or reversible lanes from eastbound to westbound is operated. In these figures, the red vertical line is the timestamp of starting to close the eastbound gates, and the green vertical line is the timestamp of starting to open the westbound gates. As a general trend, flow and occupancy of the mainline increases and speed decreases after closing the eastbound gates, while flow and occupancy of the mainline decreases and speed increases after opening the westbound gates. Please note that Figure 7 is plotted for one loop detector in the eastbound, and Figure 8 is plotted for one loop detector in the westbound for one random day. To have a better understanding of these trends and compare different loop detectors and days of week, similar figures are plotted in Appendix B for all days of the week and for each direction.

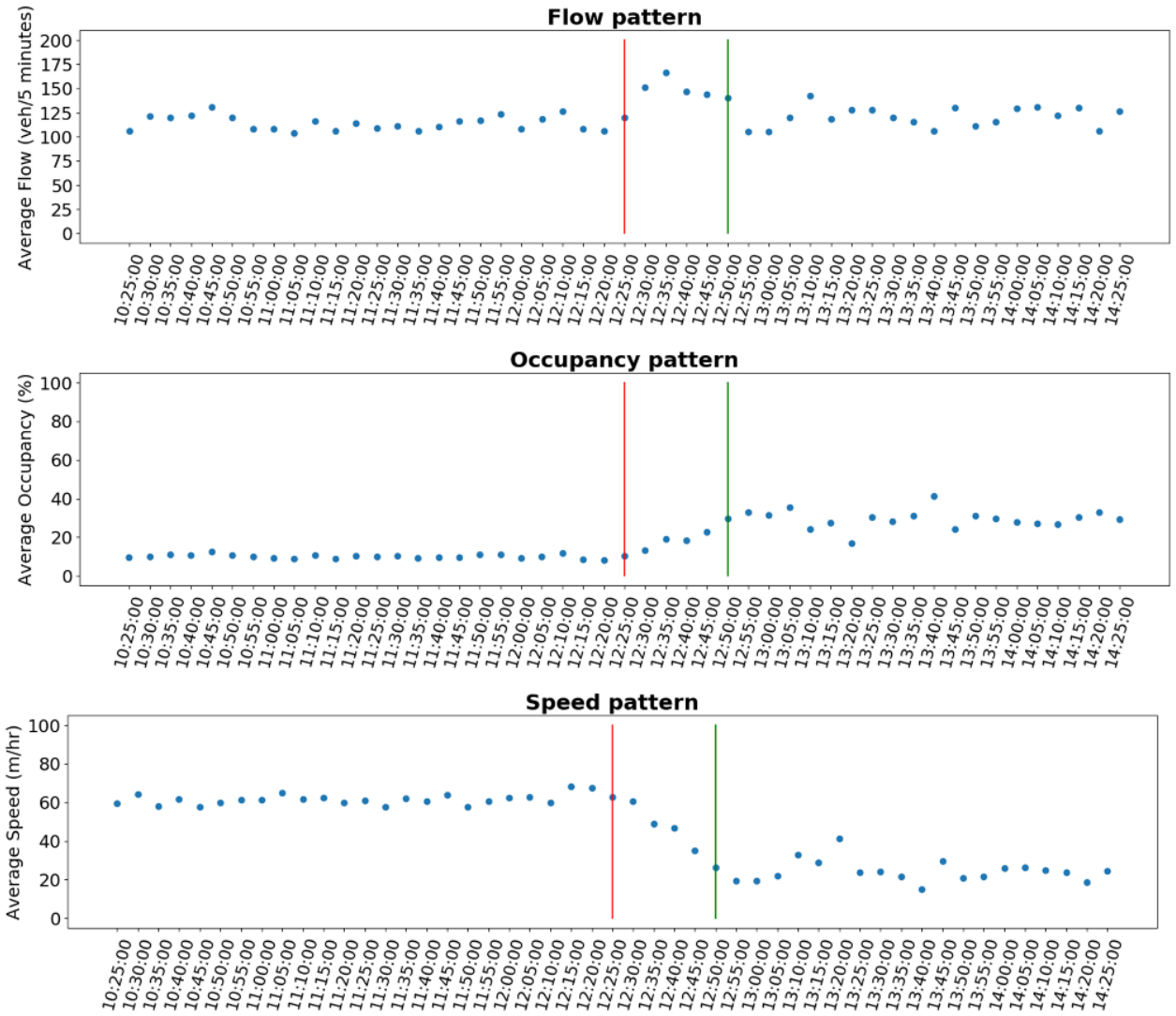

Figure 7. Graph. Impact of reversing operation on traffic pattern—eastbound (closing gates).

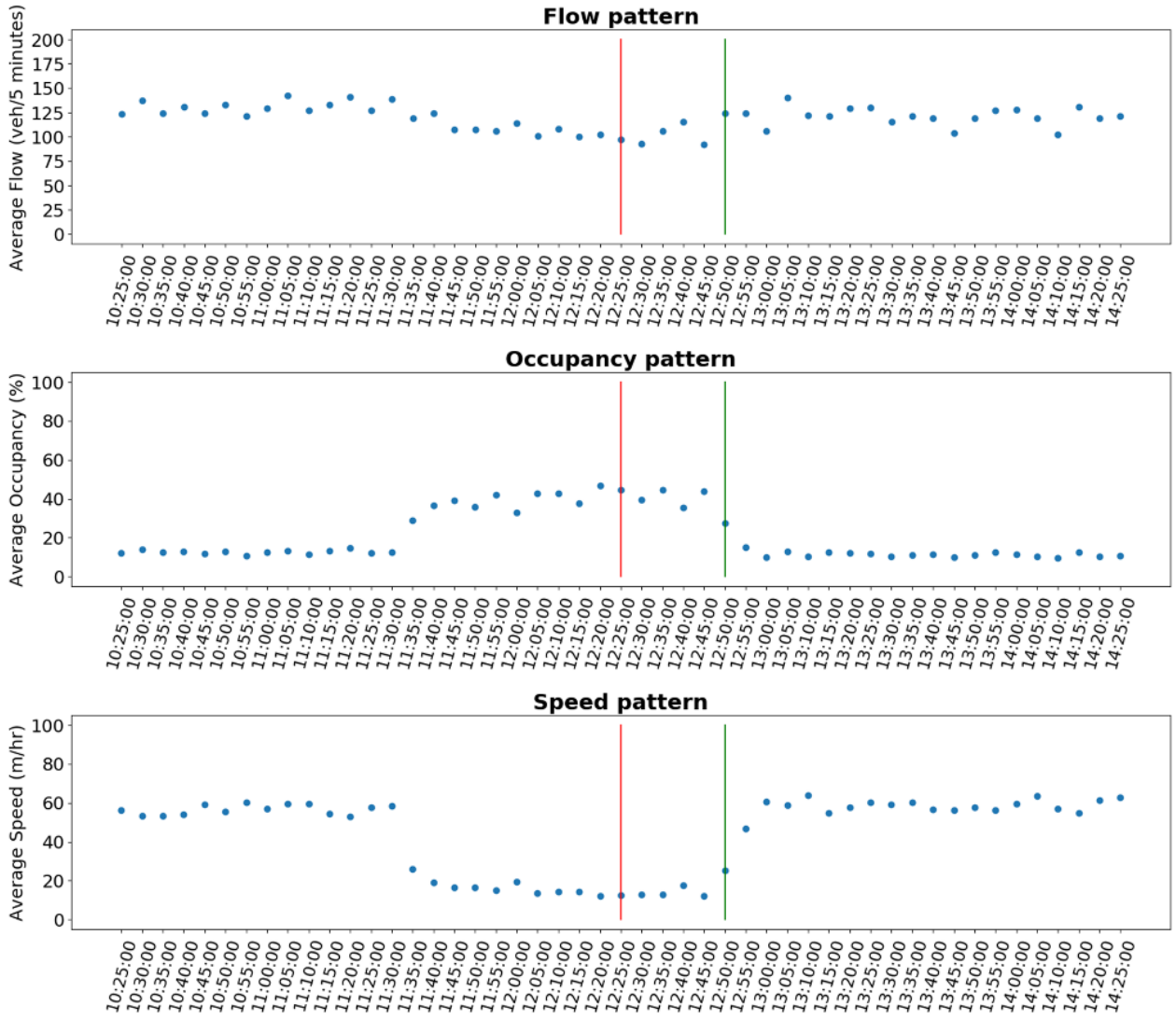

Figure 8. Graph. Impact of reversing operation on traffic pattern—westbound (opening gates).

A comprehensive analysis of Figure 7 and Figure 8 as well as Appendix B can help to find the best traffic variables that are capturing the impact of the reversing operation clearly. In addition, the impact of the operation on the eastbound and westbound can be compared on different days of the week. Comparing these plots for different days, traffic variables, and even locations of the corridor provides valuable information about how different factors can impact the pattern of traffic. However, as the most important factor, the start time of the operation can significantly change these patterns. To this end, the main goal of this study is to find the best time to start the operation time so that the corridor can pass traffic efficiently.

CHAPTER 5: METHODOLOGY

To determine the best operation of the reversible lanes in the Kennedy Expressway, this chapter provides a detailed explanation of a data-driven approach. In this approach, the objective is to develop data-driven techniques that take effective temporospatial traffic factors of the studied corridor and predict the target index (i.e., delay) for that corridor. To this end, different explanatory variables as well as target indices are generated, and several machine learning models are trained.

To measure the performance of reversible lanes in passing the traffic, three target indices to capture delay of the corridor are generated based on the suggestion of NCHRP report 398 (Lomax et al. 1997), as follows:

Index 1) Delay Rate

The delay rate is the ratio of time loss for the vehicles that are involved in the congestion in a specific road segment. This index is calculated and expressed in minutes per mile. Figure 9 presents how this index is calculated.

$$Delay\ Rate = Actual\ travel\ rate\ (min/mile) - Accepted\ travel\ rate\ (min/mile)$$

Figure 9. Equation. Delay rate calculation.

Where travel rate can be calculated as expressed in Figure 10:

$$Travel\ Rate = \frac{Travel\ time\ (minutes)}{Segment\ length\ (miles)} = \frac{60}{Average\ Speed\ (mph)}$$

Figure 10. Equation. Travel rate calculation.

In Figure 9, actual travel rate represents the travel rate experienced by vehicles, and accepted travel rate is the travel rate under free-flow speed.

Index 2) Total Delay

Total delay is the total time loss experienced by all vehicles involved in the congestion in a specific road segment. This index is expressed in vehicle-hours and is calculated in Figure 11 and Figure 12.

$$Total\ Delay = [Actual\ travel\ time\ (hour) - Accepted\ travel\ time\ (hour)] * Count$$

Figure 11. Equation. Total delay calculation.

$$Total\ Delay = \left[\frac{Segment\,Length\ (mile)}{Speed\ mean\ (mph)} - \frac{Segment\,Length\ (mile)}{Free\ flow\ speed\ (mph)}\right] * Count$$

Figure 12. Equation. Total delay calculation (expanded).

Index 3) Delay Ratio

The delay ratio identifies the magnitude of the mobility problem in relation to actual conditions, which is a dimensionless index, and is calculated through Figure 13.

$$Delay\ Ratio = \left[\frac{Delay\ rate\ (\frac{minutes}{miles})}{Actual\ travel\ rate\ (\frac{minutes}{miles})}\right]$$

Figure 13. Equation. Delay ratio calculation.

To calculate these three indices for the whole corridor (i.e., both directions), each direction of the corridor is calculated separately and then added up to create a corridor delay. In addition, our objective is to generate the delay indices of the corridor for a wide time interval so that it comprehensively represents the whole delay condition. To this end, these indices are calculated 1 hour before the operation start time until 1 hour after the start time.

Index 4) Delay Factor

A statistical method—factor analysis—is also applied to generate a new index using the three delay indices. Factor analysis is typically used to describe variability among the observed variables that are correlated. The three delay indices are correlated, so this method is selected for this study. Therefore, the variations in the three observed variables (i.e., indices) will mainly reflect the variations in one unobserved variable, which will be generated through a factor analysis procedure. Eventually, this method searches for joint variations in response to unobserved latent variables and linearly models the observed variables as a combination of the potential factors. Finally, the three delay indices are employed to generate a new delay factor through the factor analysis procedure using the Python programming language.

There are three sources of data used in this study: loop detector, reversible lanes sequence log, and weather condition. After generating different variables and experimenting with their impact on the developing model procedure, weather condition, operation duration (i.e., the duration between closing the first gate until opening the first gate), and traffic variables are used in the data-driven models. However, since the traffic pattern is different on weekdays and weekends, the research team also decided to use a dummy variable (day) to differentiate between weekdays and weekends. In addition, reversing the direction of the reversible lanes is usually done twice a day (i.e., once around noon toward the outbound direction and once around midnight toward the inbound direction); on weekends, the reversing operation might happen more than twice a day. The focus of this study is on switching the direction toward outbound around noon, because there is traffic congestion in both directions. Traffic is not critical around midnight because there is not any congestion in either direction. Also, since the whole reversing operation takes at least 15–20 minutes to complete, it is not reasonable to switch the direction of the reversible lanes several times during rush hours and leave these two lanes unused for approximately 20 minutes.

To start training machine learning models using the mentioned target indices and explanatory variables, the process is started with the inbound to the outbound operation of regular cases. Regular cases are the days in which the reversing operation is done in the correct order and the duration of the operation is not unexpectedly long, i.e., several hours. To this end, the following machine learning techniques are employed for training the models due to their powerful performance in the prediction of scale variables.

K-NEAREST NEIGHBORS

K-nearest neighbors (KNN) is a popular machine learning technique that needs many data points. The target variable is predicted without developing a mathematical model. The model's parameters are not defined in advance, and no smoothing procedure is applied to the data because it needs to be authentic. KNN is widely used as a supervised machine learning technique for classification and regression problems. The KNN technique searches and finds similar data points to a given data point in order to classify that data point in classification problems or to estimate the best value for that data point in regression problems (Han, Pei, and Kamber 2011). Because target variables are continuous indices in this study, the KNN regression algorithm is employed. Feature selection is an important step in this technique because data points are presented in n-dimensional variable space based on the number of explanatory variables of the model training (i.e., n is the number of explanatory variables). Then, the number of k-neighbors should be defined for the model so that for any new data record from the test data set, the model finds its nearest k-neighbors in the training data set and takes the average of the target variable's value for those neighboring data points. In other words, the method searches for nearest neighbors among all historical data points and uses them for the prediction of new records. There are different measurements that can be used to find the nearest data points to a given data point. In this study, the Euclidean metric is employed to find the distance between data points in the n-dimensional variable space. The Euclidean distance between two data points is defined in Figure 14, where $X_1 = (x_{11}, x_{12}, \ldots, x_{1n})$ and $X_2 = (x_{21}, x_{22}, \ldots, x_{2n})$.

$$\text{Euclidean distance } (X_1, X_2) = \sqrt{\sum_{i=1}^{n} (x_{1i} - x_{2i})^2}$$

Figure 14. Equation. Euclidean distance.

Figure 15 displays the schematic diagram of the KNN model. For instance, to predict the speed value of the orange point in a 2D variable space with k equal to 3, the three green points in the orange circle are selected as neighbors of the orange point and the target value for this point is estimated by taking the average of the target value for the three green points.

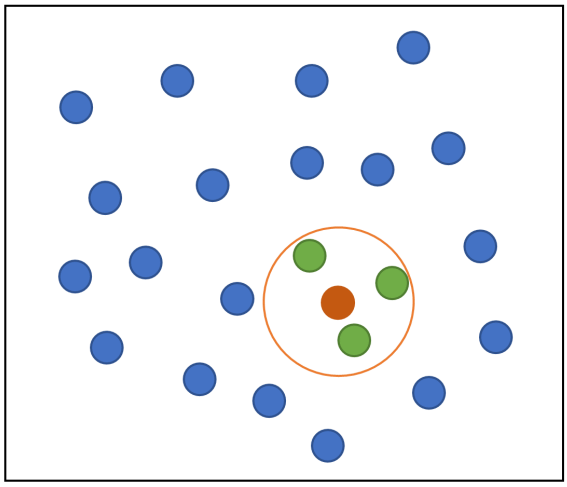

Figure 15. Illustration. Schematic diagram of the KNN model.

DECISION TREE

A decision tree, which has a tree-based structure, is one of the most popular supervised machine learning techniques and can handle both categorical and numerical data. A set of nodes and branches and several paths construct the structure of this technique; a root corresponds to the best predictor and leaf nodes correspond to the prediction of the dependent variable.

On each node of the tree, decision rules are made, and branches indicate the outcomes. In the model-training process at each node, the best attribute is selected using a feature selection method. Using this heuristic procedure, the decision of splitting the node into two or more branches is also made. To measure the split quality in the decision tree regressor model, different functions such as mean squared error (MSE), Friedman_MSE, and mean absolute error (MAE) could be used. This study uses the MSE technique, which is equal to variance reduction, as the feature selection criterion. The MSE function is presented in Figure 16:

$$\mathrm{MSE} = \frac{1}{n}\sum_{i=1}^{n}(x_i - \mu)^2$$

Figure 16. Equation. Mean squared error.

μ denotes the average of x_i when *i* goes from 1 to *n*. The value with the smallest MSE is selected to split the tree. The node-splitting process uses the reduction of variance method so that the weighted variance on the lower-level nodes is less than the upper-level node variance. Figure 17 presents the structure of the decision tree.

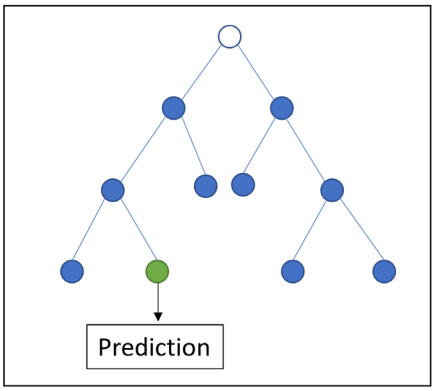

Figure 17. Illustration. Schematic diagram of the decision tree model.

RANDOM FOREST

Another supervised machine learning method is random forest, which is used for both categorical and numerical data as a classifier or regressor (Han, Pei, and Kamber 2011). Random forest consists of several decision trees voting for the target variable prediction. Decision trees are combined using bootstrap aggregation or bagging, a technique that combines machine learning models to improve the accuracy compared to an individual model. To train a random forest model, multiple random samples are selected from the training data set with replacement. Then, a decision tree is developed for each sample, and it predicts the target variable. Finally, the target variable is predicted by taking the average value of the predictions from all developed decision trees.

Random forest is robust to noisy data, and it can resolve a shortcoming of the decision tree: high sensitivity to the training data. Indeed, aggregating several trees can increase the accuracy and decrease the probability of overfitting that can happen in an individual tree, because it decreases the variance of decision trees (Han, Pei, and Kamber 2011). Figure 18 presents the structure of the random forest model.

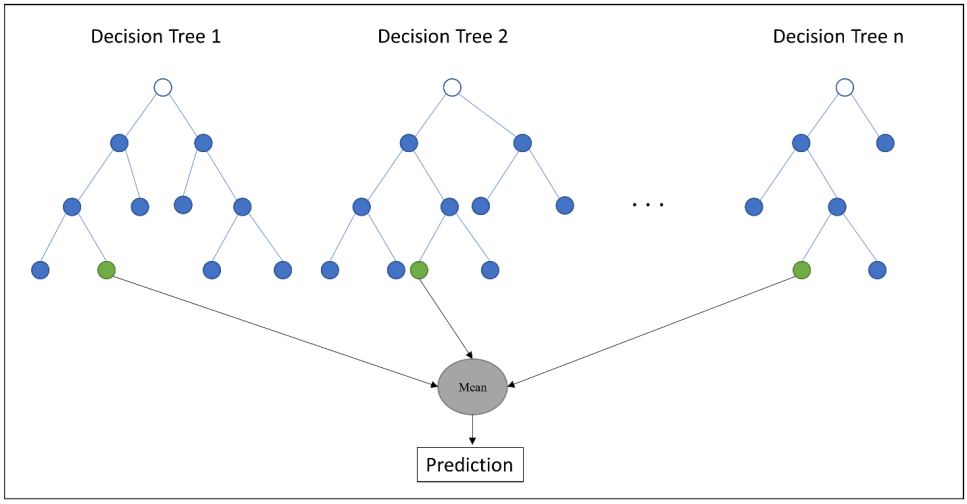

Figure 18. Illustration. Schematic diagram of random forest model.

CHAPTER 6: RESULTS

Feature selection is an important step in training machine learning models. In this study, after generating different features, the features are tested in the procedure of training the three machine learning models. Eventually, speed and count are selected as traffic variables in the models. They are aggregated into 5-minute intervals for each direction of the studied corridor. Among non-traffic variables, three variables (duration, weather, and day) are generated and employed in the final models. Note that when data size is not big enough in machine learning models, usually the number of explanatory variables is decreased to the most effective ones to avoid complexity and overfitting. Table 3 displays the explanatory variables applied in training the final machine learning models.

Table 3. Description of Explanatory Variables

Variable	Description
Duration	The duration between closing the first gate and opening the first gate.
Weather	Weather condition: 1: Fair or a few clouds 2: Cloudy with haze or light fog 3: Light rain or drizzling 4: Heavy rain, snow, thunderstorm, or fog
Day	Dummy variable for day of the week: 0: Weekend 1: Weekday
Count_E	The number of vehicles collected by the eastbound loop detectors aggregated in 5-minute intervals.*
Count_W	The number of vehicles collected by the westbound loop detectors aggregated in 5-minute intervals.*
Speed_E	The speed of vehicles passing eastbound loop detectors aggregated in 5-minute intervals.*
Speed_W	The speed of vehicles passing westbound loop detectors aggregated in 5-minute intervals.*

* It includes 12 time-series variables from the operation time to 1 hour before the operation time (5-minute interval aggregation).

Using the explanatory variables presented in Table 3 and the four delay indices as target variables, three machine learning models (K-nearest neighbors, decision tree, and random forest) are trained. Table 4 presents the accuracy of the trained model with respect to each of the delay indices.

Table 4. Accuracy of Machine Learning Models

	K-Nearest Neighbors	Decision Tree	Random Forest
Index 1) Delay Rate	64.5%	71.8%	87.7%
Index 2) Total Delay	62.7%	75.8%	90.5%
Index 3) Delay Ratio	66.2%	84.9%	**93.7%**
Index 4) Delay Factor	59.5%	74.5%	88.7%

Based on Table 4, the random forest model outperforms the other models, and the best model's performance is achieved when index 3 (delay ratio) is used as the target variable. Therefore, the random forest model and delay ratio as the target delay index will be used for post-analysis in the rest of this study. To better compare the three machine learning models, Figure 19 displays the predicted value against the true value of the delay ratio for the testing data set. Comparing the accuracy of these three models, the random forest model outperforms the other two models with an accuracy of 93.7%. The decision tree and K-nearest neighbors models achieve an accuracy of 84.9% and 66.2%, respectively. Therefore, the random forest model is selected to predict the delay ratio in the post-analysis.

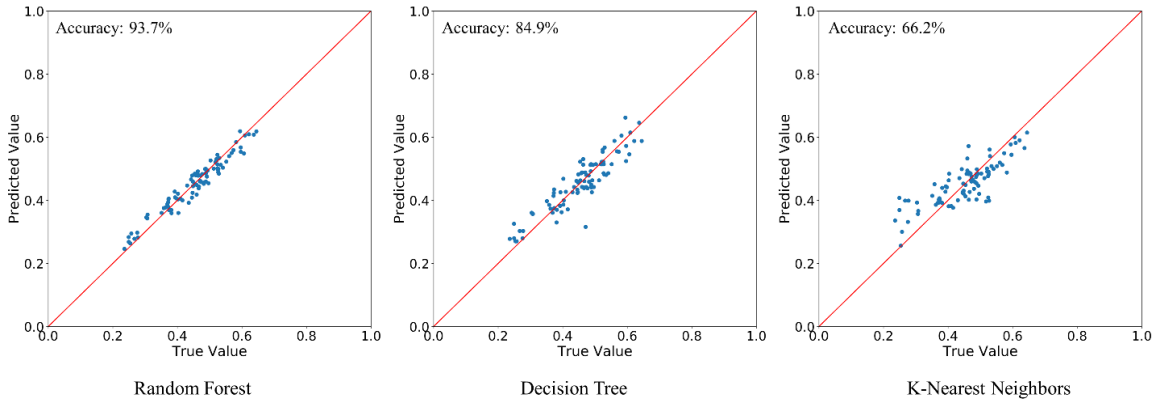

Figure 19. Graph. Accuracy of machine learning models.

Using the trained random forest model and the value of the variable presented in Table 3, the delay ratio can be presented for the other times of day. Given that the operation duration does not change for a specific day, the delay can be predicted in the corridor if the operation has been done at other times of that day. To this end, it is possible to observe how the delay in the corridor is changing if the operation started 5 minutes earlier, 10 minutes earlier, etc. Please note the model can only run for earlier times than the actual time of operation because the traffic data after the actual operation time is already impacted by the operation and cannot be used as the input data for the models. Therefore, using this approach, the delay ratio is predicted for the corridor by shifting the operation start time to earlier 5-minute steps for an interval of several hours. Figure 20, Figure 21, and Figure 22, which correspond to random days, present the results of plotting the delay ratio from the actual time of operation to 5-minute earlier times for starting the operation. Figure 20 presents a day in which the operation is started at 13:25. This is an example of a bad operation start time, because starting the operation about 65 minutes earlier would result in a lower value of index 3 (i.e., delay ratio), which is more preferred. Figure 21, in contrast, is an example of a day in which the operation started at 12:20, when the value of the delay ratio index is relatively low. However, this operation can still be started within a 75-minute interval earlier than the actual operation start time so that the value of the delay ratio index does not change significantly. Finally, Figure 22 is an example of a good operation start time. The operation is started at 12:15 and the best values of the delay ratio are achieved in the actual time of operation; starting the operation earlier will result in more delay in the corridor. Applying the final random forest model on the valid data of all available days provides similar patterns to what is observed in Figure 20, Figure 21, and Figure 22. Therefore, post-analysis of

these patterns for every day of the week is essential in providing an offline timetable for the operation and coming up with a robust approach to find the best time for starting the operation in real time. However, because the inference of the model on some days does not lead to interpretable patterns, applying statistical tests and data-driven techniques in the post-analysis of the model is essential to come up with the best offline and real-time instruction for starting the operation. Note that the focus of this study is switching the direction of the reversible lanes toward the outbound direction, which happens around noon. Appendix C provides the inference of the random forest model on different days.

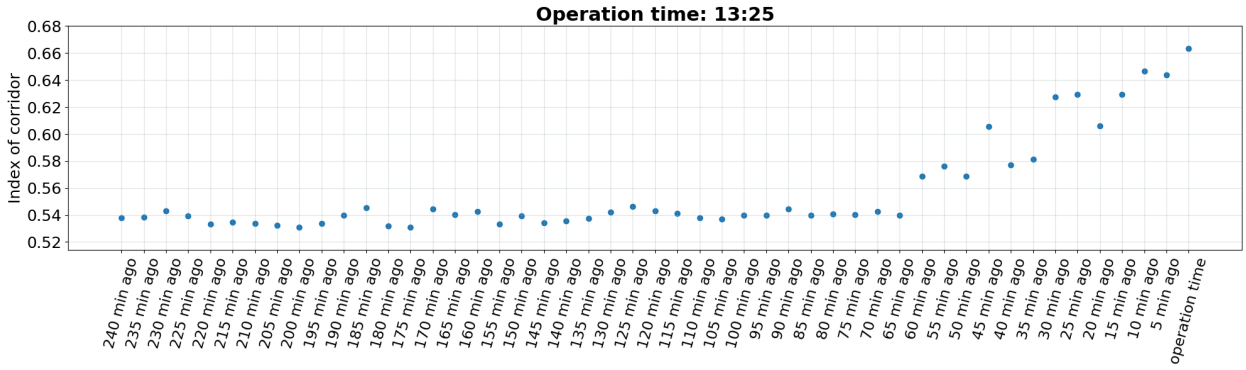

Figure 20. Graph. Model inference for earlier operation start time—a bad example.

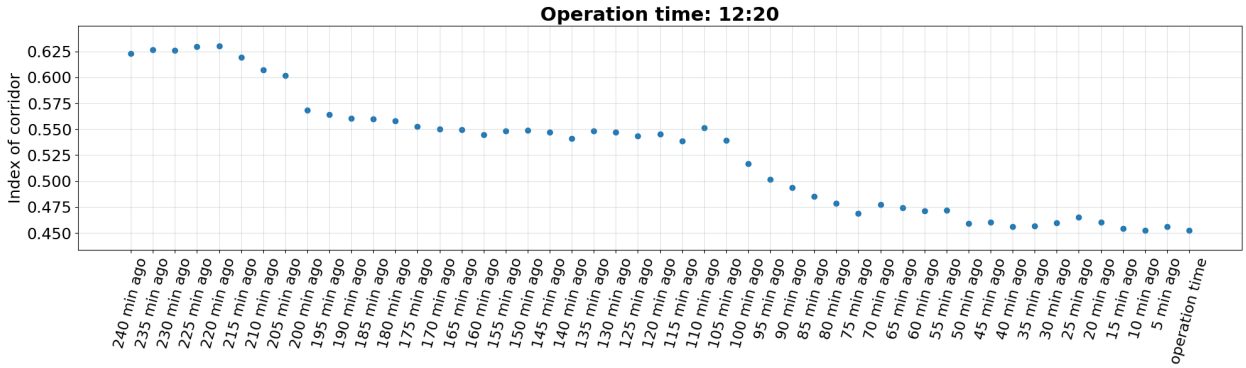

Figure 21. Graph. Model inference for earlier operation start time—an acceptable example.

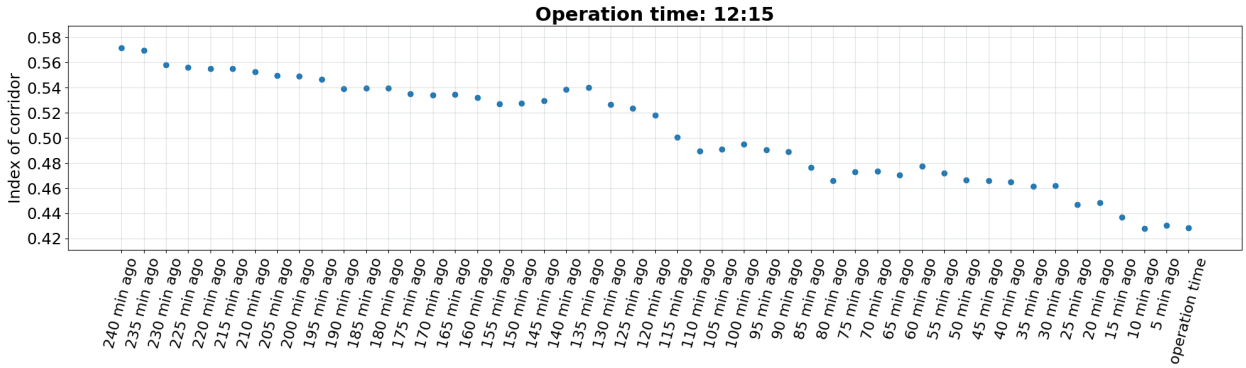

Figure 22. Graph. Model inference for earlier operation start time—a good example.

CHAPTER 7: POST-ANALYSIS

Using the inference of the random forest model, the delay index is available for a wide range of times, all days of the week. Among the four delay indices, the delay ratio index is used in the post-analysis. To come up with the best time of operation (i.e., minimum delay in the corridor), the predicted delay index is used through two approaches: offline and real time. Ideally, these two approaches can be integrated to achieve the highest accuracy.

OFFLINE OPERATION TIMETABLE

In the offline approach, a suggested time for starting the reversing operation (i.e., toward outbound, which happens around noon) is provided for each day of the week. Therefore, to come up with this timetable, the best time of operation can be found for each day (i.e., the time in which the delay index is minimum). By taking the average of these times for each day of the week, a timetable can be suggested. However, before providing this timetable, it is required to find out if the difference of operation start time on different days of the week is significant. To test it, a two-way ANOVA is employed in which the impact of two categorical factors on the mean of a quantitative variable is tested. The setup of the two-way ANOVA test can be written as presented in Figure 23:

$$Y_{ijk} = \mu + \alpha_i + \beta_j + \alpha\beta_{ij} + \epsilon_{ijk}$$

Figure 23. Equation. ANOVA model equation.

Where μ is the overall mean response, α_i is the first factor (i = 1, 2, …, a), β_j is the second factor (j = 1, 2, …, b), and $\alpha\beta_{ij}$ is the interaction of two factors, in which *a* and *b* are the number of categories in the first and second factors, respectively. ϵ_{ijk} is the error term, which follows N(0,σ^2), and *k = 1, 2, …, n* in which *n* is the number of observations.

To run this test, the delay index is the quantitative variable, and day of week and time of day are the two categorical factors. Day of week has seven categories; however, time of day can be categorized into different intervals. To categorize time of day, the time interval is divided from 9:00 a.m. to 3:00 p.m. into 24 categories so that each category is a 15-minute interval. Table 5 provides the results of applying the two-way ANOVA test on these factors. Then, time of day is categorized into 12 30-minute intervals from 9:00 a.m. to 3:00 p.m., and the two-way ANOVA test is applied again. Table 6 presents the results of this test.

Table 5. Two-way ANOVA Test Results (15-minute Intervals)

Response: Delay Index					
Variable	Df	Sum Sq	Mean Sq	F value	Pr(>F)
Time-15	17	0. 30338	0. 017846	5.8037	4.221e-11 ***
Days	6	0. 58775	0. 097959	31.8577	< 2.2e-16 ***
Time-15_Days	65	0. 28944	0. 004453	1.4482	0.02404 *
Residuals	245	0. 75335	0. 003075		

* Signif. codes: '***' 0.001 '**' 0.01 '*' 0.05

Table 6. Two-way ANOVA Test Results (30-minute Intervals)

Response: Delay Index					
Variables	Df	Sum Sq	Mean Sq	F value	Pr(>F)
Time-30	9	0. 21728	0. 024142	7.6504	4.748e-10 ***
Days	6	0. 61213	0. 102022	32.3300	< 2.2e-16 ***
Time-30_Days	37	0. 21777	0. 005886	1.8651	0.002692 **
Residuals	281	0. 88674	0. 003156		

* Signif. codes: '***' 0.001 '**' 0.01 '*' 0.05

Note that in Table 5, the variable "Time-15" is expected to have a degree of freedom of 23 because it has 24 categories; however, six categories do not include any observation from the data set, which results in a degree freedom of 17. Similarly, in Table 6, the variable "Time-30" is expected to have a degree of freedom of 11 because it has 12 categories; however, two categories do not include any observation from the data set, which results in a degree freedom of 9.

The results of the two-way ANOVA tests in Table 5 and Table 6 indicate that day of week and time of day and their interaction can significantly impact the delay index; therefore, the best time to start the operation cannot be the same for all days of the week. That means regardless of the time intervals' size, changing levels of day of week and time of day factors results in changing the delay index. However, after comparing Table 5 and Table 6, a 30-minute interval is selected to categorize the time of day factor because the interaction of factors is significant at the 0.01 significance level for the 30-minute intervals while it is significant at the 0.05 significance level for 15-minute intervals. Table 7 presents the average time of the actual starting operation for each day of the week as well as the suggested time to start the reversing operation toward the outbound direction.

Table 7. Offline Operation Timetable

Day of week	Actual time	Suggested time	Suggested 15-minute interval	Suggested 30-minute interval
Monday	12:10	11:02	10:55–11:10	10:47–11:17
Tuesday	11:56	11:29	11:22–11:37	11:14–11:44
Wednesday	12:08	11:41	11:34–11:49	11:26–11:56
Thursday	12:21	11:36	11:29–11:44	11:21–11:51
Friday	13:36	10:57	10:50–11:05	10:42–11:12
Saturday	13:54	10:33	10:25–10:40	10:18–10:48
Sunday	14:02	10:35	10:28–10:43	10:20–10:50

Figure 24 compares the distribution of the operation's starting time between different days of the week, once using the actual time of operation and once using the suggested time of operation (i.e., the time in which the predicted delay index is minimum).

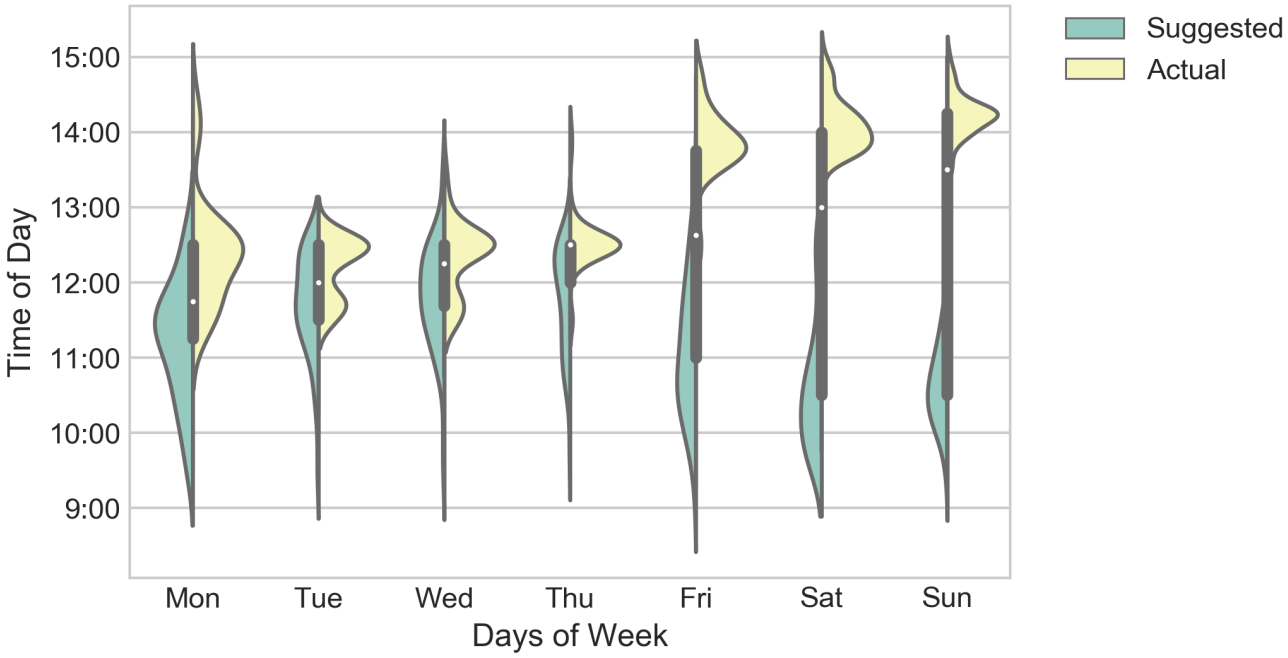

Figure 24. Diagram. Distribution of time to start the operation: actual time vs suggested time.

There are two main differences between the actual and suggested operation time distributions. First, the distribution of the starting operation time on weekdays is different between the actual and suggested operation start times. Second, in the actual time in Figure 24, the distribution of the starting operation time on weekends is located above the weekdays' distribution, meaning reversing the direction of the reversible lanes toward the outbound direction on weekends usually starts later than on weekdays. However, the distributions of starting operation time on weekends are located below those of weekdays in the suggested start time of operation.

REAL-TIME OPERATION TIME SUGGESTION

In the real-time approach, a technique that can suggest the best time to start the reversing operation toward the outbound direction is required. Because delay index time-series data of almost two years is available (i.e., the output of the random forest model for consecutive 5-minute intervals), one can find the best time to start the operation by simply observing the pattern of the delay index in real time. However, an accurate tool is required to fulfill this responsibility.

Among data-driven techniques, long short-term memory (LSTM) is a powerful deep learning model that can perform significantly with time-series data. Therefore, an LSTM model is trained in this approach to find the best time to start the operation in real time. This binary classification model should take the past 10 consecutive delay index values as the input and predict whether it is a good

time to start the operation. To this end, the time-series input data and the value of the target variable (i.e., 1 or 0) for each row of data should first be defined. Figure 25, which is the output of the random forest model for a random day, presents how the data is prepared for training the LSTM model. The first step in the preparation of data is to find the best times to start the operation each day, which is displayed with five green points in Figure 25 (i.e., this is almost the lowest 10% of the data in a four-hour interval). Afterward, the first 10 points are selected as the first row of input data, and because the 10th point of this row of data is not among the best time to start the operation (i.e., it is not among the green points), a value of zero is assigned to this row of data as the value of its target class. Shifting this 10-point window forward by one point, the second row of input data can be extracted, and its target class of zero is assigned similarly to the first row of data. Accordingly, this procedure can be repeated by moving the 10-point window forward, and, consequently, many rows of data can be extracted from the time-series delay data of each day. Please note that a value of one is assigned to the target class of the 19th row of data, which is extracted from the example day presented in Figure 25. This is because the 10th point of the 19th row of data is one of the green points, which are the best times to start the operation.

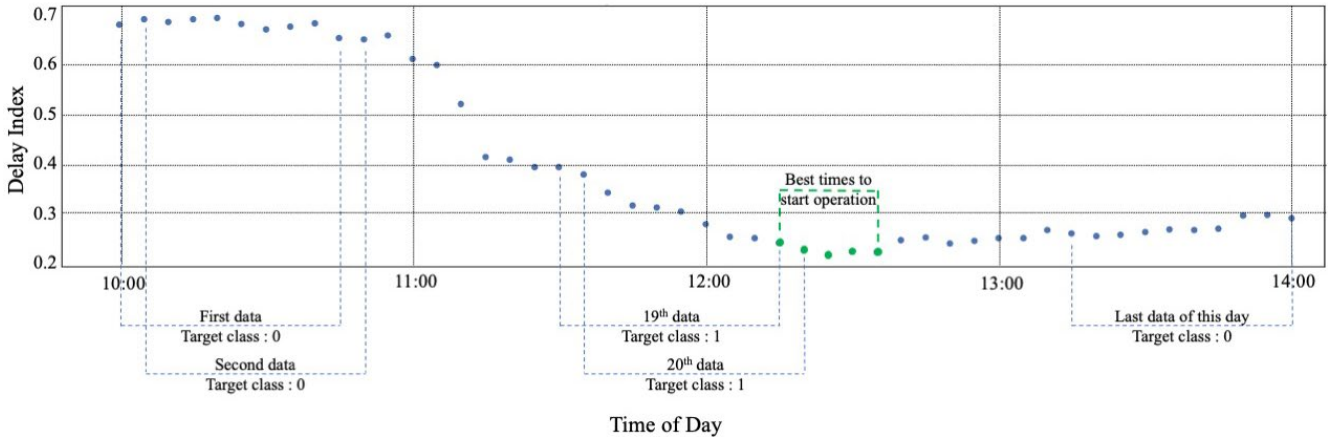

Figure 25. Graph. Preparation of the time-series data for the deep learning model.

Recurrent Neural Network (RNN) is a type of deep learning model that includes input, output, and hidden layers similar to the other neural network. However, unlike the shallow learning techniques, RNN models have a temporal loop that connects the hidden layer to itself, meaning that the hidden layer not only impacts the output but also gives feedback on itself. Figure 26 displays a general structure of RNN models. However, it should be noted that there is another dimension in the RNN model structure shown in Figure 26. In fact, each neuron in Figure 26 is not just a neuron; each neuron represents a layer.

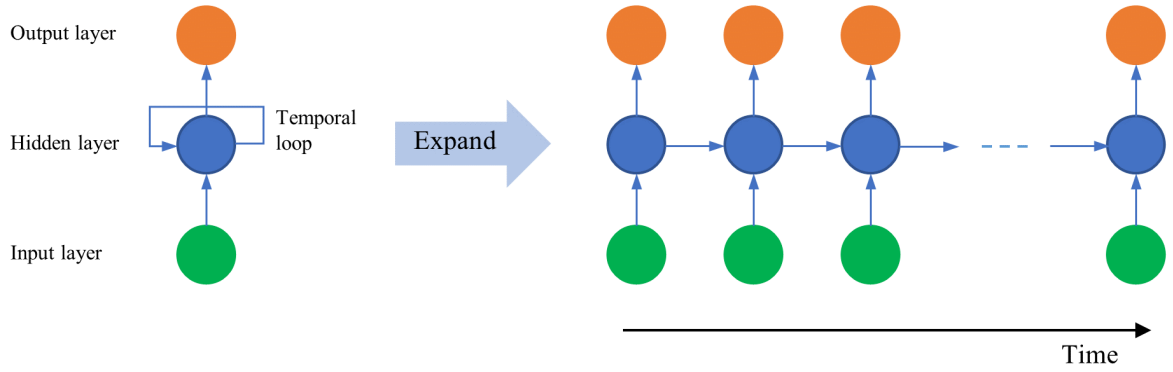

Figure 26. Illustration. Structure of RNN model.

The main concept of the RNN model is that there is a sort of short-term memory (i.e., the links between hidden layers from one timestamp to the next one) that remembers what was in the previous neuron. However, a big issue in RNN models is the vanishing gradient; the gradients decrease moving from time *t* to previous times' layers through back-propagating the weights' procedure. In contrast, when gradients are small, it is harder for the model to adjust the weights and show the impact of that layer (i.e., time). One of the most successful models to solve this issue and to get along with time-series data is LSTM.

The LSTM model is composed of a memory cell and three gates: input, forget, and output (Bianchi et al. 2017). The cell is the internal unit of processing, and gates regulate the information flow to and from the cell. In LSTMs, the main information flow occurs in the cell state. The forget gate makes the decision to remove information from the previous cell state h[t-1]. The input gate decides about updating the new state h[t]. The output gate decides on the output part from the state. A set of parameters are trained through gradient descent to control the decision of the gates. For this purpose, in this study, the Adam approach is used to update the parameters. The following equations shown in Figures 27–32 present the computation functions in which the cell state is updated and output is computed.

$$\text{forget gate:} \quad \sigma f[t] = \sigma\,(Wf \cdot x[t] + Rf \cdot y[t-1] + bf)$$

Figure 27. Equation. LSTM equations—forget gate.

$$\text{candidate state:} \quad \tilde{h}[t] = g1(Wh \cdot x[t] + Rh \cdot y[t-1] + bh)$$

Figure 28. Equation. LSTM equations—candidate state.

$$\text{input gate:} \quad \sigma u[t] = \sigma\,(Wu \cdot x[t] + Ru \cdot y[t-1] + bu)$$

Figure 29. Equation. LSTM equations—input gate.

$$\text{cell state:} \quad h[t] = \sigma u[t] \,(\cdot)\, \tilde{h}[t] + \sigma f[t] \,(\cdot)\, h[t-1]$$

Figure 30. Equation. LSTM equations—cell state.

$$\text{output gate:} \quad \sigma o[t] = \sigma(Wo \cdot x[t] + Ro \cdot y[t-1] + bo)$$

Figure 31. Equation. LSTM equations—output gate.

$$\text{output:} \quad y[t] = \sigma o[t] \,(\cdot)\, g2(h[t])$$

Figure 32. Equation. LSTM equations—output.

in which, x[t] is the input at time t; σ(·) is a sigmoid function; g1(·) and g2(·) denote the pointwise nonlinear activation function; (·) denotes the entry wise multiplication between two vectors; Ro, Ru, Rh, and Rf represent weight matrices of the recurrent connections; Wo, Wu, Wh, and Wf are weight matrices for the inputs of LSTM cells; and bo, bu, bf, and bh are bias vectors (Bianchi et al. 2017). The Adam optimizer is used in the developed model, and the losses are computed as binary cross entropy. The hidden layers of the model consisted of the Sigmoid activation function. The hyperparameters of this model, such as batch size and the number of LSTM layers, hidden layers, neurons in each layer, and epochs, are tuned through the hyperparametric tuning procedure.

To train the LSTM model, the data set is split randomly into a training set (75%) and a testing set (25%). Table 8 presents the results of tunning hyperparameters of the LSTM model.

Table 8. Model Hyperparameters

Parameters	**LSTM**
Number of epochs	500
Batch size	32
Activation function	Sigmoid
Optimizer	Adam
Loss	Binary Cross Entropy
Learning rate	0.001

To evaluate the performance of the trained LSTM model, three measures (accuracy, detection rate, and false alarm rate) are employed in this study, as displayed in the equations shown in Figures 33–35.

$$\text{Accuracy} = \frac{Number\ of\ true\ reports}{Total\ number\ of\ cases} \times 100$$

Figure 33. Equation. Model accuracy calculation.

$$\text{Detection Rate} = \frac{Number\ of\ true\ accident\ report}{Total\ number\ of\ accident} \times 100$$

Figure 34. Equation. Detection rate calculation.

$$\text{False Alarm Rate} = \frac{Number\ of\ false\ accident\ report}{Total\ number\ of\ cases} \times 100$$

Figure 35. Equation. False alarm rate calculation.

Table 9 presents the confusion matrix and performance of the LSTM model. While this model performs well with a high accuracy and detection rate, its false-alarm rate is relatively high. There would be times that the model signals it is time to start the operation while it is not exactly a good time to start it. To address this issue, the offline and real-time approaches should be combined to ignore false alarms and improve accuracy, meaning the operator can consider only model alarms, which are happening in the intervals presented in Table 7. One reason for the relatively high false-alarm rate could be low traffic volume and, consequently, a lower delay index value in weekend mornings, which caused the model to learn that those times can be considered to start the operation.

Table 9. Model Performance Results

Performance Measures	LSTM
True Negative	2211
False Positive	804
False Negative	54
True Positive	271
Accuracy (%)	74.3
Detection Rate (%)	83.4
False Alarm Rate (%)	24.1

To better understand the performance of the trained LSTM model, the receiver operating characteristic (ROC) curve of this model is displayed in Figure 36. This figure plots the true positive rate against the false positive rate; a higher area under the curve means better performance of the model. Therefore, the trained LSTM model with an area under the curve of 85.5% has a good performance in predicting the best time to start the reversing operation in real time.

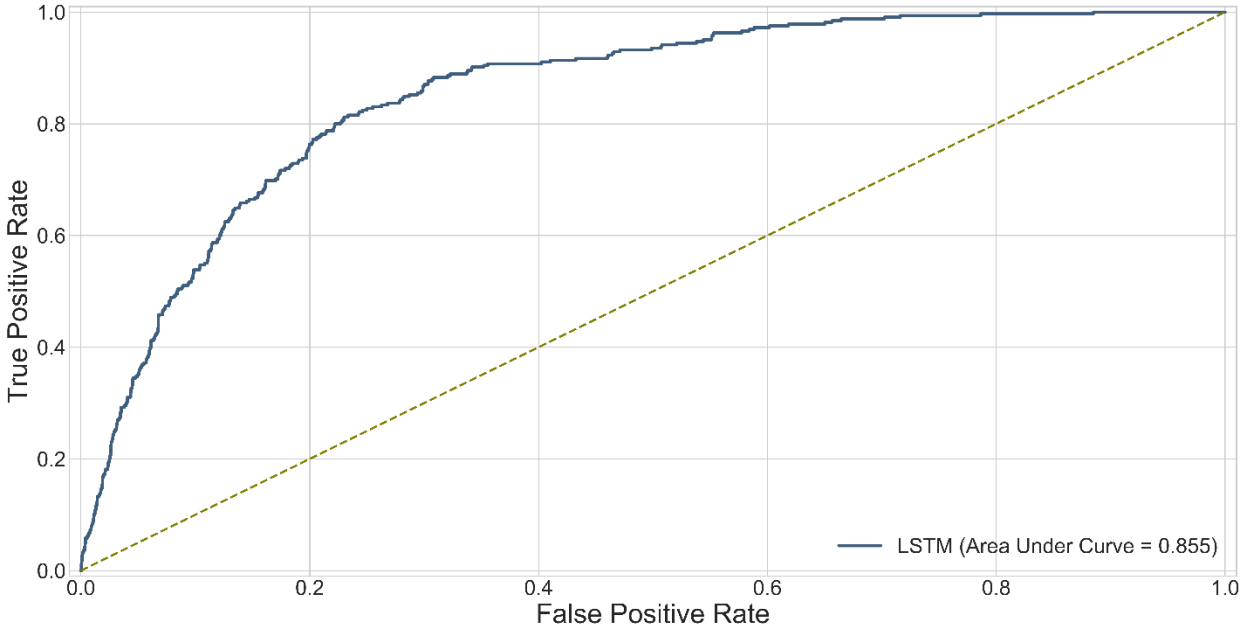

Figure 36. Graph. ROC curve of the LSTM model.

CHAPTER 8: OPTIMIZATION APPROACH

NOTATIONS

Sets

$\boldsymbol{C}$	Set of cells, $i \in C$
$\boldsymbol{C_R}$	Set of source cell
$\boldsymbol{C_o}$	Set of ordinary cells
$\boldsymbol{C_M}$	Set of merging cells
$\boldsymbol{C_D}$	Set of diverging cells
$\boldsymbol{A}$	Set of links, $a \in A$
$\boldsymbol{A_o}$	Set of ordinary links
$\boldsymbol{A_M}$	Set of merging links
$\boldsymbol{A_D}$	Set of diverging links
$\boldsymbol{\varsigma^+_i}$	Set of successors of cell i
$\boldsymbol{\varsigma^-_i}$	Set of predecessors of cell i
$\boldsymbol{P}$	Set of paths, $p \in P$
$\boldsymbol{T}$	Set of time intervals, $t \in T$

Parameters

$\boldsymbol{d_t}$	Total demand at time interval t
$\boldsymbol{\mu}$	Infinitesimal parameter to avoid zero denominator
$\boldsymbol{T}$	Maximum departure time
$\boldsymbol{T_f}$	Maximum time horizon
$\boldsymbol{N^i}$	Maximum occupancy of cell
$\mathbf{Q}^{\boldsymbol{i}}$	Flow capacity out of cell i at time t

$\boldsymbol{\delta}$	Ratio of forward to backward shockwave propagation

Variables

$\boldsymbol{x_{p,t}^{i}}$	Occupancy of cell i at time t and path p
$\boldsymbol{y_{p,t}^{i,j}}$	Flow of link (i, j) at time t and path p
$\boldsymbol{z_{p,t}^{i,j}}$	Auxiliary variable corresponding to $y_{p,t}^{i,j}$
$\hat{\mathrm{y}}_{\boldsymbol{p,t}}^{\boldsymbol{i,j}}$	Auxiliary variable corresponding to $y_{p,t}^{i,j}$
$\boldsymbol{\overline{y}_{t}^{i,j}}$	Aggregate flow from cell i to j at time t
$\boldsymbol{\overline{x}_{t}^{i}}$	Aggregate cell occupancy of cell i at time t
$\boldsymbol{x'^{i,j}_{t}}$	Aggregate cell occupancy at diverging cell i at time t traveling to cell j
$\boldsymbol{r_{p,t}}$	Departure rate at time t for the flow using path p
$\boldsymbol{TT_{p,t}}$	Travel time for the flow using path p at time t
$\boldsymbol{v_{p,t,t'}}$	Auxiliary variable for average travel time estimation of path p
$\boldsymbol{\tau_{p,t,t'}}$	Auxiliary variable for maximum travel time estimation of path p
$\boldsymbol{\hat{\tau}_{p,t,t'}}$	Auxiliary variable for maximum travel time estimation of path p

INTRODUCTION

Traffic congestion is always one of the main concerns of transportation agencies. One reason for traffic congestion is travelers having similar travel behavior (Downs 2004). People travel for the same purpose during rush hours, such as traveling downtown on weekday mornings for business or health care purposes (morning commute), on weekday evenings to go home (evening commute), on weekend evenings for recreational purposes, and on special occasions (e.g., New Year's Eve, Super Bowl). When most people travel with private vehicles, these similar travel behavior patterns led to a large flow toward a certain area at a certain time in a limited capacity system, which causes congestion (Downs 2004).

Transportation agencies have committed to reduce traffic congestion through construction and non-construction strategies. Construction strategies such as adding new highways or lanes to existing highways, expanding the public transportation network, and improving land use are effective, but expensive (FHWA 2017). Reversible lanes are an effective and economical non-construction strategy

(Bede, Szabó, and Péter 2010). The concept of the reversible lane system is to increase directional capacity to match with expected periodic unbalanced directional traffic demand. They enable transportation agencies to make better use of underused roads by adjusting capacity with demand. When the demand pattern changes, reversible lanes can allocate road capacities to the direction with the highest demand such as during morning and evening rush hours (Bede, Szabó, and Péter 2010).

The concept of the reversible lane system is simple, but it is difficult to manage and operate. Reversible lanes should be managed in a way that maximizes efficiency in both directions. Currently, the direction of most reversible lanes is changed manually by traffic operators by looking at cameras (Frejo et al. 2015). Without any travel demand or travel time estimation, manual control can be easily carried out based on a traffic operator's professional judgment. However, manual control results in misjudgment and causes the operation not to be performed at an optimal time. In addition, manual control cannot keep up with the increasing demand, whereas the operation of reversible lanes based on dynamic traffic analysis can be practiced at its best time.

The literature suggests using the optimization approach for dynamic control of reversible lanes (Zhao et al. 2014; Wu et al. 2009). To capture travelers' route choice behavior with the optimization approach, a dynamic traffic assignment (DTA) is needed. DTA is a generalization of static traffic assignment (STA). STA assumes that travelers depart at the same time and, consequently, assumes a fixed demand for an origin-destination (OD) pair. However, the reality of networks is that travelers depart at different times and the demand for ODs varies in time. DTA generalizes the STA assumption by capturing the reality of networks assuming time-varying link flows. DTA models explain networks and demand interactions that vary during the time, giving departure time choice options to travelers in the network. Merchant and Nemhauser (1978) were the first to systematically formulate DTA models into an analytical formulation. DTA models are classified into two groups based on the assumptions about route choice criterion: (i) deterministic dynamic traffic assignment (DDTA) models and (ii) stochastic dynamic traffic assignment (SDTA) models (Peeta and Ziliaskopoulos 2001). DDTA models assume that all travelers have perfect knowledge about traffic-flow conditions and choose the shortest path, which is impractical in reality. Indeed, travelers minimize their travel time based on their individualistic knowledge of traffic-flow conditions. This route choice behavior is relaxed in SDTA model assumptions. Once SDTA models were proposed, they received the attention of many researchers due to their legitimacy. Therefore, the concept and mathematical programming of SDTA models have been extensively developed in the literature by other studies (Meng and Khoo 2012; Gao 2012).

Considering user equilibrium (UE) in DTA models, dynamic user equilibrium (DUE) models have always drawn the interests of researchers. Studies in the literature have considered two extensions for UE in DTA models. First, the perfect traveler knowledge assumption and route choice criterion of static models should be generalized to consider the fact that links' travel times change over time (Chiu et al. 2010). The UE condition assumes that the shortest path between each OD is always taken in the network. Therefore, travel time on all the used paths between an OD is equal to the travel time of the shortest path between that OD pair, otherwise the path will not be used. Once the UE condition is reached in the network, the traffic-flow conditions will not change unless the demand or the network change. Second, extension of UE in DTA accounts for the equal travel times on the used

paths between an OD for only those travelers who departed for that OD pair at the same time. This is because travelers who departed for an OD at different times will have different travel times (Chiu et al. 2010).

The reversible lanes at the Kennedy Expressway are the most notable example of reversible lanes. The reversible lanes lie in the center of the expressway from the north of the Loop at Ohio Street to the Kennedy Expressway and Edens Expressway intersection, approximately an 8-mile distance. These reversible lanes drive two-stream lanes to the city center and the suburbs in the morning and the evening, respectively. The lanes are controlled by traffic personnel in a separate control center. A thorough dynamic traffic control algorithm using real-time data can properly manage the operation of the lanes to minimize traffic congestion in the corridor. This study seeks to optimize the operation time of reversible lanes at the Kennedy Expressway to mitigate rush-hour traffic congestion. A bi-level framework is proposed. At the upper level, transportation decision-makers seek to minimize the total delay in both directions of the expressway. The control decision variable at the upper level is operation time of the reversible lanes. At the lower level, travelers seek to address their travel needs while minimizing their travel time. The control decision for travelers is to select the optimal route. The operation time chosen in the upper level affects travelers' route choice, and the travelers' route choice affects the operation time decided at the upper level.

LITERATURE REVIEW

In the literature, for reversible lanes management, several dynamic traffic controls such as ramp metering and variable speed limit have been implemented. However, relatively few studies have considered the optimization approach for controlling reversible lanes (Wu et al. 2009; Zhao et al. 2014). For example, Zhao et al. (2014) proposed a lane-based optimization model for operation of arterial reversible lanes. With a similar approach, Wu et al. (2009) suggested a bi-level programming model demand to operate reversible lanes. These studies broke new ground in the context of managing reversible lanes. However, they did not consider time-dependent OD demand. To capture time-dependent OD demand, dynamic traffic assignments (DTA) models are needed.

DTA models can be divided into analytical- or simulation-based models. Analytical models are mathematical program formulations that provide a theoretical base and validate the findings of other models. Analytical tractability, however, comes at the cost of the traffic-flow model's accuracy. Analytical models can be classified into three classes: mathematical programming, optimal control theory, and variational inequality (Balakrishna, Ben-Akiva, and Koutsopoulos 2007; Peeta and Ziliaskopoulos 2001). Optimal control theory and variational inequality, however, can be included in the general description of mathematical programming. Simulation models capture most dynamic traffic-flow realities, yet the theoretical guarantees of solution existence, uniqueness, and stability are lacking.

In mathematical programming–based models time is considered a discrete variable. Merchant and Nemhauser (1978) were the first to formulate dynamic traffic assignment as mathematical programming. The study aimed to minimize the total system cost, which implies system optimum (SO), and solve this SO DTA problem in a single-destination network with a fixed demand. The study

uses link-exit functions to model traffic flow and link performance functions to calculate travel time. The study yields non-convex programming formulation, which leads to first-in, first-out (FIFO) principal violation. Modeling traffic flow based on link-exit functions (link-based) causes FIFO principal violation (Carey and Subrahmanian 2000). In actual travel behavior, vehicles violate the FIFO principal by overtaking other vehicles, but the physical violation of FIFO principal is different from the violation in theory, which unreasonably assumes vehicles "jump" over each other in congested areas.

Meeting FIFO conditions in single-destination networks is easy, but these conditions are complicated in multiple-destination networks and should be met in a clear and detailed manner (Peeta and Ziliaskopoulos 2001). Therefore, Carey (1987) improved Merchant and Nemhauser's formulation to a well-mannered convex nonlinear programming formulation. Another common occurrence in SO formulation is "holding back" of the vehicles, which happens when some minor or certain flows are held back in favor of major ones to reduce total system delay (Ziliaskopoulos 2000; Carey and Subrahmanian 2000; Peeta and Ziliaskopoulos 2001). Later, Ziliaskopoulos (2000) proposed a linear programming formulation for single-destination networks in SO DTA problems. The study models traffic flows based on the cell transmission model (CTM) (Daganzo 1994, 1995), which captures more traffic-flow realities in case of propagation than link-based models.

Dynamic traffic assignment formulation under UE conditions is even more complicated than system optimum. A study by Janson et al. (1991) is one of the first on UE DTA problems. The study develops a link-based convex nonlinear programming formulation for UE DTA problems. However, the traffic flows are modeled based on the static link performance function and do not consider instantaneous travel times on a path, resulting in incapability of capturing traffic-flow realities (Peeta and Ziliaskopoulos 2001).

Many previous studies formulated both SO and UE DTA problems as an optimal control problem, where time is considered a continuous variable. A study by Friesz et al. (1989) is one of the earliest studies to formulate a link-based SO and UE DTA problem for single-destination networks. The proposed SO formulation can be considered a continuous-time extension of Merchant and Nemhauser's formulation. The study also develops a time-dependent extension of Beckman's formulation under static UE conditions. Using the optimal control theory, Ran et al. (1993) formulated a link-based UE problem, and Ran et al. (1989) fomulated a link-based SO problem. Although the optimal control theory is capable of describing traffic-flow dynamics in an interesting way, it has several limitations. The limitations include a lack of effective solution algorithms for general problems as well as precise constraints to guarantee FIFO conditions are met and avoid vehicle holding back issue, and potentially unrealistic traffic-flow modeling (Peeta and Ziliaskopoulos 2001).

Variational inequality (VI) is a general unified framework that can formulate different classes of UE DTA problems such as optimization, fixed point, and complementarity (Peeta and Ziliaskopoulos 2001). VI was first introduced by Dafermos (1980) for static traffic equilibrium problems. Extensive research implies that VI approaches have increasingly attracted many researchers' attention due to their capabilities (Nagurney 1999; Facchinei and Pang 2004; Friesz, Bernstein, and Stough 1996). Friesz et al. (1993) developed a continuous-time VI model that considers both departure time and path choice. The formulation captures most traffic realities. The travel cost on links is calculated using

both link performance function and a penalty for early/late arrival function. The FIFO principal is also met under restrictive constraints. The formulation is for infinite-dimensional problems. However, due to these considerations, the proposed formulation is complicated. VI can model traffic flows in a more solid way compared to mathematical programming and optimal control theory. VI addresses analytical tractability problems and, thus, models traffic flows more realistically. Besides, extensions and sensitivity analysis can be easily executed. However, the extensive computation disables VI formulation from being computationally tractable (Peeta and Ziliaskopoulos 2001).

In all categories of DTA models, from different classes of analytical models to simulation-based models, modeling traffic-flow propagation has been always challenging. Many researchers have attempted to maintain the balance of capturing traffic-flow realities with computation tractability (Peeta and Ziliaskopoulos 2001). DTA models use three approaches to model traffic flows: link exit functions, point queue, and physical queue. In link-based models, a link exit function relates travel delay on a link to the inflow at the link. Although link-based models have been the most popular traffic-flow model and are widely used in analytical DTA models, they are incapable of satisfying FIFO conditions and traffic propagation issues. In DTA models, FIFO is an essential requirement that should be met by traffic-flow models. Queue-based traffic-flow models, in contrast, guarantee FIFO nature by default. However, point-queue based traffic-flow models have typically been used for single bottle necks and have barely been applied to general networks because they cannot capture congestion effects and physical spatial dimensions of queues, which accounts for the traffic propagation (Ramadurai et al. 2009).

Most previous studies using physical queue traffic-flow models applied the cell transmission model (CTM) to solve the DTA problem. CTM was first proposed by Daganzo (1994, 1995) for simulating the nature of traffic flows on a single highway link. Then, Ziliaskopoulos (2000) proposed a linear programming formulation of CTM by describing traffic propagation based on a set of linear constraints. This linear programming formulation was later improved by Ukkusuri et al. (2008) for UE DTA problems. However, the linear formulation of CTM is not accurate due to the incapability of addressing traffic propagation issues in some cases and FIFO violation in networks with multiple destinations. Therefore, Ramadurai et al. (2009) suggested a complementarity formulation of CTM to address the traffic propagation problem. This study simplifies the computations by treating all sorts of cells (ordinary, diverging, merging, sink, and source). However, the traffic flow is modeled based on point queue models. Because of the capability of complementarity formulation to address traffic propagation problem in CTM, later studies mostly focused on developing complementarity constraints in CTM for different networks and problems. Han et al. (2011) developed a complementarity formulation of CTM for UE DTA problems that considers a single OD pair network. Ukkusuri et al. (2012) extended the formulation to multiple origins and destinations.

CTM can be easily adapted to different frameworks, and, thus, it has a wide range of applications, from network design and network analysis to ramp metering and congestion pricing. Table 10 summarizes the application of CTM. A study conducted in southern California by Gomes and Horowitz (2006) solved an on-ramp metering problem using asymmetric CTM to minimize congestion on urban freeways. Meng and Khoo (2010) applied a modified CTM to mitigate congestion among on-ramps on freeways to solve a fair ramp metering problem. Lo and Szeto (2005) used CTM to solve the

congestion pricing problem in a more realistic manner. Ukkussuri and Waller (2008) incorporated CTM in the proposed network design model under dynamic user equilibrium conditions. CTM is also applied to evaluate the impact of Advanced Traveler Information Systems on travel time (Lo and Szeto 2004).

Table 10. CTM Applications—A Synthesis of Selected Literature

Reference	CTM applications			
	Network design	**Congestion mitigation**	**Congestion pricing**	**Advice on routes for travelers with advanced traveler information systems**
Abdelghany et al. (2000)	Yes	–	–	–
Ukkusuri and Waller (2008)	Yes	–	–	–
Gomes and Horowitz (2006)	–	Yes	–	–
Meng and Khoo (2010)	–	Yes	–	–
Lo and Szeto (2005)	–	–	Yes	Yes
Lo and Szeto (2004)	–	–	–	Yes
Al-Deek et al. (1998)	–	–	–	Yes

METHODOLOGY

The reversible lane operation time problem is formulated as a bi-level program consisting of upper- and lower-level models (Figure 37). The bi-level framework is widely used in transportation planning literature (Seilabi et al. 2020; Tabesh 2020). This section formulates the upper- and lower-level models. At the upper level, a transportation agency decision-maker decides the optimal time to reverse the direction of the reversible lanes to minimize the total travel time. At the lower level, travelers seek to address their travel needs while minimizing their travel time. The control decision for travelers is to select the optimal route. The operation time chosen in the upper level affects travelers' route choice, and the travelers' route choice affects the operation time decided at the upper level. Due to the dynamic nature of the problem CTM, a DTA model is used to model the lower-level model.

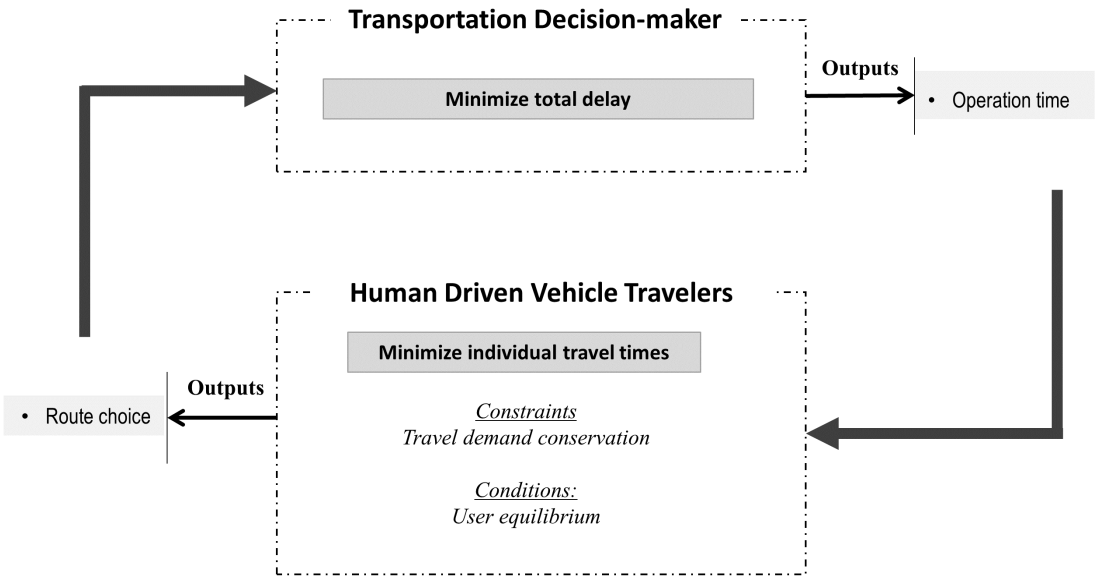

Figure 37. Graph. Bi-level structure of the problem.

Preliminaries

Let C and A denote a set of cells and links (cell connectors), respectively. C_R, C_O, C_M and C_D represent the set of the source, ordinary, merging and diverging cells, respectively. A_O, A_M, and A_D represent the set of the ordinary, merging and diverging links, respectively. ς_i^+ and ς_i^- represent the set of the successors and predecessors of cell i. In addition, O and D denote a set of ODs with indices r and s, respectively. P denotes the set of paths between each OD. T denotes the set of time intervals. Sets C_R, C_O, C_M, C_D, ς_i^+ and ς_i^- are a subset of C and sets A_O, A_M, and A_D is a subset of A.

In this report, each path between an OD pair is divided into homogeneous cells, as proposed by Daganzo (1994, 1995). Based on the concept of homogeneity, cells have an equal length of the distance through which travelers can travel at free-flow speed in a time interval. Three successive cells are represented by k, i, and j. When path p goes through the cell i, we represent that by $p \ni i$. $p \ni (i,j)$ means path p goes through the link (i,j).

Upper-level Model

At the upper level, as stated earlier, by reversing the reversible lane at the optimum operation time, the transportation decision-makers seek to minimize the total delay (Z). Let $x_{p,t}^i$ denote the occupancy of cell i at time t and path p and τ represent the duration of each time interval. The travel time experienced by each user at time interval t and path p is $\tau x_{p,t}^i$ because, according to the cell transmission model, users have to stay in the cell for the duration of the time interval. Therefore, the upper-level objective function can be formulated as follows in Figure 38:

$$\min Z = \sum_{t\in T}\sum_{p\in P}\sum_{i\in C} \tau x_{p,t}^{i} - t_0 \sum_{t\in T} d_t$$

Figure 38. Equation. Upper-level objective function.

where t_0 indicates the free-flow travel time.

Lower-level Model

The lower-level model is related to travelers' route choice in response to the policies and actions of the transportation agency decision-maker in the upper level. To capture the travelers' route choice behavior, this study modifies the cell transmission model proposed by Ukkusuri et al. (2012). Let $\bar{x}_t^i$ denote the aggregate occupancy of cell i at time t, and $x'^{i,j}_t$ denote the aggregate occupancy of cell i traveling to cell j at time t. Let $y_{p,t}^{i,j}$ denote the flow of link (i,j) at time t and path p, and $\bar{y}_t^{i,j}$ denote the aggregate flow of link (i,j) at time t. Let $r_{p,t}$ denote the departure rate of commuters at time interval t and path p. The lower-level model can be formulated as follows in Figures 39–51:

$$0 \le \sum_{t\in T} r_{p,t} \perp TT_p - C_t \ge 0 \qquad \forall p \in P, t \in T$$

Figure 39. Equation. Lower-level model—constraint 1.

$$0 \le C_t \perp \sum_{p\in P} r_{p,t} - d_t \ge 0 \qquad \forall t \in T$$

Figure 40. Equation. Lower-level model—constraint 2.

$$TT_p = \frac{\sum_{t\in T}\sum_{i\in C} \tau x_{p,t}^{i}}{\sum_{t\in T} r_{p,t}} \qquad \forall p \in P$$

Figure 41. Equation. Lower-level model—constraint 3.

$$x_{p,0}^{i} = 0 \qquad \forall i \in C, p \in P$$

Figure 42. Equation. Lower-level model—constraint 4.

$$y_{p,0}^{i,j} = 0 \qquad \forall (i,j) \in A, p \in P$$

Figure 43. Equation. Lower-level model—constraint 5.

$$x_{p,t}^{i} = r_{p,t-1} + x_{p,t-1}^{i} - y_{p,t-1}^{i,j} \qquad \forall i \in C_R, p \in P, t \in T$$

Figure 44. Equation. Lower-level model—constraint 6.

$$x_{p,t}^{i} = x_{p,t-1}^{i} + y_{p,t-1}^{k,i} \qquad \forall i \in C_S, p \in P, t \in T$$

Figure 45. Equation. Lower-level model—constraint 7.

$$x_{p,t}^{i} = x_{p,t-1}^{i} + y_{p,t-1}^{k,i} - y_{p,t-1}^{i,j} \qquad \forall i \in C_O, p \in P, t \in T$$

Figure 46. Equation. Lower-level model—constraint 8.

$$y_{p,t}^{i,j} = \min\left(\bar{x}_t^i, Q^i, Q^j, \delta\left(N^j - \bar{x}_t^j\right)\right) \cdot \frac{x_{p,t}^i}{\bar{x}_t^i + \mu} \qquad \forall (i,j) \in A, p \in P, t \in T$$

Figure 47. Equation. Lower-level model—constraint 9.

$$x'^{i,j}_t = \sum_{\forall (i.j) \in P} x_{p,t}^{i} \qquad \forall (i,j) \in A, t \in T$$

Figure 48. Equation. Lower-level model—constraint 10.

$$\bar{x}_t^i = \sum_{j \in \varsigma_i^+} x'^{i,j}_t \qquad \forall i \in C, t \in T$$

Figure 49. Equation. Lower-level model—constraint 11.

$$y_{p,t}^{i,j} = \min\left(x'^{i,j}_t, Q^j, \delta\left(N^j - \bar{x}_t^j\right)\right) \cdot \min\left(1, \frac{Q^i}{\sum_{j' \in \varsigma_i^+} \min\left(x'^{i,j'}_t, Q^{j'}, \delta\left(N^{j'} - \bar{x}_t^{j'}\right)\right)}\right) \cdot \frac{x_{p,t}^i}{x'^{i,j}_t + \mu} \qquad \forall (i,j) \in A, p \in P, t \in T$$

Figure 50. Equation. Lower-level model—constraint 12.

$$y_{p,t}^{k,i} = \min\left(Q^k, \bar{x}_t^k\right) \cdot \min\left(1, \frac{\min\left(Q^i, \delta\left(N^i - \bar{x}_t^i\right)\right)}{\sum_{k' \in \varsigma_i^-} \min\left(Q^{k'}, \bar{x}_t^{k'}\right)}\right) \cdot \frac{x_{p,t}^k}{\bar{x}_t^k + \mu} \qquad \forall (k,i) \in A, p \in P, t \in T$$

Figure 51. Equation. Lower-level model—constraint 13.

where μ denotes infinitesimal parameter to avoid zero denominator. Q^i and N^i denote the flow capacity and jam density of cell i, respectively. δ denotes the ratio of forward-to-backward shockwave propagation and d_t denotes the travel demand between the OD. Constraint 1 ensures that travelers' travel time at each path is equal. Constraint 2 ensures the demand conservation constraint, and constraint 3 calculates the mean travel time of path p. Constraints 4 and 5 initiate the cell transmission model. Constraints 6–8 compute cell occupancy of cell i. Constraints 10 and 11 calculate the aggregate occupancy of cell i at time t and the aggregate occupancy of cell i traveling to cell j at time t, respectively. Finally, constraints 9, 12, and 13 determine the path flows traveling from cell i to cell j at time interval t and path p.

COMPUTATIONAL EXPERIMENTS

In this section, numerical experiments are carried out to demonstrate the applicability of the proposed model. This section solves the proposed bi-level model using the Kennedy Expressway corridor translated to cells. In CTM, links are divided into cells and cell connectors. The Kennedy Expressway and reversible lanes are divided into homogeneous cells. Based on the concept of homogeneity, cells have an equal length of the distance through which users can travel at free-flow speed in a time interval. The time intervals are 1.25 minutes and the length of the cells is 1.5 miles, because the free-flow speed at Kennedy Expressway is 70 mi/hr. The Kennedy Expressway network (Figure 52) has 20 cells and 21 cell connectors, which consist of source cells (shown in yellow), sink cells (shown in red), diverging cells and links (shown in blue), merging cells and links (shown in green), and ordinary cells and links (shown in black).

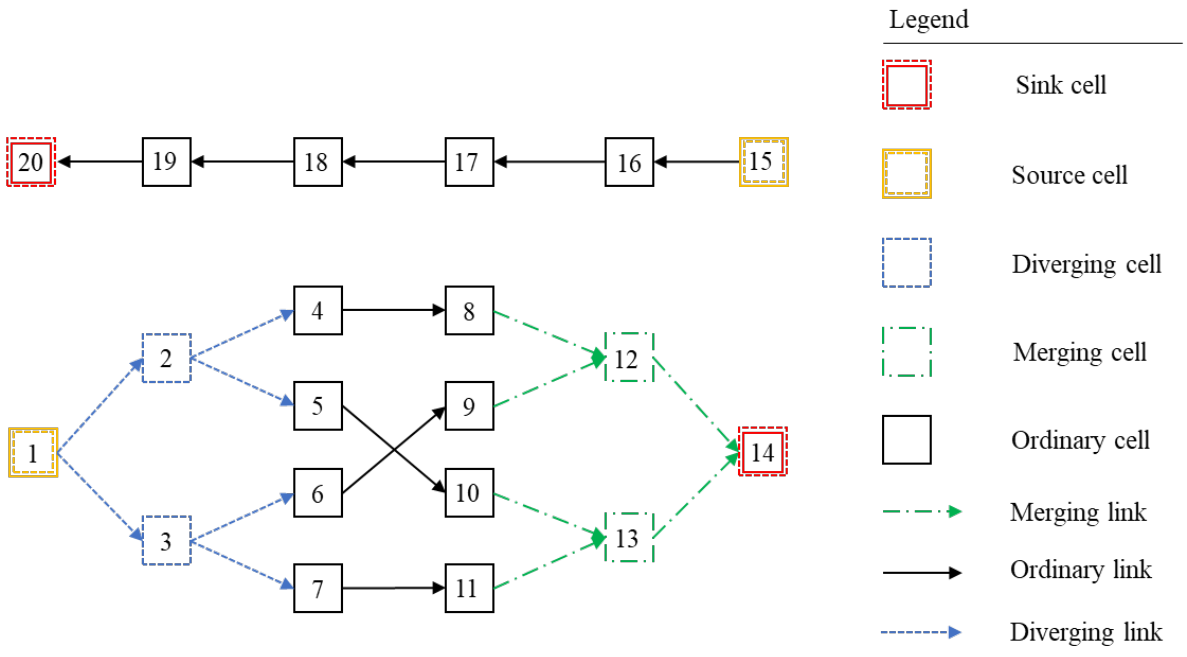

Figure 52. Flow chart. Kennedy Expressway network before reversible lane operation time.

At the operation time decided in the upper-level model, the reversible lanes toward one direction are closed until travelers evacuate the reversible lanes. Hence, the network shown in Figure 52 changes to the network shown in Figure 53.

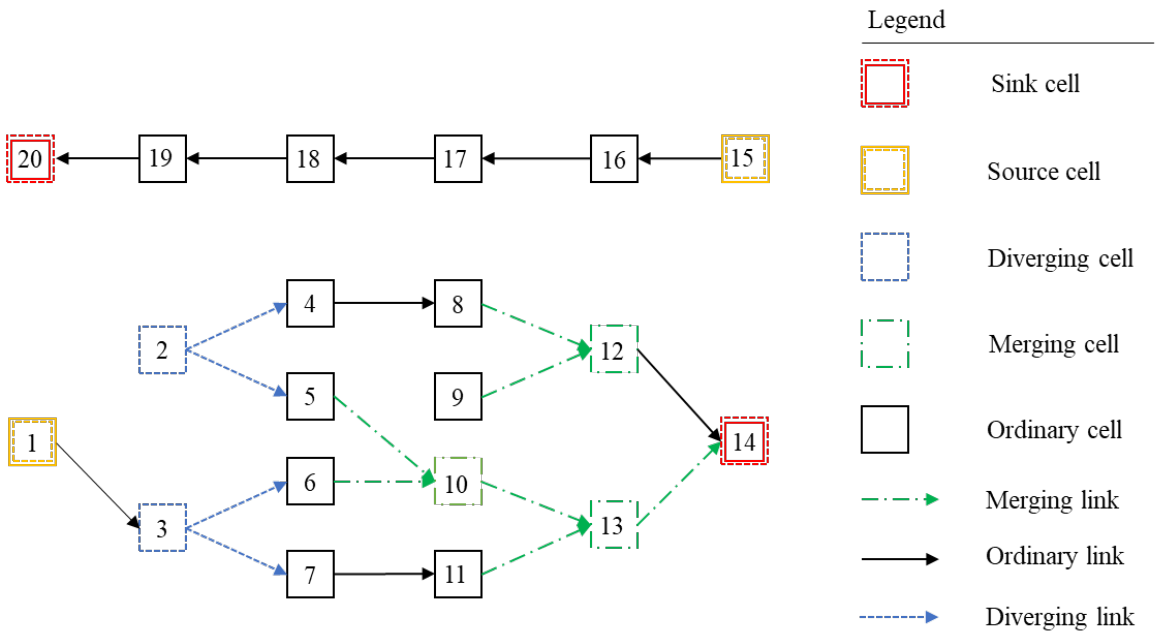

Figure 53. Flow chart. Kennedy Expressway network during reversible lane operation time.

After evacuation of the reversible lanes, the reversible lanes are opened to the other direction and the network is changed to the network shown in Figure 54.

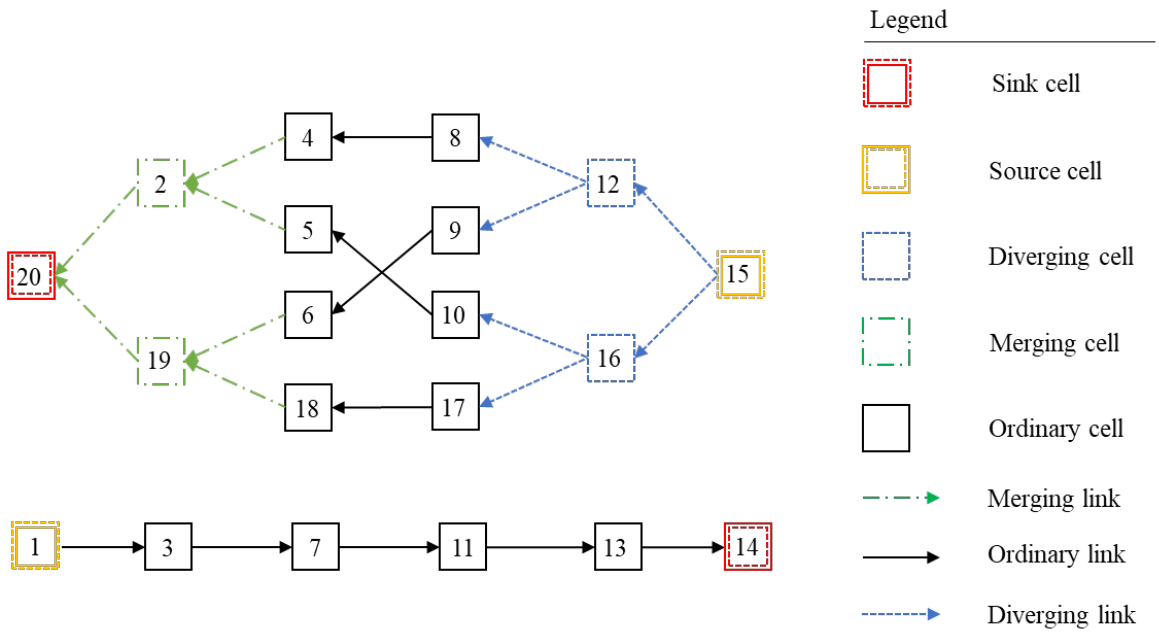

Figure 54. Flow chart. Kennedy Expressway network after reversible lane operation time.

This study proposes an optimal time interval for starting the reversing operation for each day of the week. The optimal operation time is determined by minimizing total delay using a dynamic optimization model. Then, the average of these optimal operation times with a variance is suggested as the optimal time interval. Eventually, an offline timetable is provided including the optimal operation time interval for each day of the week. Prior to obtaining different optimal operation times for each weekday, as discussed in Chapter 7, a two-way ANOVA test is done to evaluate whether the difference between operation times of different weekdays is significant. Table 11 is a provided offline timetable. The table represents the average of the suggested optimal operation start time, 15- and 30-minute suggested operation time intervals, and compares the average of actual start time of the reversing operation for each day of the week.

Table 11. Offline Operation Timetable

Day of week	Actual time	Suggested time	Suggested 15-minute interval	Suggested 30-minute interval
Monday	12:10	11:24	11:13–11:28	11:01–11:31
Tuesday	11:56	11:44	11:32–11:47	11:19–1:49
Wednesday	12:08	11:48	11:38–11:53	11:28–11:58
Thursday	12:21	11:28	11:17–11:32	11:06–11:36
Friday	13:36	11:01	10:54–11:08	10:44–11:14
Saturday	13:54	10:57	10:43–10:58	10:28–10:58
Sunday	14:02	11:11	10:57–11:12	10:43–11:13

Figure 55 presents the distribution of the actual start time of the reversing operation for each day of the week, while Figure 56 illustrates the distribution of the suggested start time. As shown in Figure 55, the actual time that the operation began on weekdays from Monday to Thursday is around noon. On Friday and the weekends, however, the operation was performed later in the afternoon. The distribution of the suggested start times in Figure 56 illustrates the reversing operation on Friday and the weekends should be carried out even earlier compared to the weekdays. In addition, when Figure 55 and Figure 56 are compared, the distribution of the suggested optimal operation time on weekdays is below the distribution of the actual operation time, implying that the operation on weekdays should have started earlier.

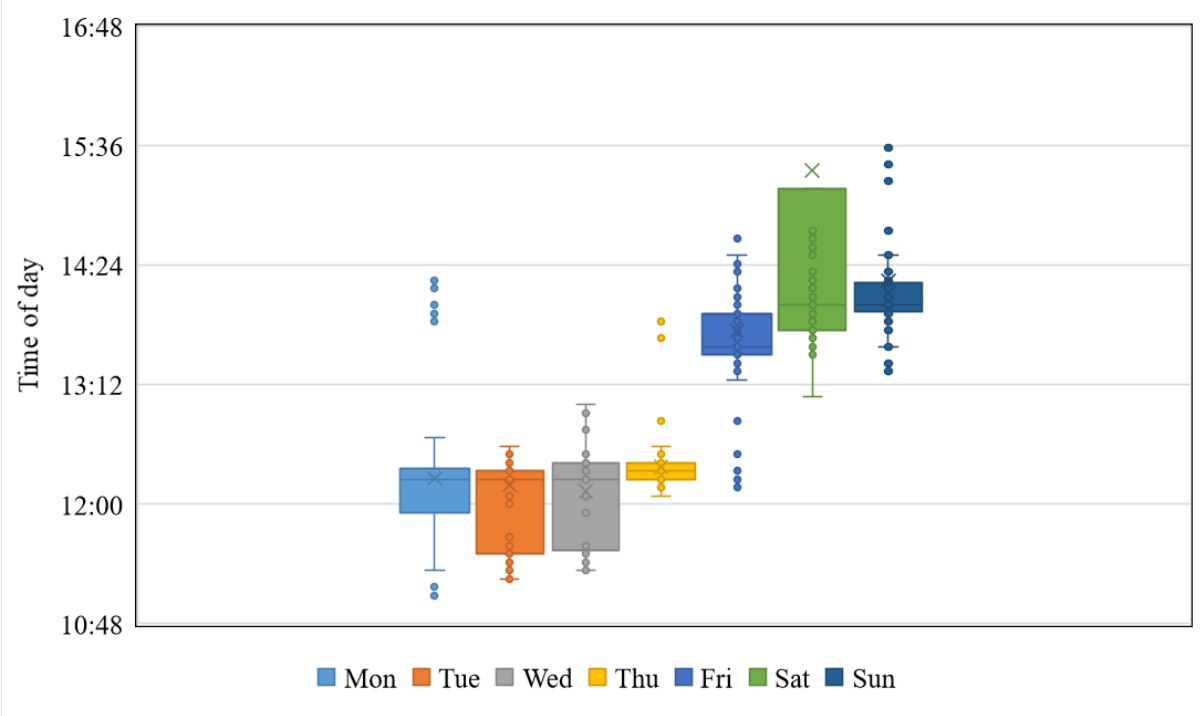

Figure 55. Graph. Diagram of time to start the operation—actual time.

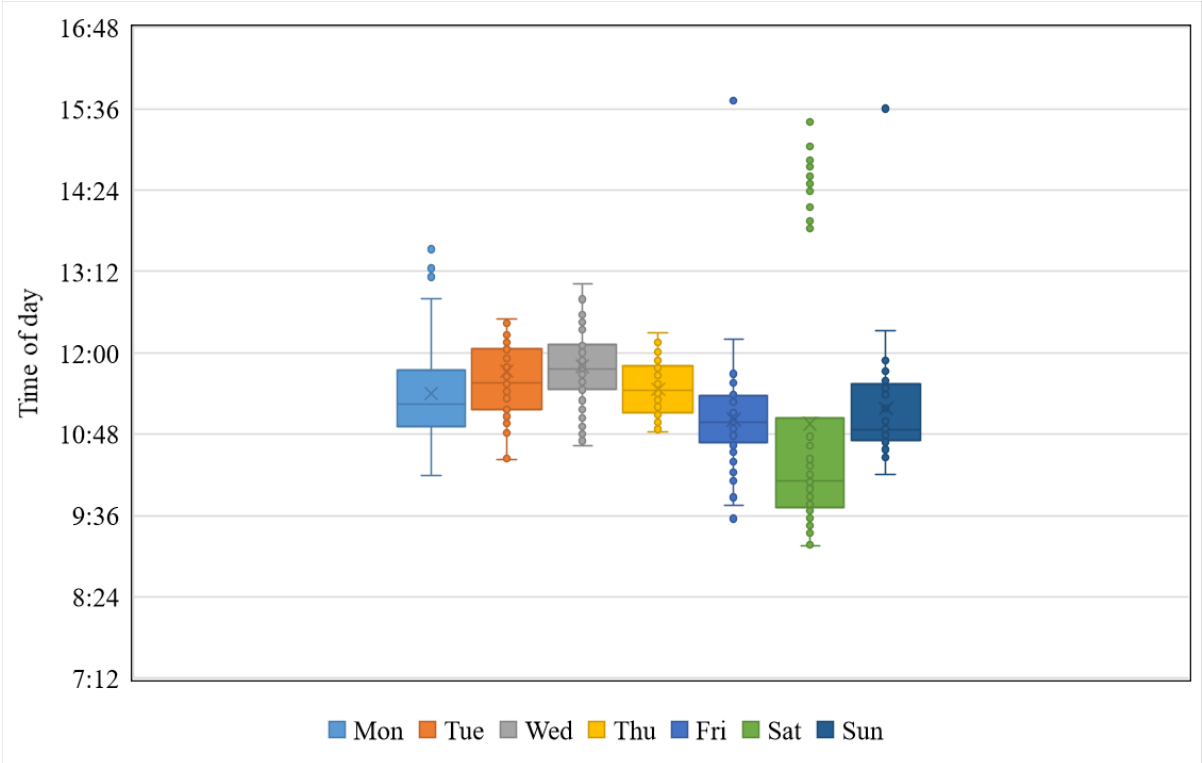

Figure 56. Graph. Diagram of time to start the operation—suggested time.

CHAPTER 9: SUMMARY AND CONCLUSION

In this research we evaluated and improved the operation of the reversible lanes in the Kennedy Expressway. The main purpose of these reversible lanes is to help the congested direction of the expressway pass the traffic flow. Therefore, after a comprehensive review of related studies, the available sources of data were cleaned and preprocessed. Then, the current reversing operation was evaluated. Afterwards, a data-driven approach was proposed in which a real-time technique and an offline timetable were introduced for operation of reversible lanes. Finally, an optimization technique was employed and another offline timetable was proposed to improve the operation of the Kennedy Expressway reversible lanes to improve the performance of these lanes in passing traffic.

In the data-driven approach, three machine learning models—random forest, decision tree, and K-nearest neighbors—were trained using several explanatory variables and four delay indices as target variables. The random forest model was selected as the best model due to its prediction accuracy. In addition, the best model's performance was achieved when delay ratio was used as the target variable. Therefore, the random forest model, which had an accuracy of 93.7%, and delay ratio as the target delay index were used for post-analysis. Using the inference of the random forest model, the delay index would be available for a wide range of times, all days of the week. Therefore, to determine the best time of operation (i.e., minimum delay in the corridor), the predicted delay index was used to find the best time of operation, and the offline timetable was suggested by taking the average of best operation times each day of the week. To test if the difference of operation start time on different days of the week is significant, a two-way ANOVA was also employed. In addition, to find the best time of operation in real time, an LSTM binary classifier model is trained that can take the past 10 consecutive delay index values as the input and predict whether it is a good time to start the operation.

In the optimization approach, a bi-level framework is proposed. At the upper level, transportation decision-makers seek to minimize the total delay at both directions of the expressway. The control decision variable at the upper level is the operation time of the reversible lanes. At the lower level, travelers seek to address their travel needs while minimizing their travel time. The control decision for travelers is to select the optimal route. The operation time chosen in the upper level affects travelers' route choice, and the travelers' route choice affects the operation time decided at the upper level. The objective in this approach is to find an optimal time interval for starting the reversing operation for each day of the week. The optimal operation time was determined by minimizing the total delay using a dynamic optimization model. Then, the average of these optimal operation times with a variance is suggested as the optimal time interval. Eventually, an offline timetable is provided including the optimal operation time interval for each day of the week similar to what we have provided in the offline section of the data-driven approach.

Finally, in order to achieve the highest accuracy, we can suggest the integration of two offline timetables calculated in the data-driven and optimization approaches, as shown in Table 12. Table 12 represents the integration of 15- and 30-minute suggested operation time intervals of the two offline approaches for each day of the week. Accordingly, a combination of offline and real-time techniques

results in ignoring false alarms of the real-time technique and improves the accuracy. This means the operator can consider only model alarms, which are happening in the intervals presented in Table 12.

Table 12. Integration of Offline Operation Timetables

Day of week	Suggested short intervals (Integration of 15-minute intervals)	Suggested long intervals (Integration of 30-minute intervals)
Monday	10:55–11:28	10:47–11:31
Tuesday	11:22–11:47	11:14–11:49
Wednesday	11:34–11:53	11:26–11:58
Thursday	11:17–11:44	11:06–11:51
Friday	10:50–11:08	10:42–11:14
Saturday	10:25–10:58	10:18–10:58
Sunday	10:28–11:12	10:20–11:13

In order to evaluate the possibility of switching the direction of the reversible lanes more than twice on a weekday (i.e., four times), the traffic pattern of random weekdays was observed and analyzed. Figure 57 presents the traffic pattern of both directions of a random weekday in which two switching operations were operated. The red horizontal line is a threshold to better compare the congested condition in both directions. To add two more operations to this condition, the only possible time interval is within the time of switching toward the outbound direction around noon and toward inbound around midnight. However, based on Figure 57, in this time interval the traffic situation is similar in both directions. Therefore, blocking vehicles from using two reversible lanes for about 1 hour (i.e., each operation takes half an hour on average) would not be beneficial for the whole corridor.

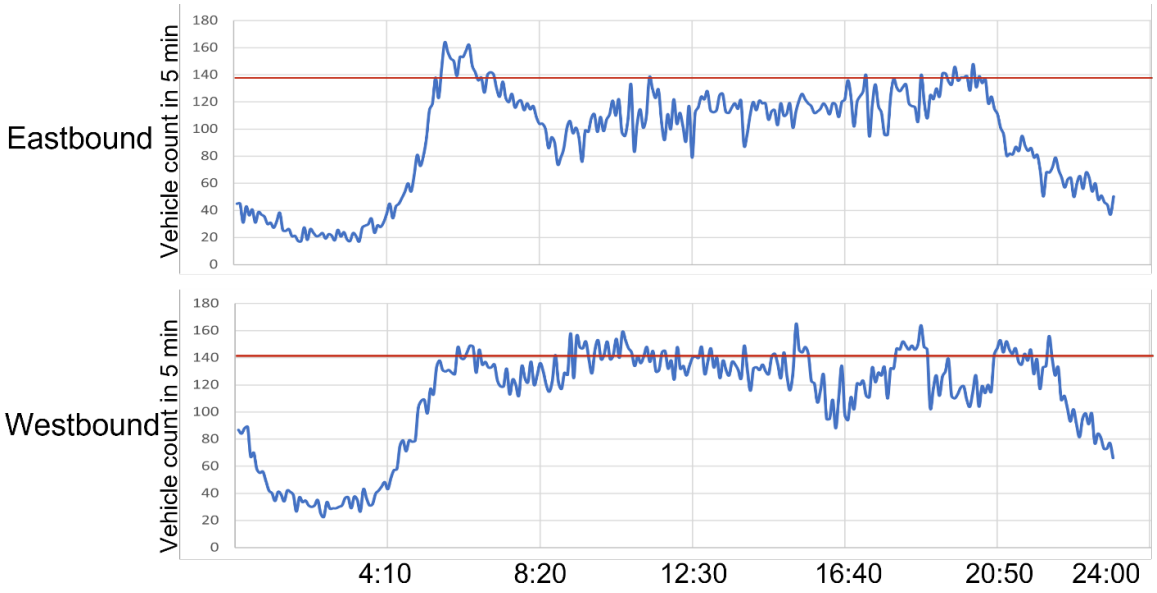

Figure 57. Graph. Example of traffic pattern on a weekday.

It is also worth noting that the focus of this study was an 8-mile segment of the Kennedy Expressway on which the reversible lanes are located. However, for future studies, it is suggested that the impact of reversible lanes on the whole network be considered through other advanced approaches.

REFERENCES

Abdelghany, A. F., K. F. Abdelghany, H. S. Mahmassani, and P. M. Murray. 2000. "Dynamic Traffic Assignment in Design and Evaluation of High-Occupancy Toll Lanes." *Transportation Research Record*, 1733 (1): 39–48. https://doi.org/10.3141/1733-06.

Al-Deek, Haitham M., Asad J. Khattak, and Paramsothy Thananjeyan. 1998. "A Combined Traveler Behavior and System Performance Model with Advanced Traveler Information Systems." *Transportation Research Part A: Policy and Practice* 32 (7): 479–493. https://doi.org/10.1016/S0965-8564(98)00010-X.

Balakrishna, Ramachandran, Moshe Ben-Akiva, and Haris N Koutsopoulos. 2007. "Offline Calibration of Dynamic Traffic Assignment: Simultaneous Demand-and-Supply Estimation." *Transportation Research Record*, 2003 (January): 50–58. https://doi.org/10.3141/2003-07.

Bede, Zsuzsanna, Géza Szabó, and Tamás Péter. 2010. "Optimalization of Road Traffic with the Applied of Reversible Direction Lanes." *Periodica Polytechnica Transportation Engineering* 38 (1): 3–8. https://doi.org/10.3311/pp.tr.2010-1.01.

Bianchi, F. M., E. Maiorino, M. C. Kampffmeyer, A. Rizzi, and R Jenssen. 2017. "Recurrent Neural Networks for Short-Term Load Forecasting: An Overview and Comparative Analysis."

Carey, Malachy. 1987. "Optimal Time-Varying Flows on Congested Networks." *Operations Research* 35 (1): 58–69. https://doi.org/10.1287/opre.35.1.58.

Carey, Malachy, and Eswaran Subrahmanian. 2000. "An Approach to Modelling Time-Varying Flows on Congested Networks." *Transportation Research Part B: Methodological* 34 (3): 157–83. https://doi.org/10.1016/S0191-2615(99)00019-3.

Chiu, Y-C, J. Bottom, M. Mahut, and A. Paz. 2010. "A Primer for Dynamic Traffic Assignment Workshop." Presented at the 89th Annual Meeting of Transportation Research Board, Janaury 10–14, 2010.

Conceição, Lígia, Gonçalo Homem de Almeida Correia, and José Pedro Tavares. 2020. "The Reversible Lane Network Design Problem (RL-NDP) for Smart Cities with Automated Traffic." *Sustainability* 12 (3): 1226.

Dafermos, Stella. 1980. "Traffic Equilibrium and Variational Inequalities." *Transportation Science* 14 (1): 42–54. https://doi.org/10.1287/trsc.14.1.42.

Daganzo, Carlos F. 1994. "The Cell Transmission Model: A Dynamic Representation of Highway Traffic Consistent with the Hydrodynamic Theory." *Transportation Research Part B* 28 (4): 269–87. https://doi.org/10.1016/0191-2615(94)90002-7.

Daganzo, Carlos F. 1995. "The Cell Transmission Model, Part II: Network Traffic." *Transportation Research Part B* 29 (2): 79–93. https://doi.org/10.1016/0191-2615(94)00022-R.

Downs, Anthony. 2004. *Still Stuck in Traffic*. Washington, DC: Brookings Institution Press.

Facchinei, Francisco, and Jong-Shi Pang. 2004. *Finite-Dimensional Variational Inequalities and Complementarity Problems*. New York: Springer. https://doi.org/10.1007/b97544.

Federal Highway Administration (FHWA). 2017. *Reducing Non-Recurring Congestion*. Washington, DC: US Department of Transportation.

Frejo, José Ramón D., Ioannis Papamichail, Markos Papageorgiou, and Eduardo F. Camacho. 2015. "Macroscopic Modeling and Control of Reversible Lanes on Freeways." *IEEE Transactions on Intelligent Transportation Systems* 17 (4): 948–59.

Friesz, Terry L., David Bernstein, Tony E. Smith, Roger L. Tobin, and B. W. Wie. 1993. "Variational Inequality Formulation of the Dynamic Network User Equilibrium Problem." *Operations Research* 41 (1): 179–91. https://doi.org/10.1287/opre.41.1.179.

Friesz, Terry L., David Bernstein, and Roger Stough. 1996. "Dynamic Systems, Variational Inequalities and Control Theoretic Models for Predicting Time-Varying Urban Network Flows." *Transportation Science* 30 (1): 14–31. https://doi.org/10.1287/trsc.30.1.14.

Friesz, Terry L., Javier Luque, Roger L. Tobin, and Byung Wook Wie. 1989. "Dynamic Network Traffic Assignment Considered as a Continuous Time Optimal Control Problem." *Operations Research* 37 (6): 893–901. https://doi.org/10.1287/opre.37.6.893.

Gao, Song. 2012. "Modeling Strategic Route Choice and Real-Time Information Impacts in Stochastic and Time-Dependent Networks." *IEEE Transactions on Intelligent Transportation Systems* 13 (3). https://doi.org/10.1109/TITS.2012.2187197.

Gomes, Gabriel, and Roberto Horowitz. 2006. "Optimal Freeway Ramp Metering Using the Asymmetric Cell Transmission Model." *Transportation Research Part C: Emerging Technologies* 14 (4). https://doi.org/10.1016/j.trc.2006.08.001.

Han, J., J. Pei, and M. Kamber. 2011. *Data Mining: Concepts and Techniques*. Waltham, MA: Morgan Kaufmann Publishers. https://doi.org/10.1016/C2009-0-61819-5.

Han, Lanshan, Satish Ukkusuri, and Kien Doan. 2011. "Complementarity Formulations for the Cell Transmission Model Based Dynamic User Equilibrium with Departure Time Choice, Elastic Demand and User Heterogeneity." *Transportation Research Part B: Methodological* 45 (10): 1749–67. https://doi.org/10.1016/j.trb.2011.07.007.

Janson, Bruce N., L. Scott Buckels, and Bruce E. Peterson. 1991. "Network Design Programming of U.S. Highway Improvements." *Journal of Transportation Engineering* 117 (4): 457–78. https://doi.org/10.1061/(ASCE)0733-947X(1991)117:4(457).

Kotagi, Punith B., and Gowri Asaithambi. 2019. "Microsimulation Approach for Evaluation of Reversible Lane Operation on Urban Undivided Roads in Mixed Traffic." *Transportmetrica A: Transport Science* 15 (2): 1613–36.

Lambert, Laurence, and Brian Wolshon. 2010. "Characterization and Comparison of Traffic Flow on Reversible Roadways." *Journal of Advanced Transportation* 44 (2): 113–22.

Liu, Chenxi. 2020. "Bi-Level Optimization Algorithm for Dynamic Reversible Lane Control Based on Short-Term Traffic Flow Prediction." Master's thesis, University of Washington.

Lo, Hong K., and W. Y. Szeto. 2004. "Modeling Advanced Traveler Information Services: Static versus Dynamic Paradigms." *Transportation Research Part B: Methodological* 38 (6).

https://doi.org/10.1016/j.trb.2003.06.001.

Lo, Hong K., and W. Y. Szeto. 2005. “Road Pricing Modeling for Hyper-Congestion.” *Transportation Research Part A: Policy and Practice* 39 (7–9). https://doi.org/10.1016/j.tra.2005.02.019.

Lomax, T., S. Turner, G. Shunk, H. S. Levinson, R. H. Pratt, P. N. Bay, and G. B. Douglas. 1997. *NCHRP Report 398: Quantifying Congestion*. Washington, DC: National Research Council.

Meng, Qiang, and Hooi Ling Khoo. 2010. “A Pareto-Optimization Approach for a Fair Ramp Metering.” *Transportation Research Part C: Emerging Technologies* 18 (4). https://doi.org/10.1016/j.trc.2009.10.001.

Meng, Qiang, and Hoo Ling Khoo. 2012. “A Computational Model for the Probit-Based Dynamic Stochastic User Optimal Traffic Assignment Problem.” *Journal of Advanced Transportation* 46 (1). https://doi.org/10.1002/atr.149.

Merchant, Deepak K., and George L. Nemhauser. 1978. “Model and an Algorithm for the Dynamic Traffic Assignment Problems.” *Transp Sci* 12 (3). https://doi.org/10.1287/trsc.12.3.183.

Nagurney, Anna. 1999. “Variational Inequality Theory.” In *Network Economics*, 3–48. Springer Nature. https://doi.org/10.1007/978-1-4757-3005-0_1.

Peeta, Srinivas, and Athanasios Ziliaskopoulos. 2001. “Foundations of Dynamic Traffic Assignment: The Past, the Present and the Future.” *Networks and Spatial Economics* 1 (3). https://doi.org/10.1023/A:1012827724856.

Ramadurai, Gitakrishnan, Elliot Anshelevich, Victor Chan, Jose Holguin-Veras, and Jong-Shi Pang. 2009. “Novel Dynamic User Equilibrium Models: Analytical Formulations, Multi-Dimensional Choice, and an Efficient Algorithm.” PhD thesis, Rensselaer Polytechnic Institute.

Ramadurai, Gitakrishnan, and Satish V. Ukkusuri. 2009. “Complementarity Formulations for User Equilibrium and Ideal System State in Dynamic Transportation Networks.” In *Transportation Research Board 88th Annual Meeting*.

Ran, B., and T. Shimazaki. 1989. “A General Model and Algorithm for the Dynamic Traffic Assignment Problems.” In *Transport Policy, Management & Technology Towards 2001: Selected Proceedings of the Fifth World Conference on Transport Research*, 463–477.

Ran, Bin, David E. Boyce, and Larry J. LeBlanc. 1993. “New Class of Instantaneous Dynamic User-Optimal Traffic Assignment Models.” *Operations Research* 41 (1): 192–202. https://doi.org/10.1287/opre.41.1.192.

Seilabi, Sania E., Mahmood T. Tabesh, Amir Davatgari, Mohammad Miralinaghi, and Samuel Labi. 2020. “Promoting Autonomous Vehicles Using Travel Demand and Lane Management Strategies.” *Frontiers in Built Environment* 6 (October): 560116. https://doi.org/10.3389/fbuil.2020.560116.

Stenneth, Leon Oliver. 2016. “Method and Apparatus for Determining Road Network Lane Directional Changes.” Google Patents.

Tabesh, Mahmood Tarighati. 2020. “Parking Facility Location and User Pricing in the Era of Autonomous Vehicle Operations.” Master’s thesis, Purdue University. https://doi.org/https://doi.org/10.25394/PGS.13363046.v1.

Ukkusuri, Satish V., and S. Travis Waller. 2008. “Linear Programming Models for the User and System Optimal Dynamic Network Design Problem: Formulations, Comparisons and Extensions.” *Networks and Spatial Economics* 8 (4). https://doi.org/10.1007/s11067-007-9019-6.

Ukkusuri, Satish V., Lanshan Han, and Kien Doan. 2012. “Dynamic User Equilibrium with a Path Based Cell Transmission Model for General Traffic Networks.” *Transportation Research Part B: Methodological* 46 (10): 1657–84. https://doi.org/10.1016/j.trb.2012.07.010.

Waleczek, Helen, Justin Geistefeldt, Dijana Cindric-Middendorf, and Gerd Riegelhuth. 2016. “Traffic Flow at a Freeway Work Zone with Reversible Median Lane.” *Transportation Research Procedia* 15: 257–66.

Wolshon, Brian, and Laurence Lambert. 2006. “Reversible Lane Systems: Synthesis of Practice.” *Journal of Transportation Engineering* 132 (12): 933–44.

Wu, J. J., H. J. Sun, Z. Y. Gao, and H. Z. Zhang. 2009. “Reversible Lane-Based Traffic Network Optimization with an Advanced Traveller Information System.” *Engineering Optimization* 41 (1): 87–97. https://doi.org/10.1080/03052150802368799.

Zhao, Jing, Wanjing Ma, Yue Liu, and Xiaoguang Yang. 2014. “Integrated Design and Operation of Urban Arterials with Reversible Lanes.” *Transportmetrica B: Transport Dynamics* 2 (2): 130–50.

Zheng, Hong, Xiaozheng He, Yongfu Li, and Srinivas Peeta. 2017. “Traffic Equilibrium and Charging Facility Locations for Electric Vehicles.” *Networks and Spatial Economics* 17 (2): 435–57. https://doi.org/10.1007/s11067-016-9332-z.

Ziliaskopoulos, Athanasios K. 2000. “Linear Programming Model for the Single Destination System Optimum Dynamic Traffic Assignment Problem.” *Transportation Science* 34 (1): 37–49. https://doi.org/10.1287/trsc.34.1.37.12281.

APPENDIX A: IMPACT OF REVERSING OPERATION ON SPEED AND TRAFFIC COUNT OF LOOP DETECTORS

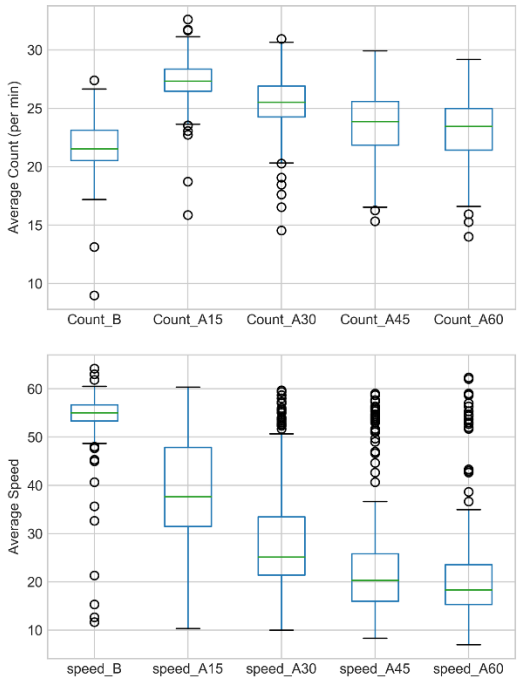

Figure 58. Graph. East 1.

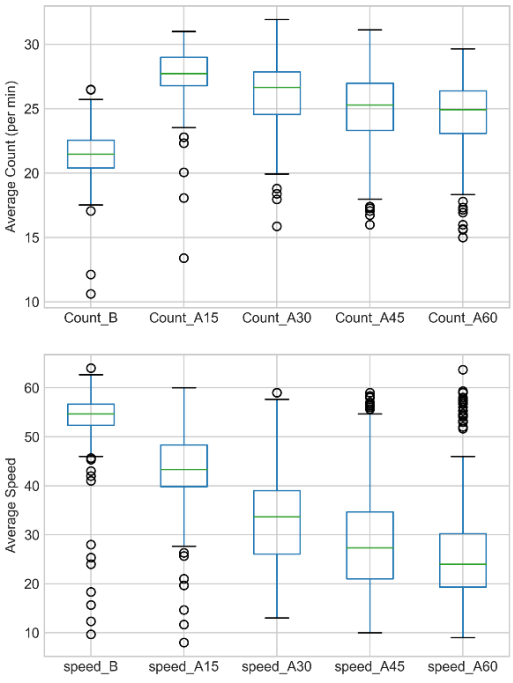

Figure 59. Graph. East 2.

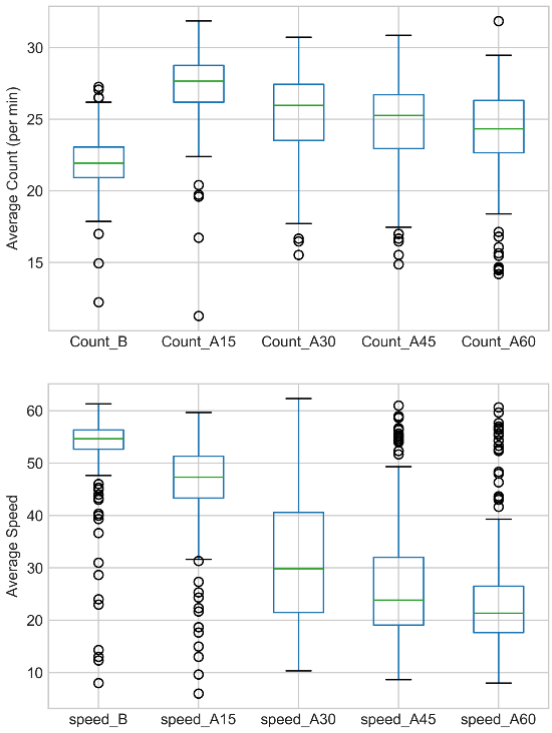

Figure 60. Graph. East 3.

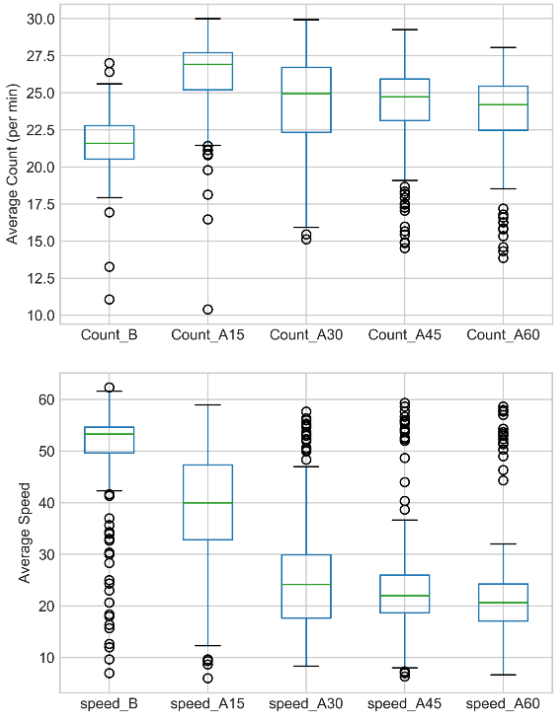

Figure 61. Graph. East 4.

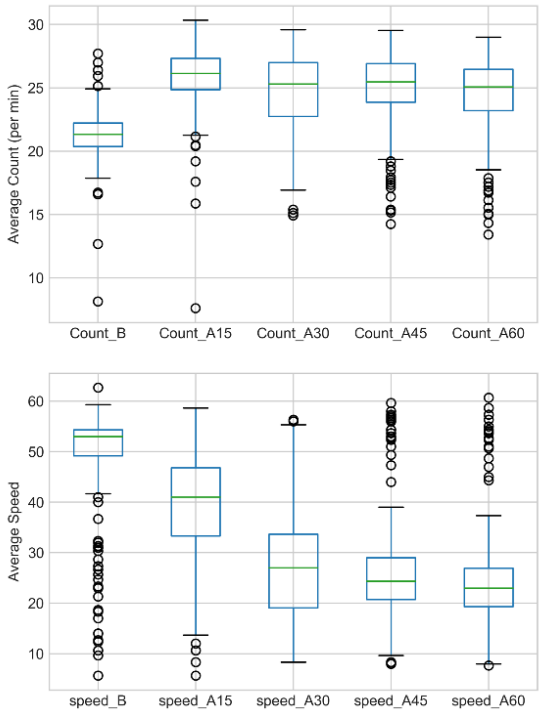

Figure 62. Graph. East 5.

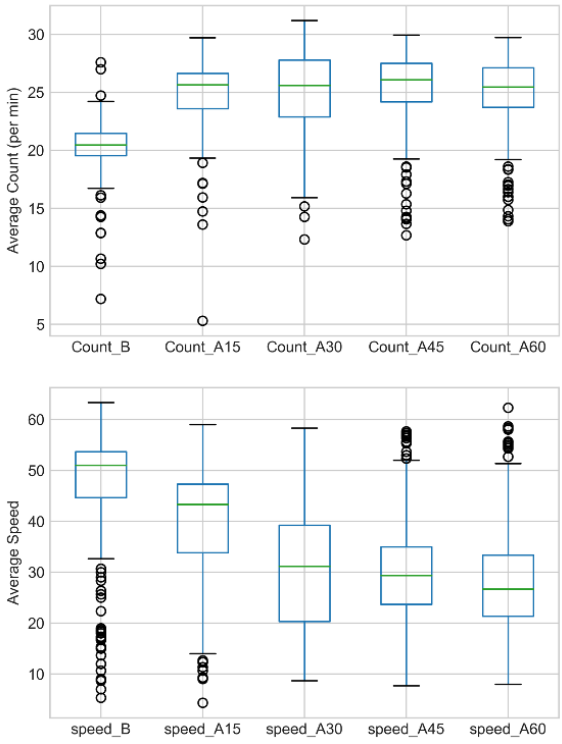

Figure 63. Graph. East 6.

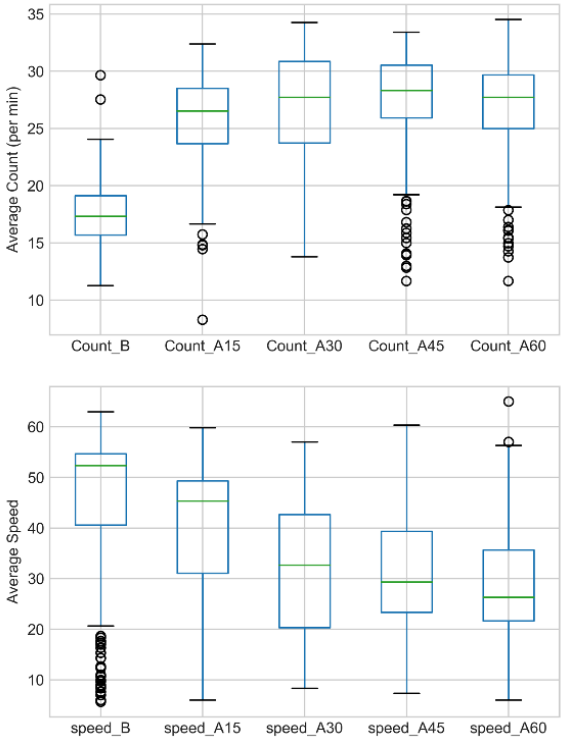

Figure 64. Graph. East 7.

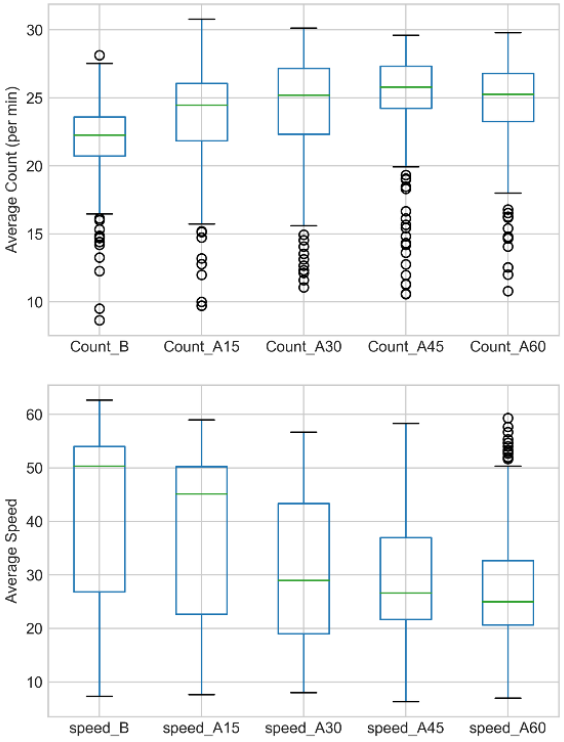

Figure 65. Graph. East 8.

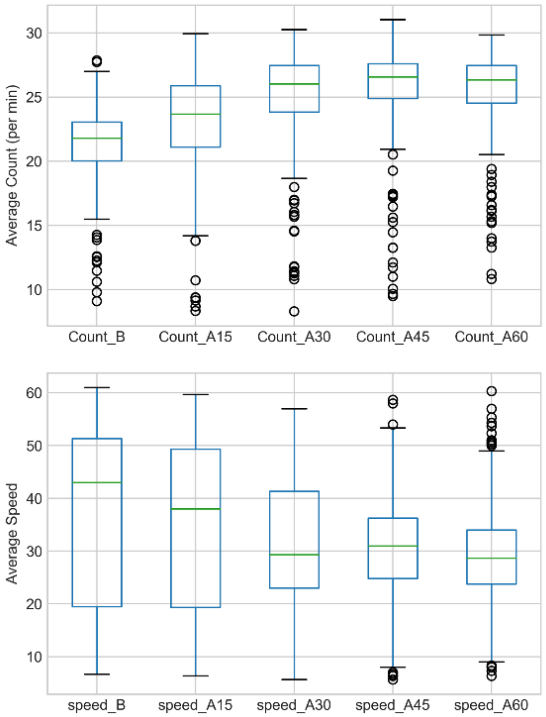

Figure 66. Graph. East 9.

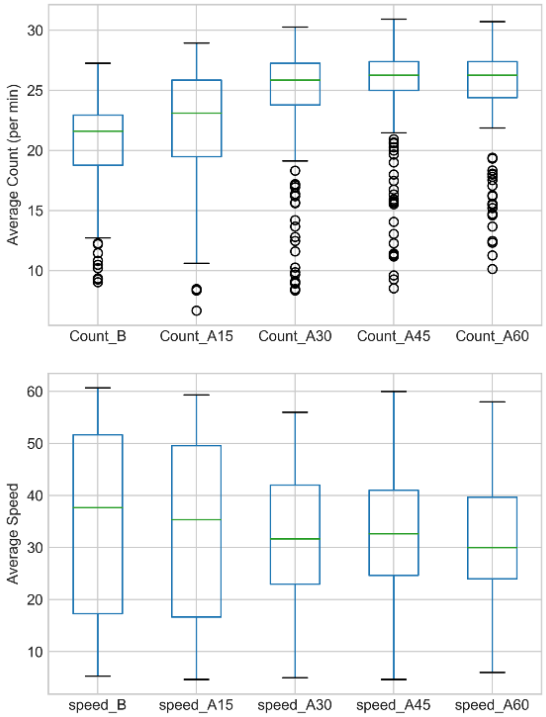

Figure 67. Graph. East 10.

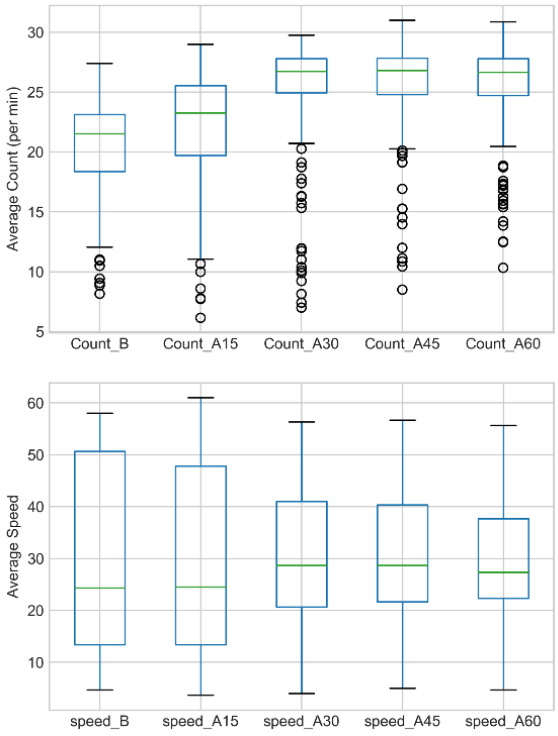

Figure 68. Graph. East 11.

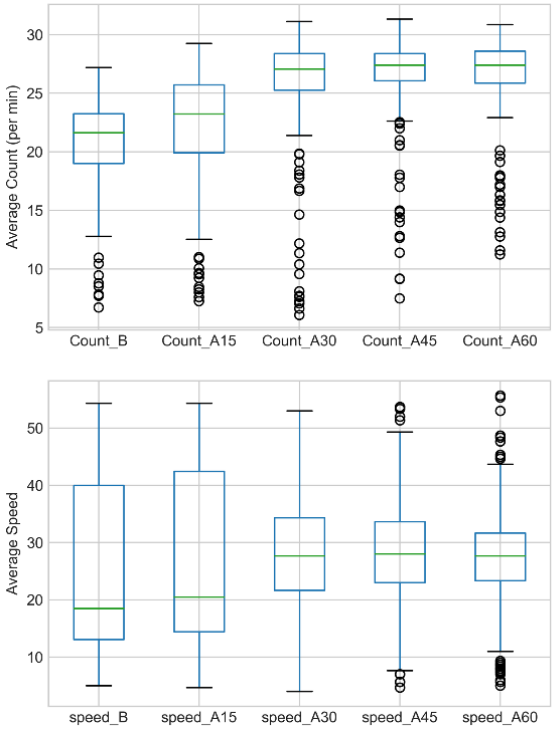

Figure 69. Graph. East 12.

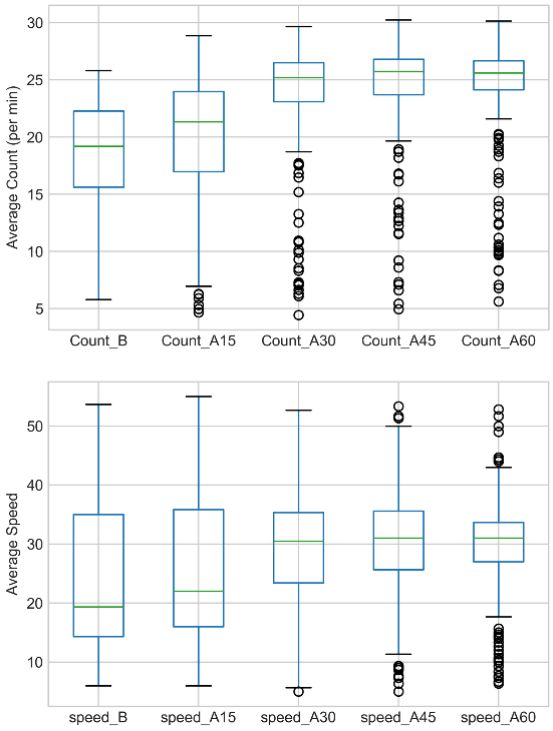

Figure 70. Graph. East 13.

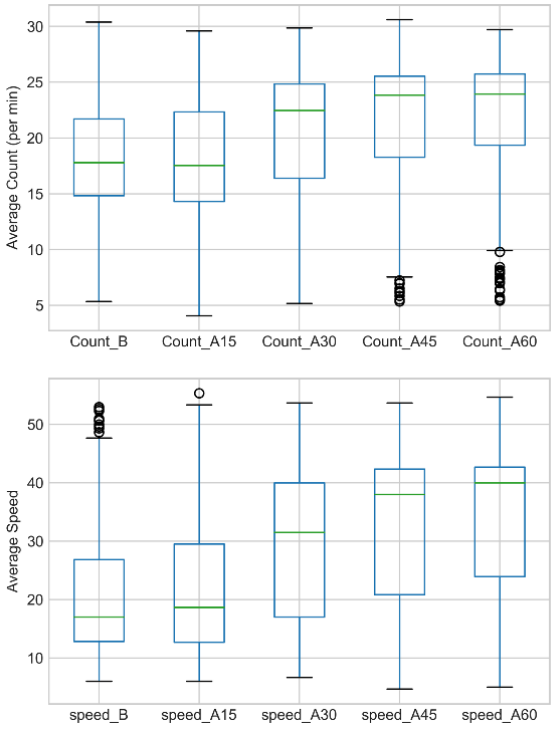

Figure 71. Graph. East 14.

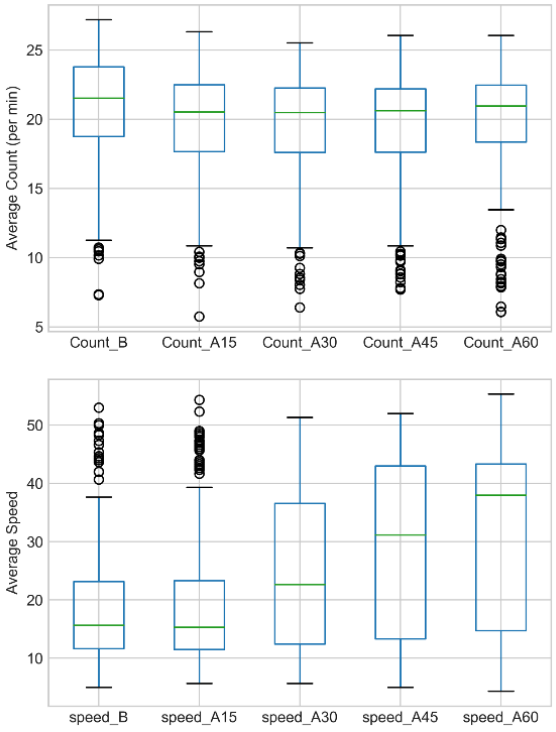

Figure 72. Graph. East 15.

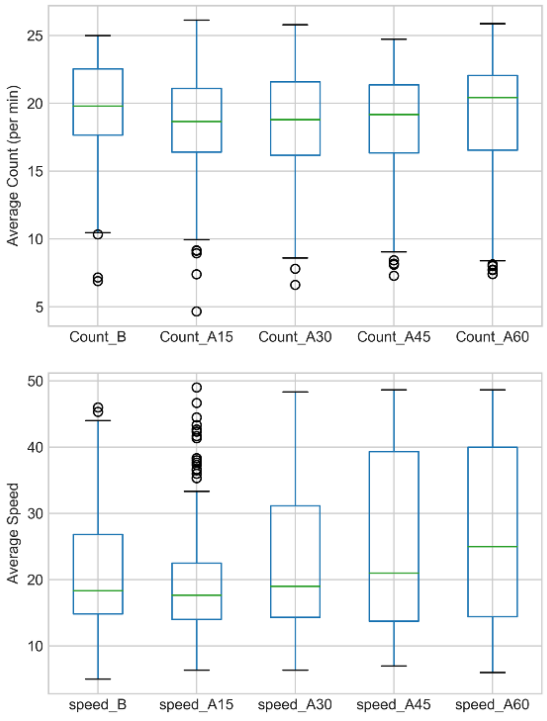

Figure 73. Graph. East 16.

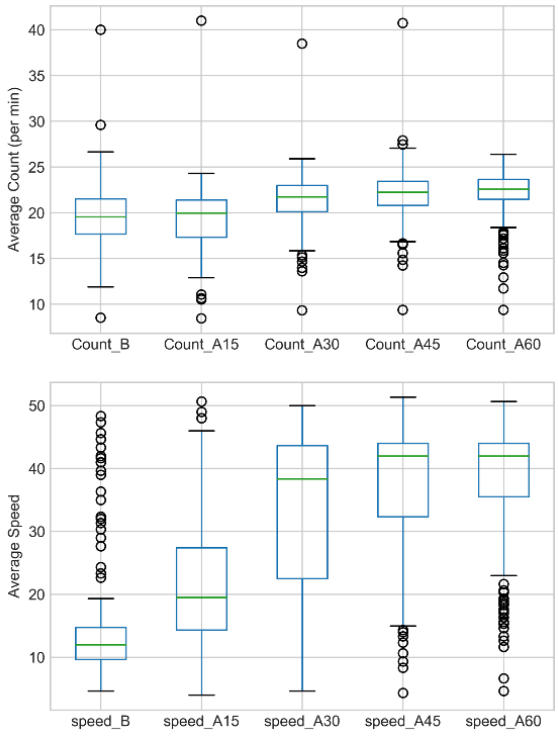

Figure 74. Graph. West 1.

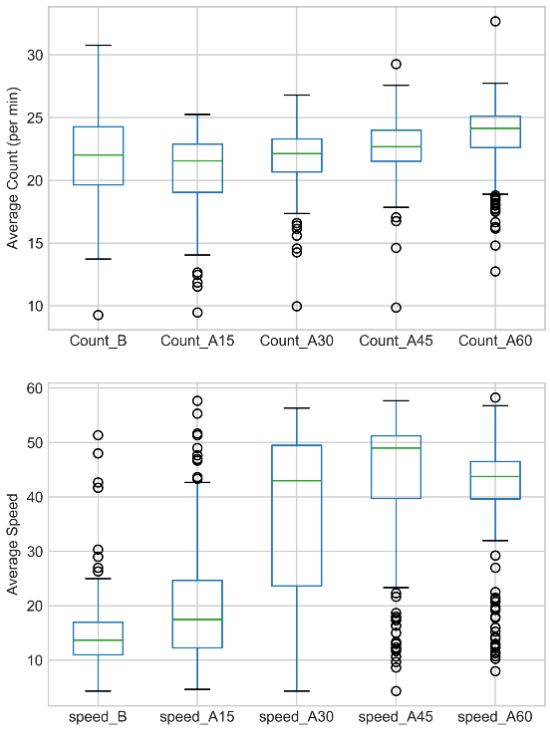

Figure 75. Graph. West 2.

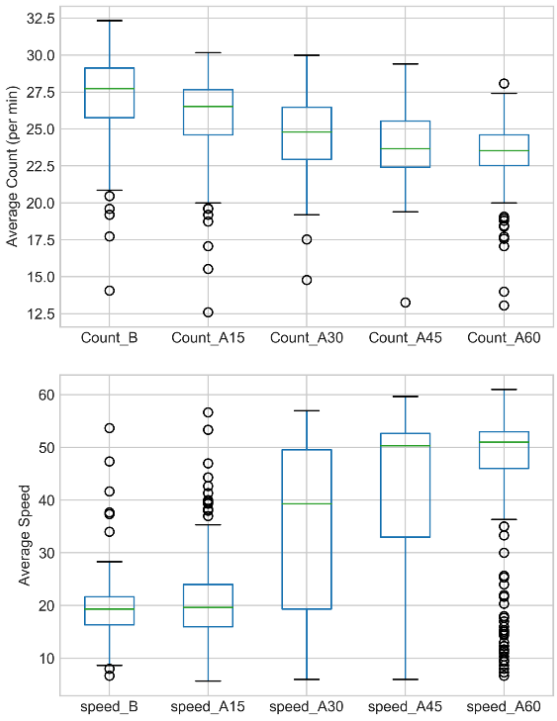

Figure 76. Graph. West 3.

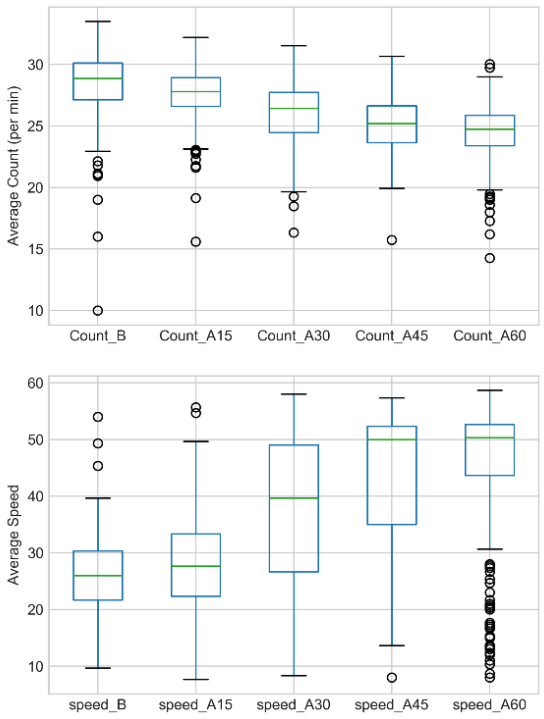

Figure 77. Graph. West 4.

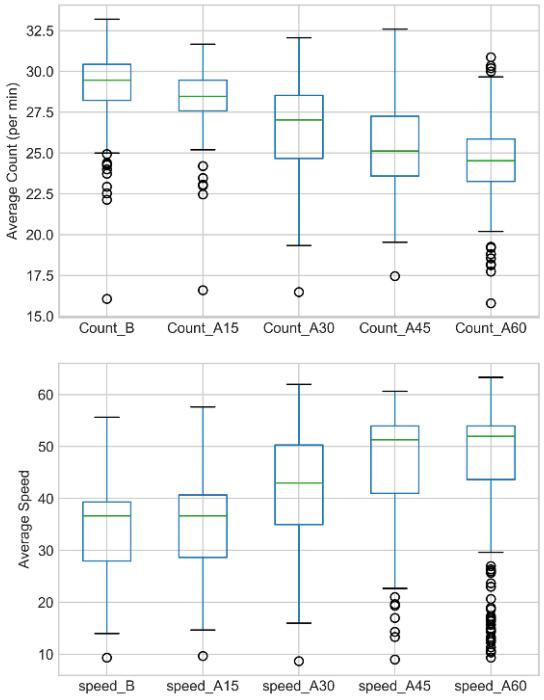

Figure 78. Graph. West 5.

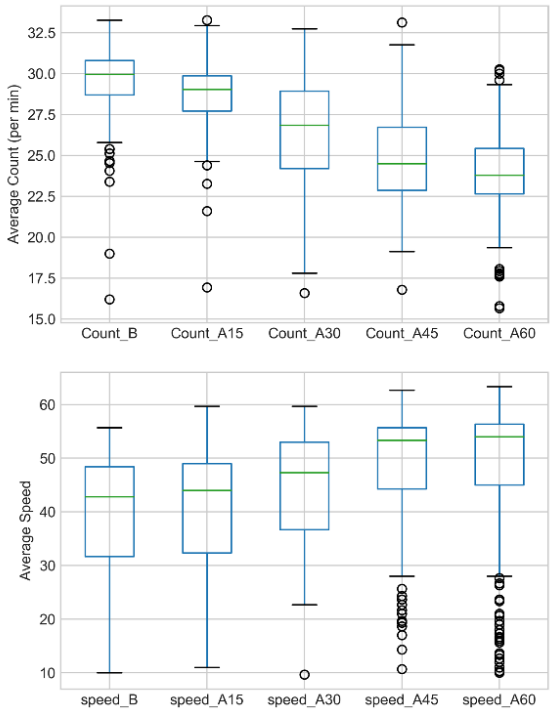

Figure 79. Graph. West 6.

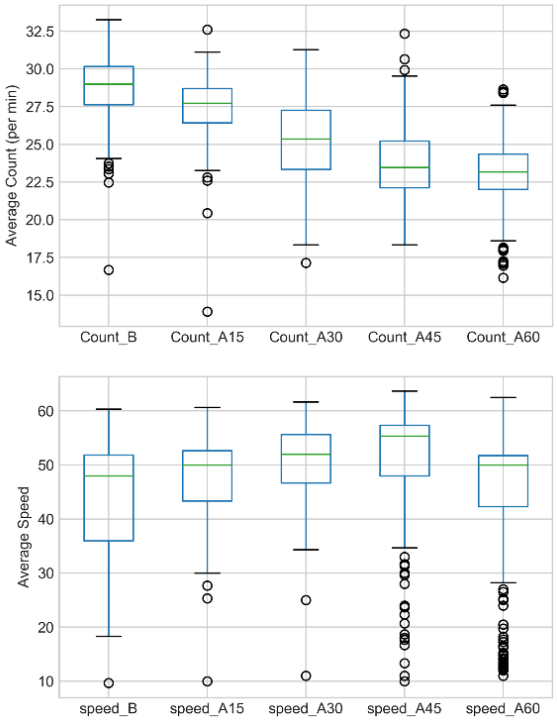

Figure 80. Graph. West 7.

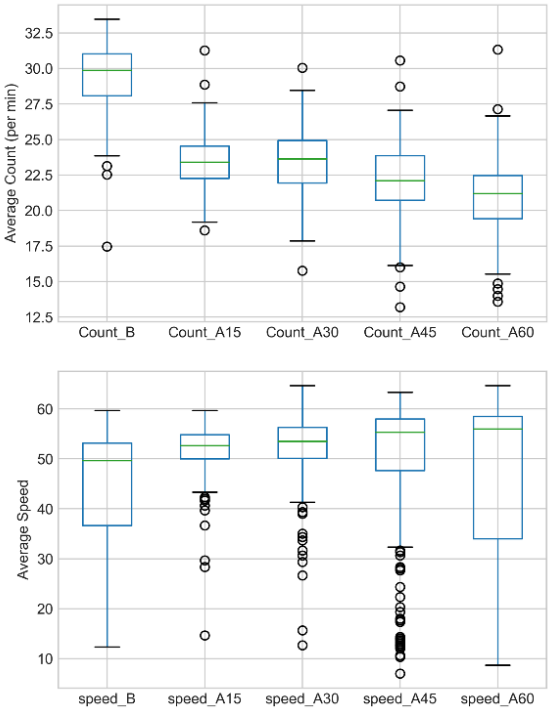

Figure 81. Graph. West 8.

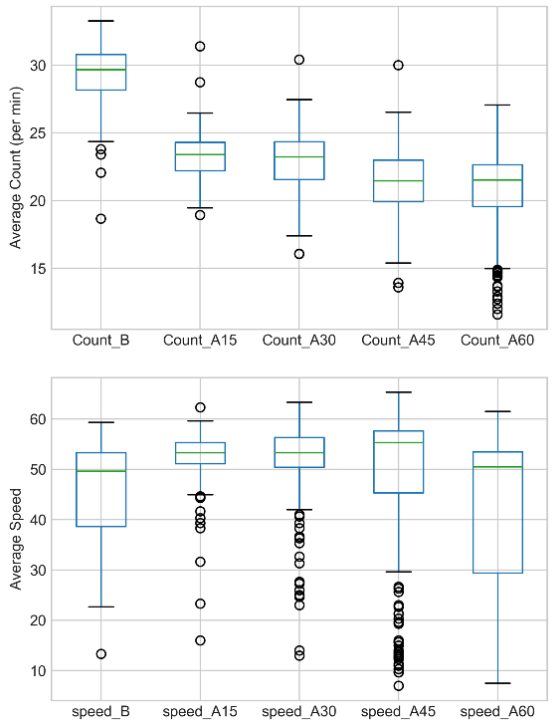

Figure 82. Graph. West 9.

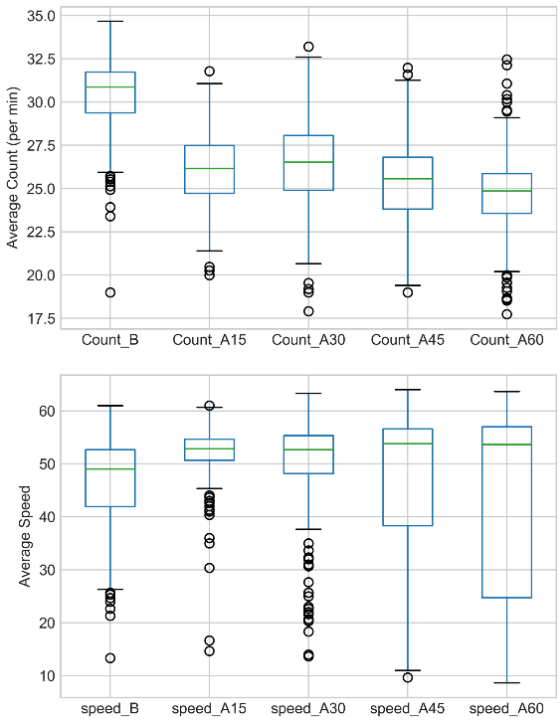

Figure 83. Graph. West 10.

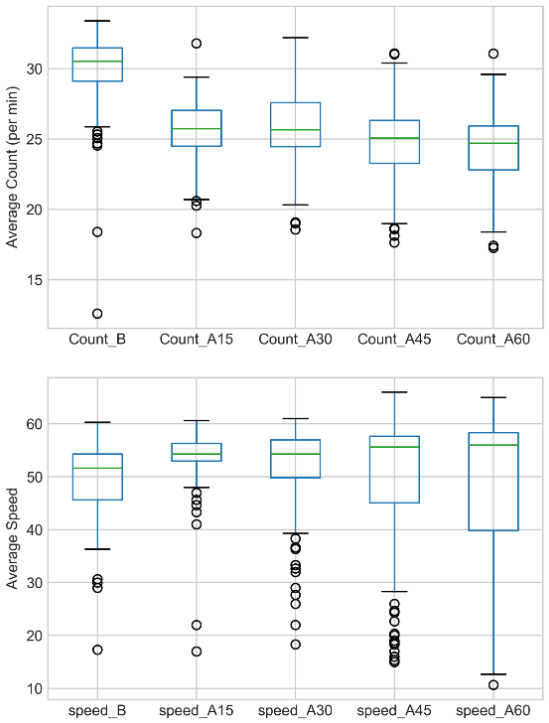

Figure 84. Graph. West 11.

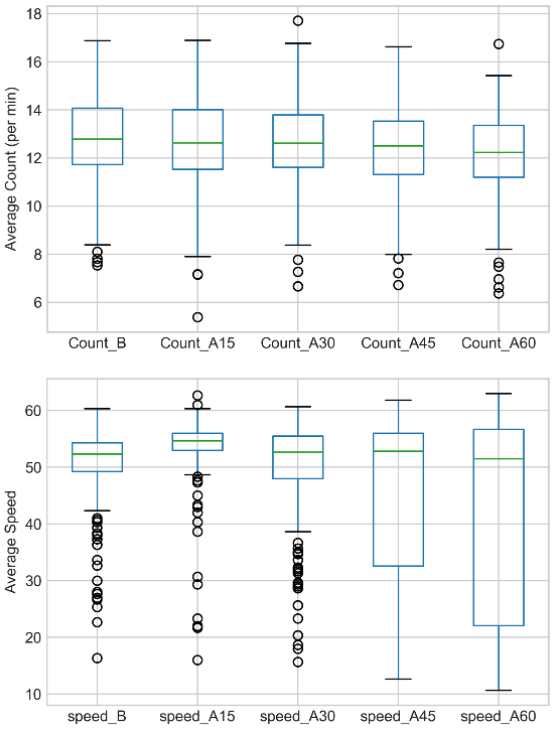

Figure 85. Graph. West 12.

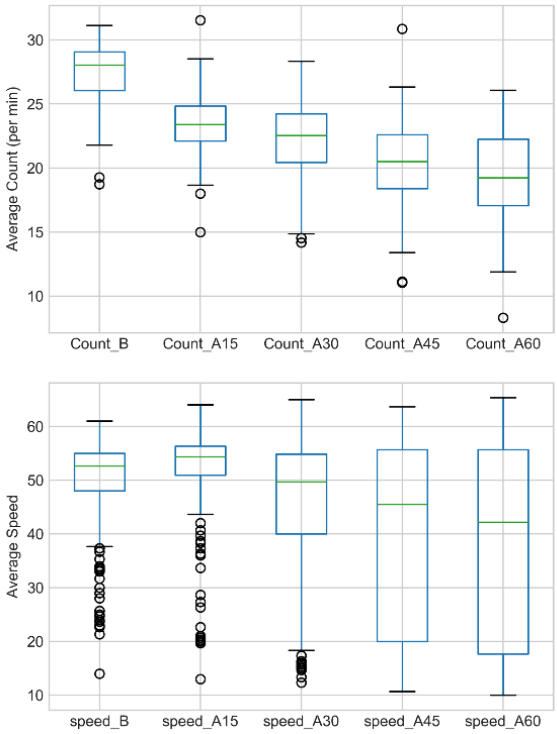

Figure 86. Graph. West 13.

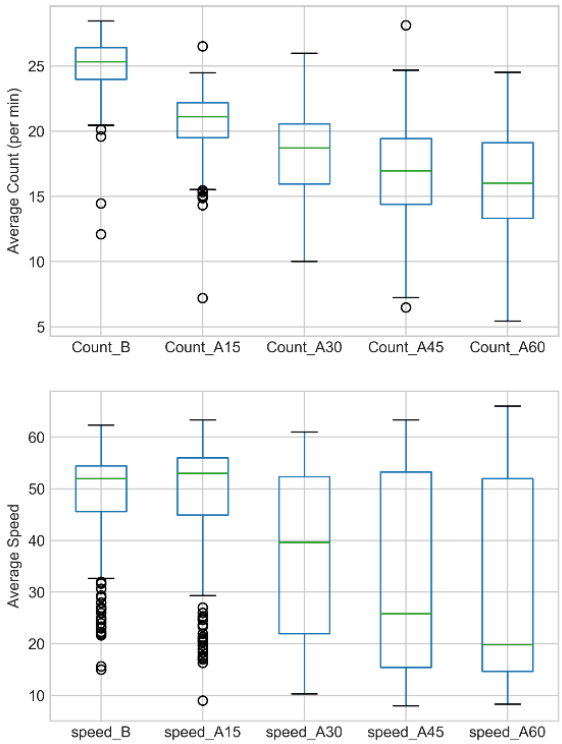

Figure 87. Graph. West 14.

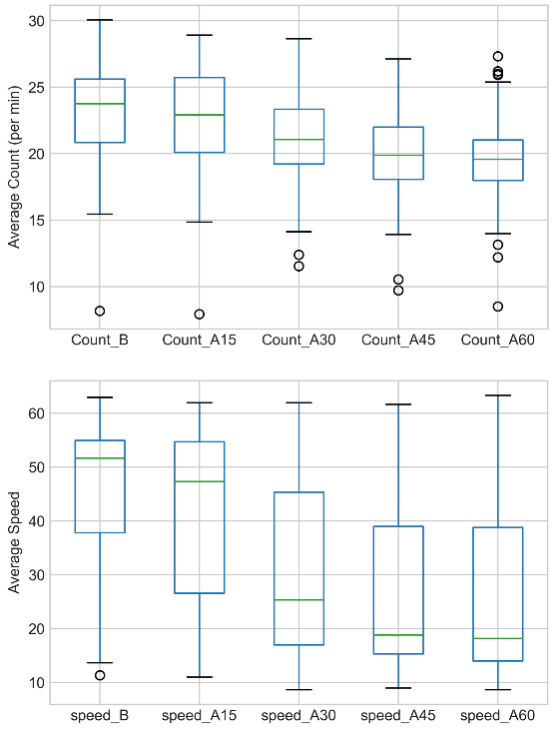

Figure 88. Graph. West 15.

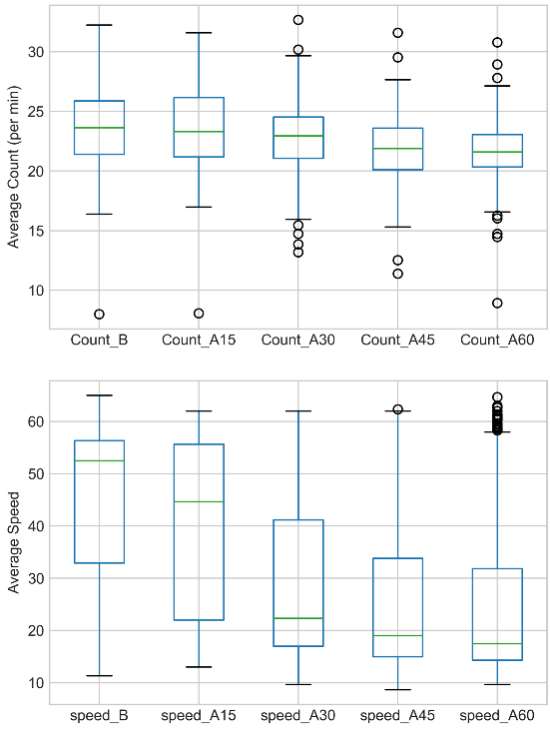

Figure 89. Graph. West 16.

APPENDIX B: IMPACT OF REVERSING OPERATION ON PATTERN OF TRAFFIC

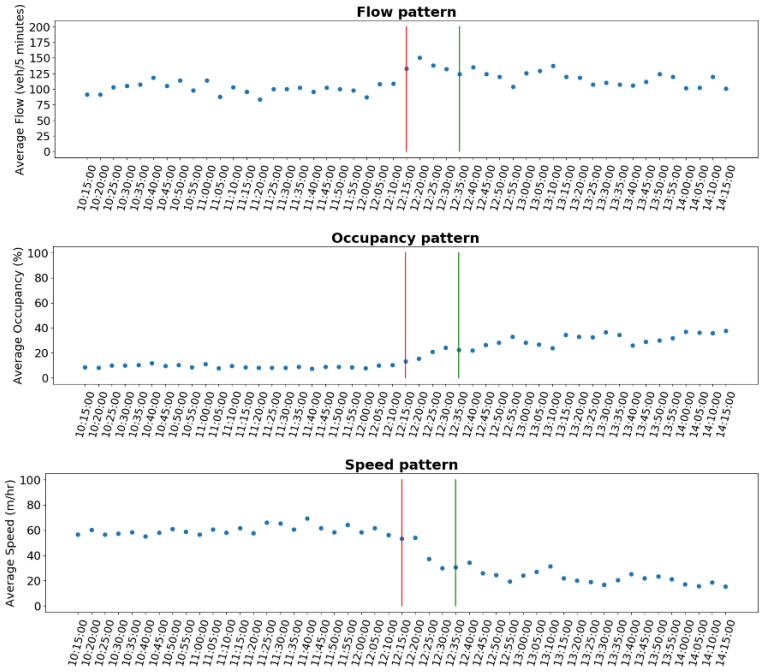

Figure 90. Graph. Monday: Eastbound.

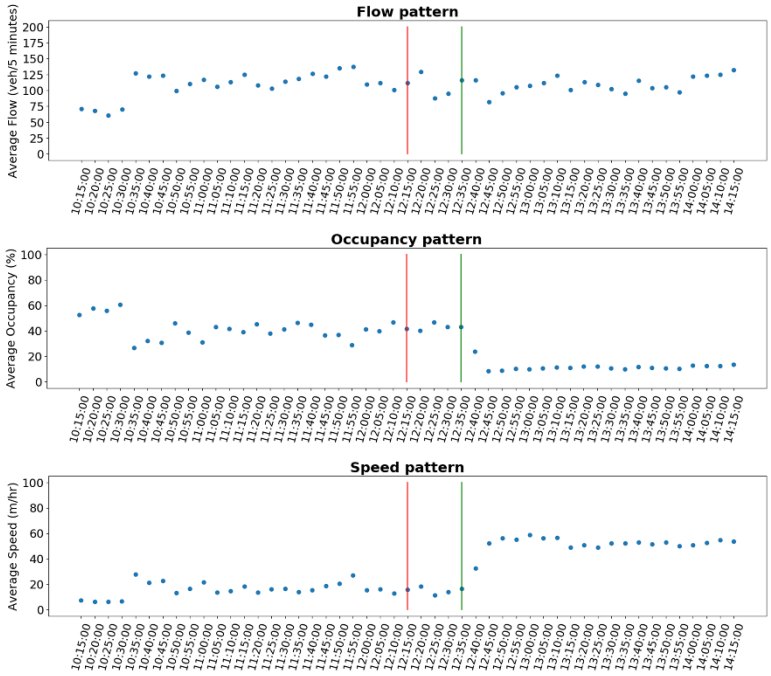

Figure 91. Graph. Monday: Westbound.

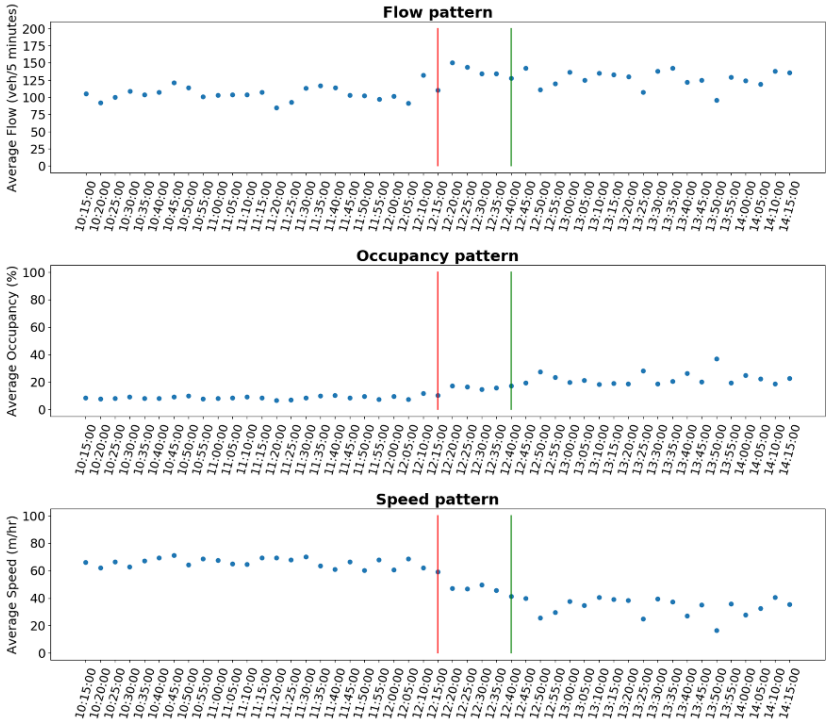

Figure 92. Graph. Tuesday: Eastbound.

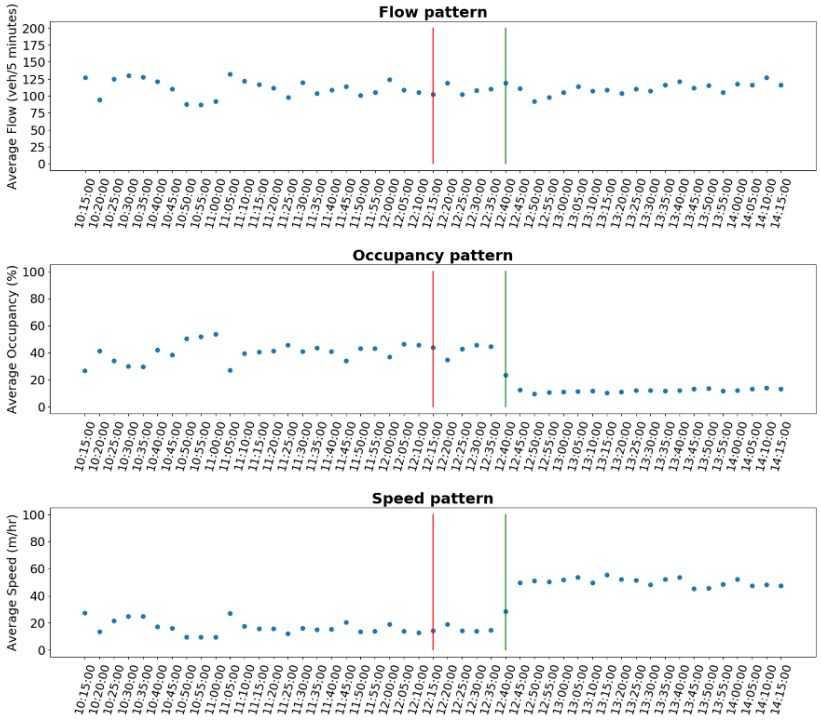

Figure 93. Graph. Tuesday: Westbound.

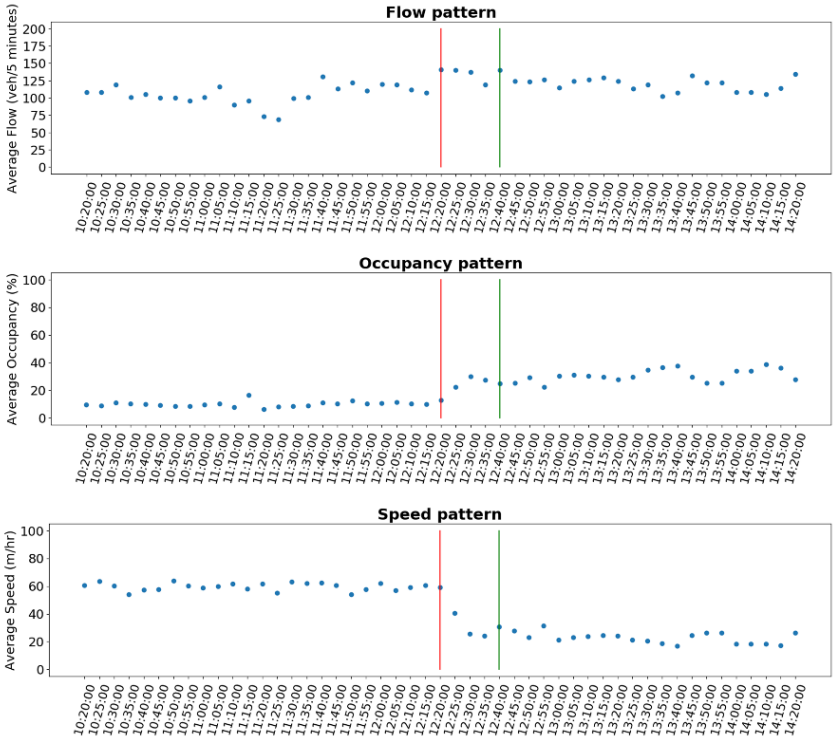

Figure 94. Graph. Wednesday: Eastbound.

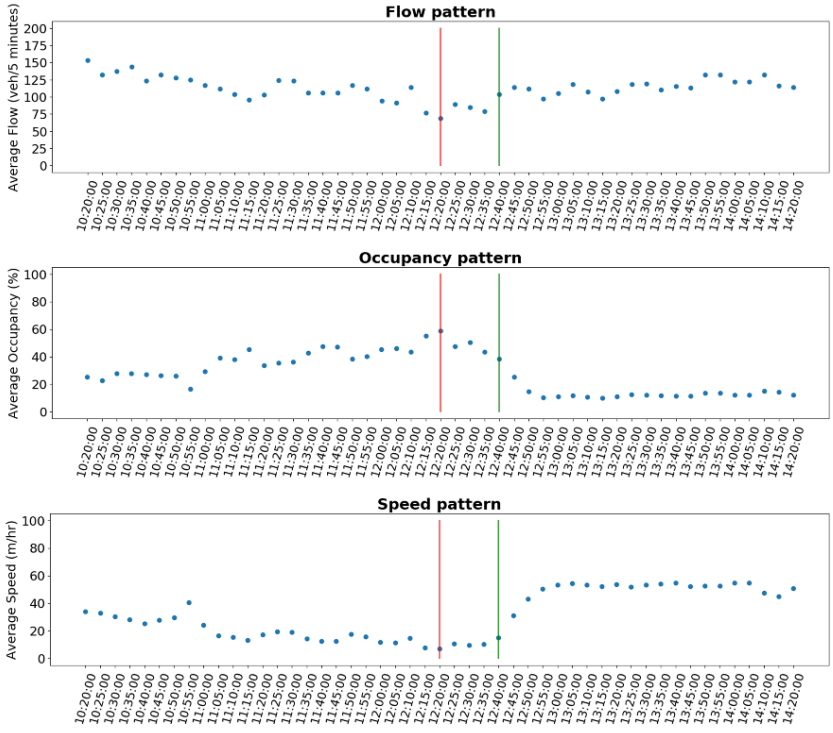

Figure 95. Graph. Wednesday: Westbound.

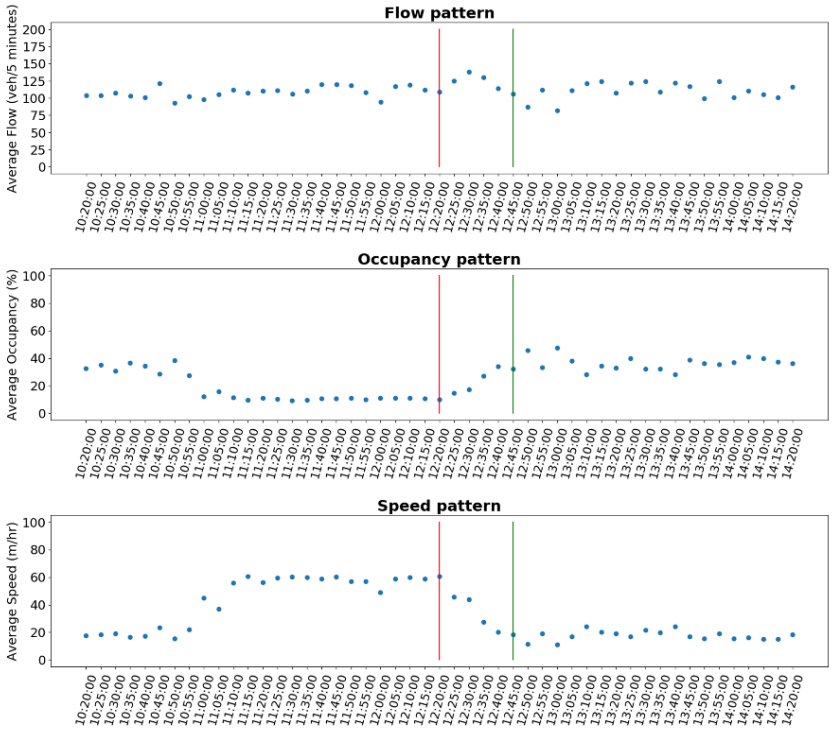

Figure 96. Graph. Thursday: Eastbound.

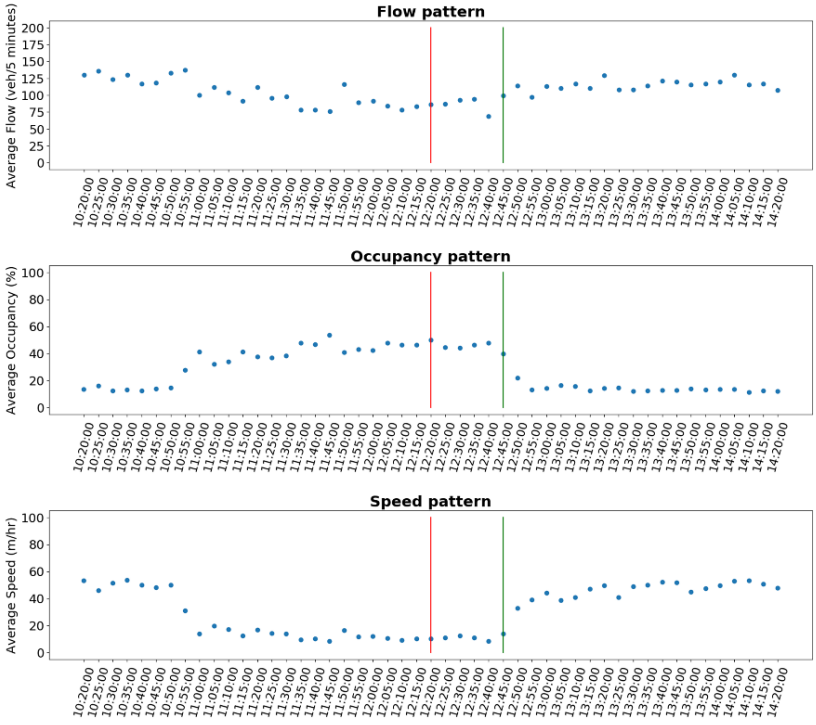

Figure 97. Graph. Thursday: Westbound.

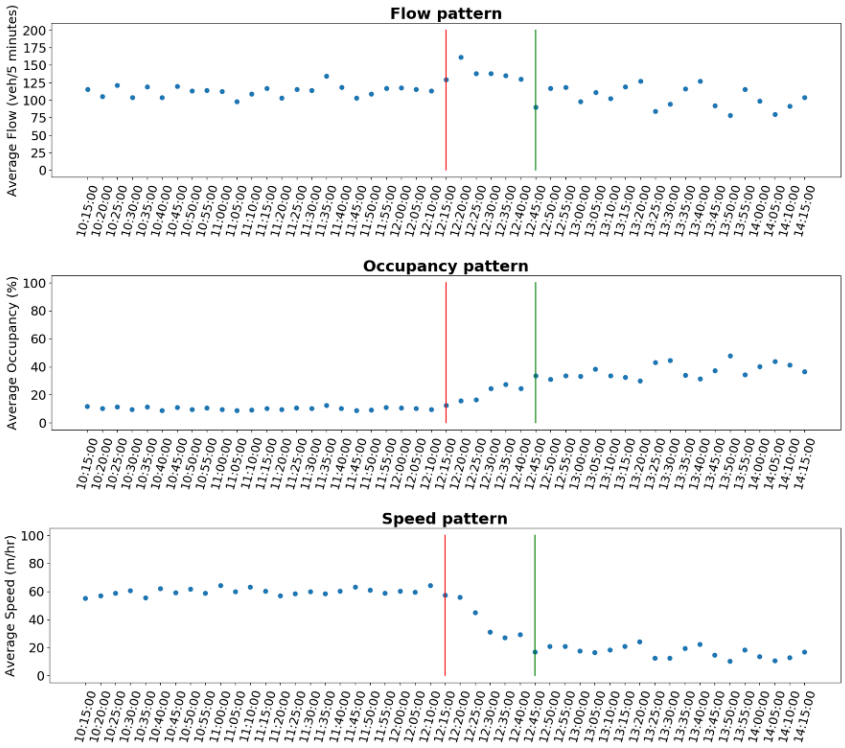

Figure 98. Graph. Friday: Eastbound.

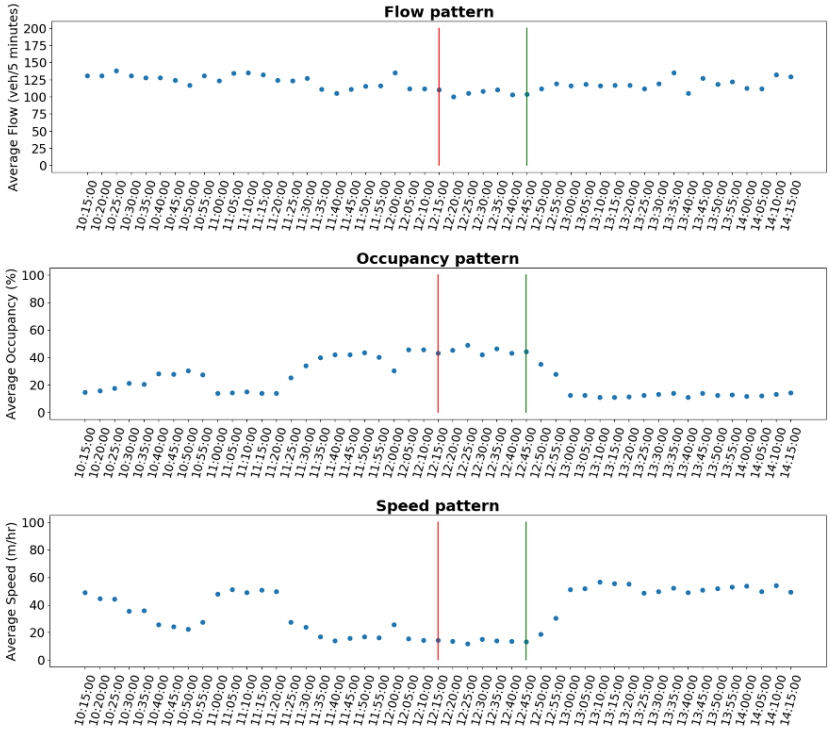

Figure 99. Graph. Friday: Westbound.

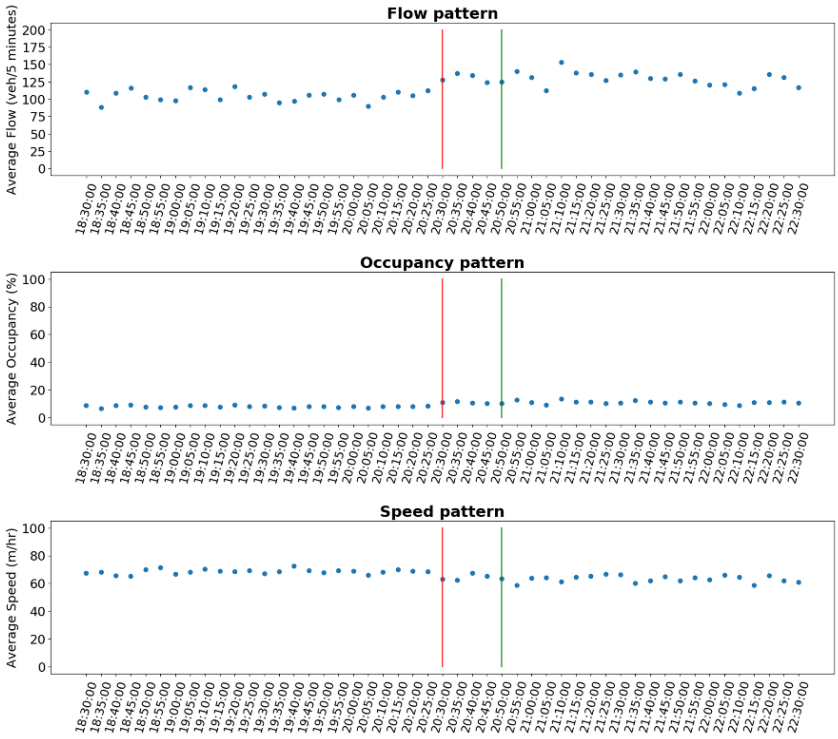

Figure 100. Graph. Saturday: Eastbound.

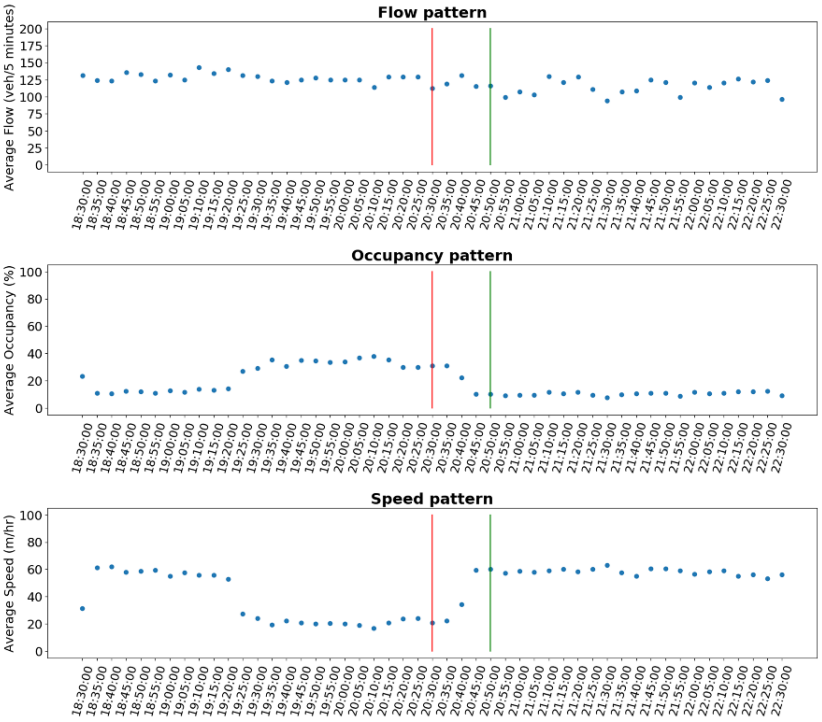

Figure 101. Graph. Saturday: Westbound.

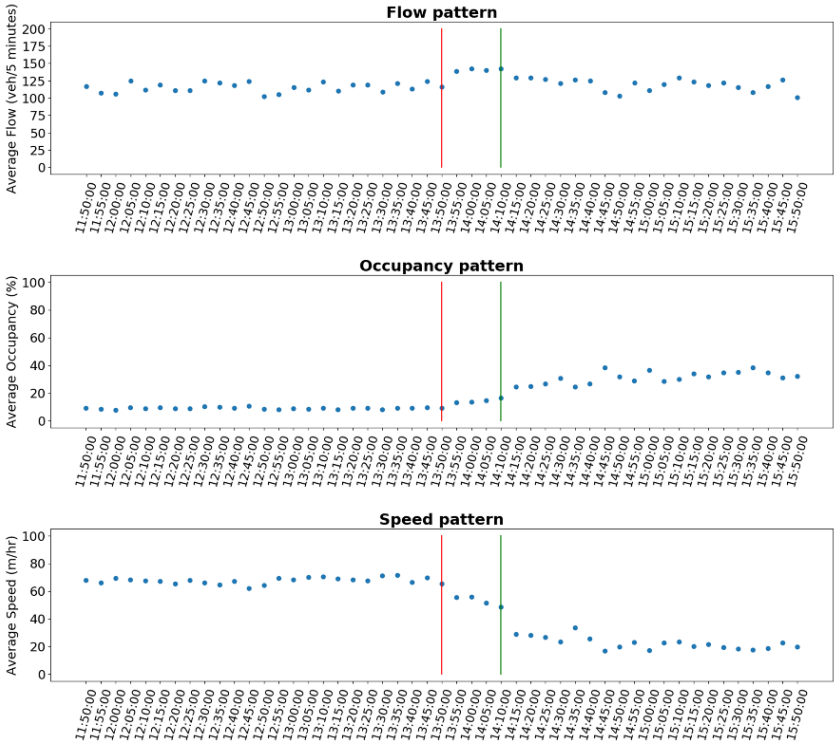

Figure 102. Graph. Sunday: Eastbound.

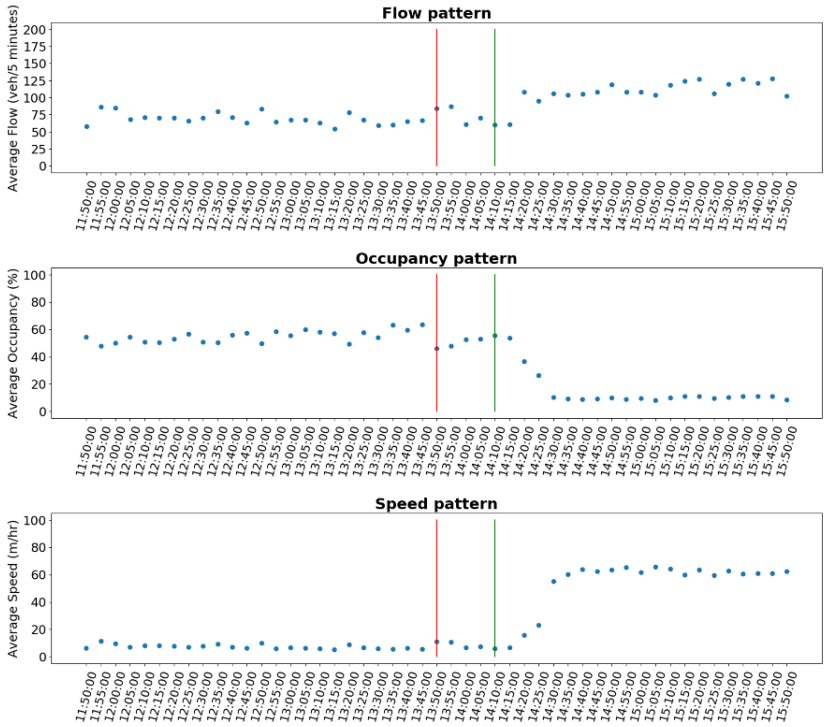

Figure 103. Graph. Sunday: Westbound.

APPENDIX C: INFERENCE OF THE RANDOM FOREST MODEL ON RANDOM DAYS

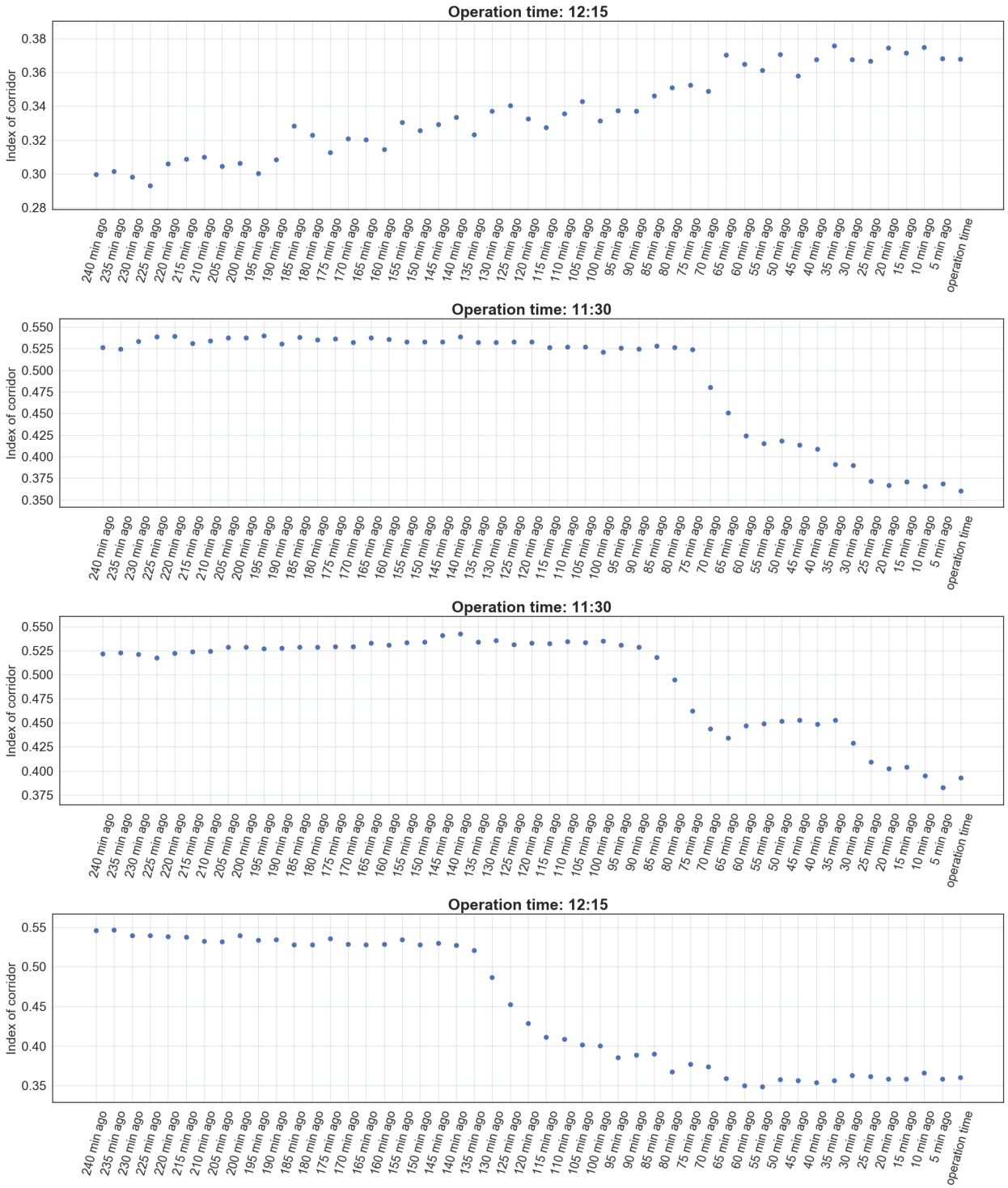

Figure 104. Graph. Monday.

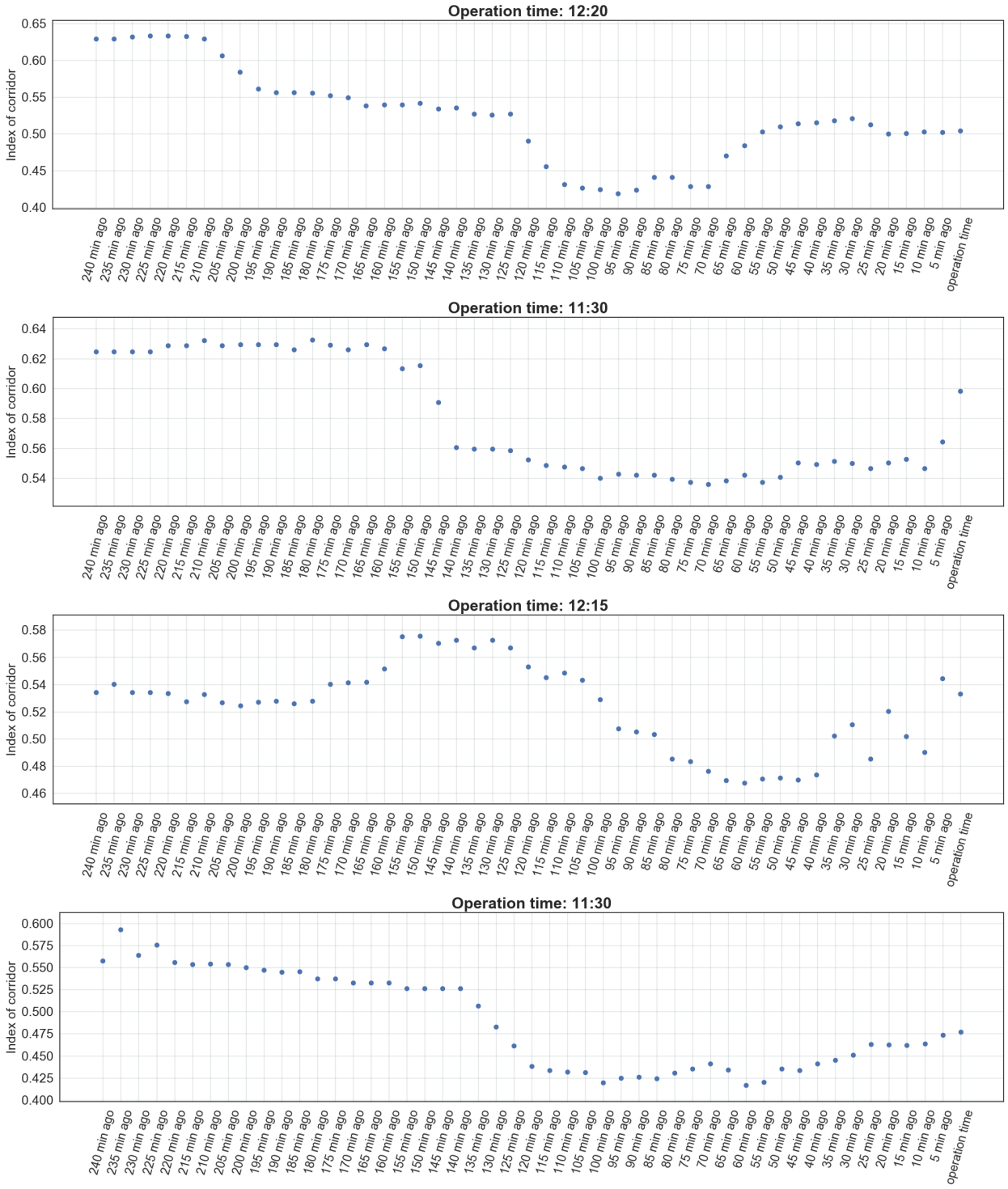

Figure 105. Graph. Tuesday.

Figure 106. Graph. Wednesday.

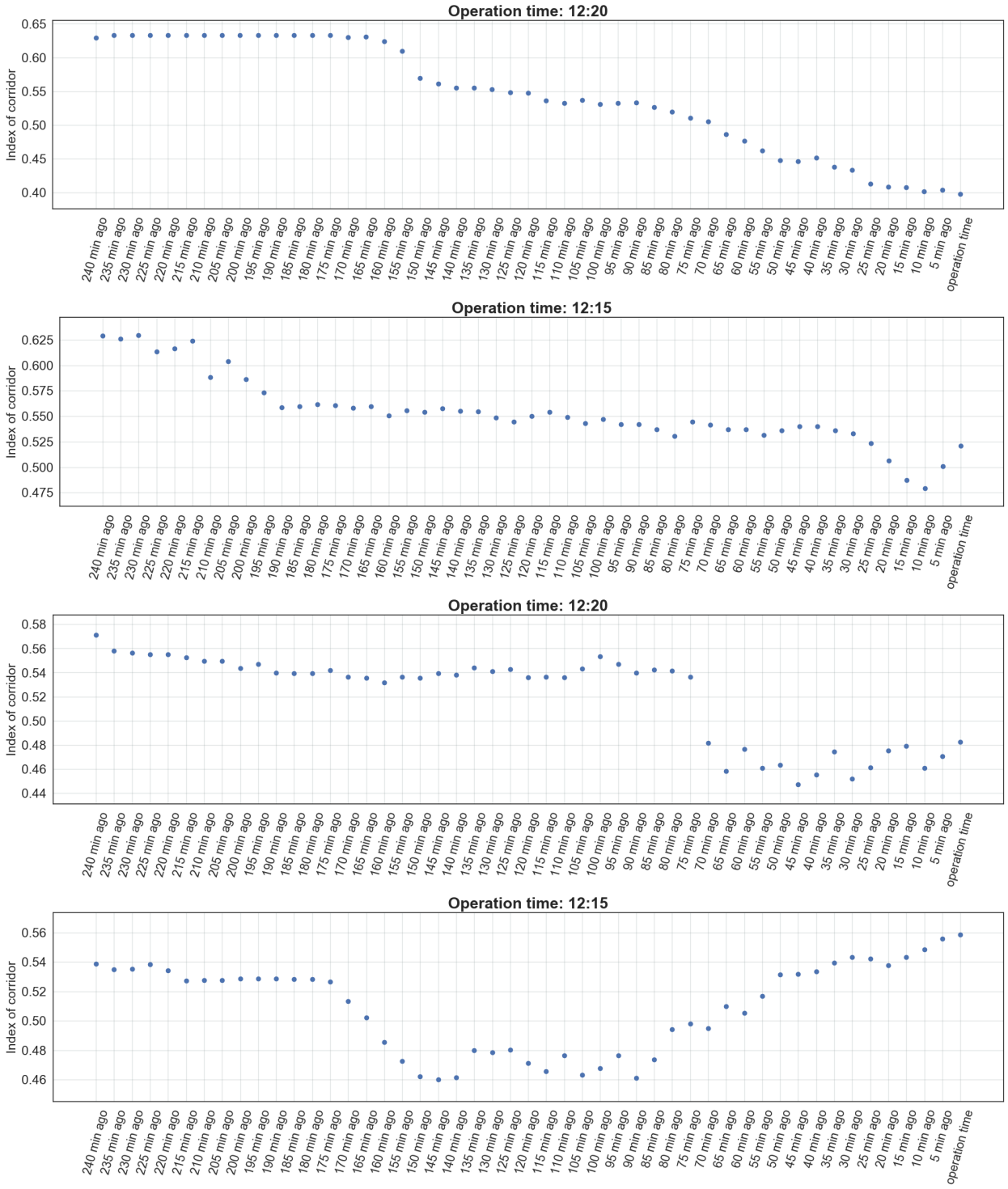

Figure 107. Graph. Thursday.

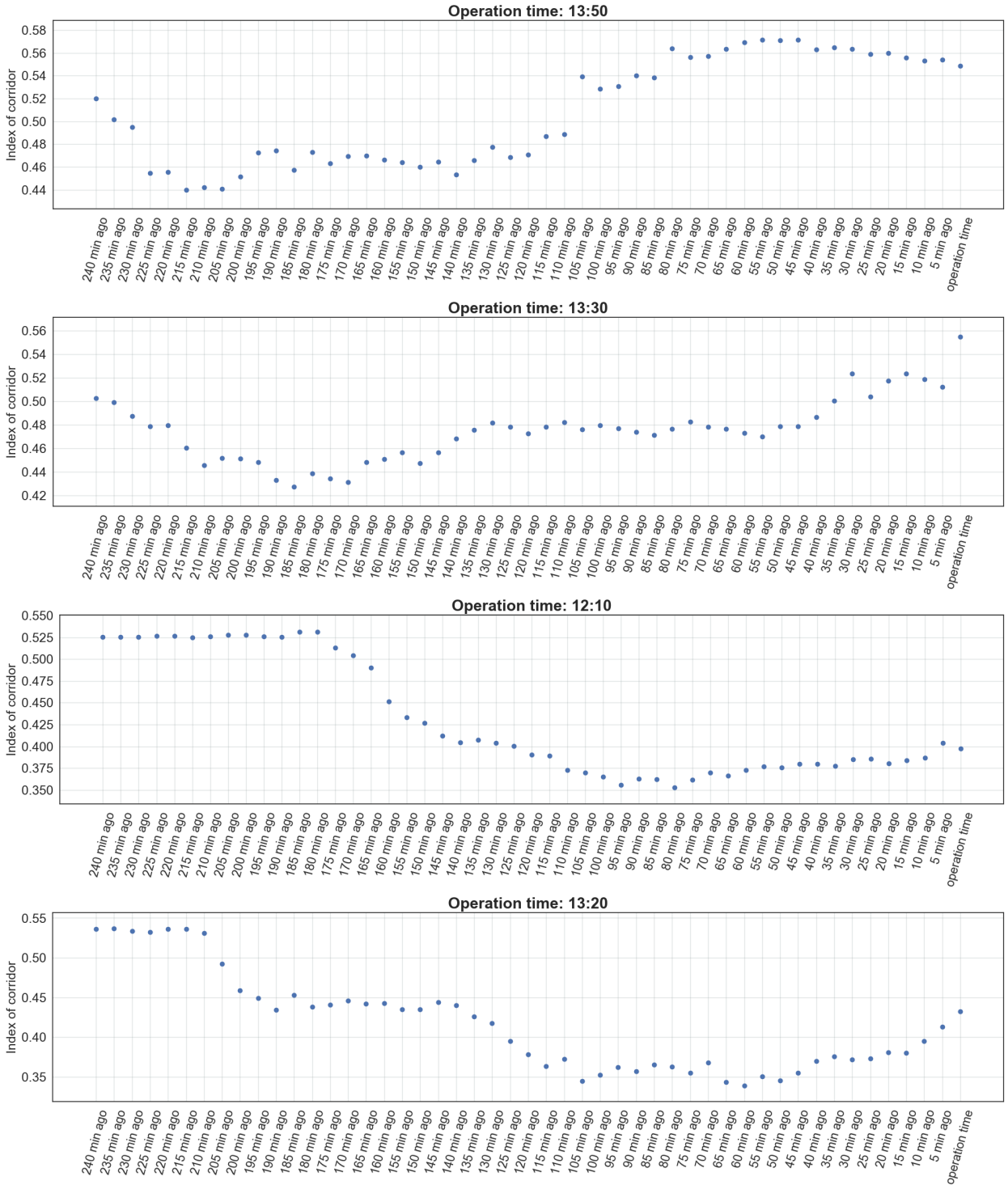

Figure 108. Graph. Friday.

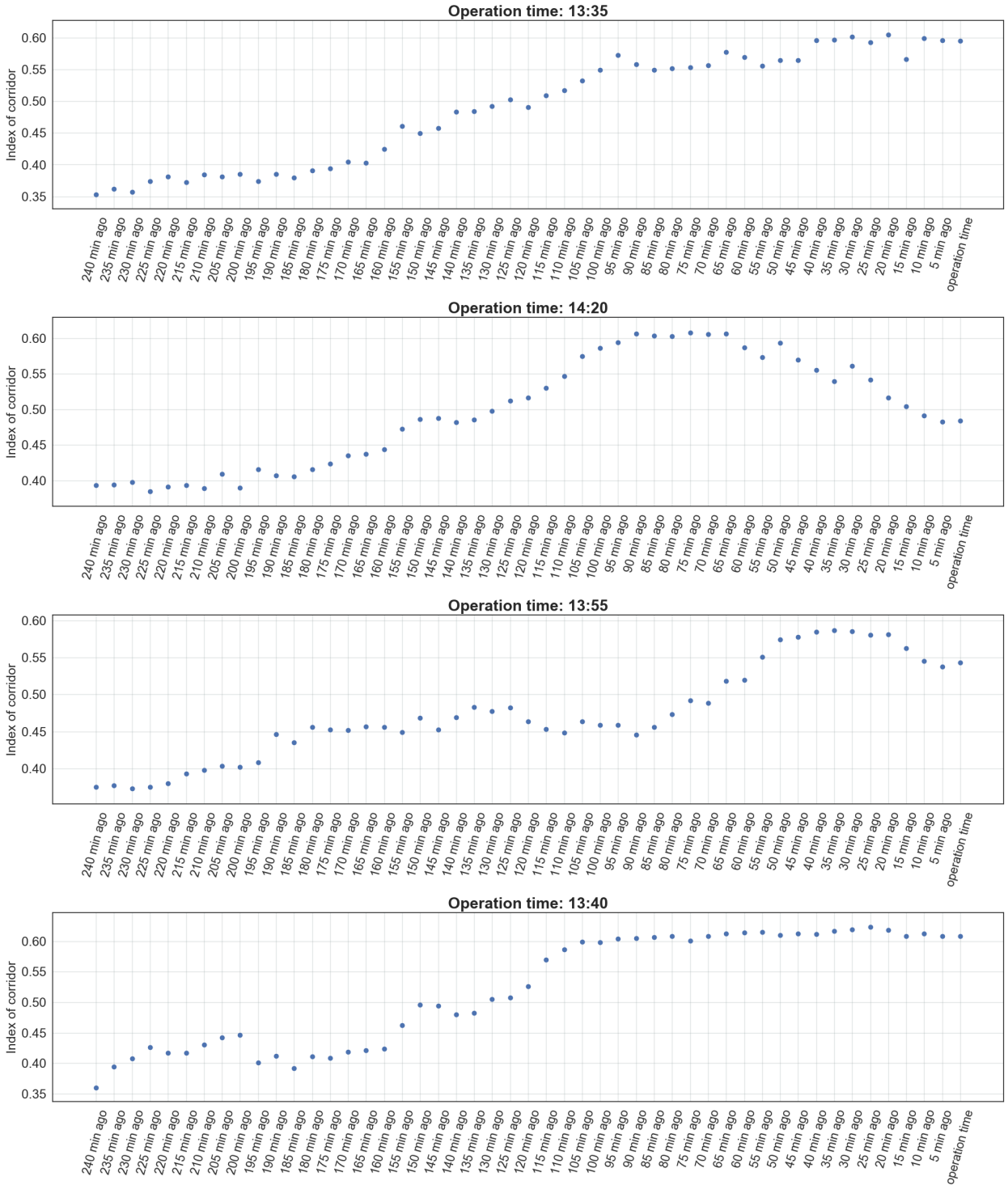

Figure 109. Graph. Saturday.

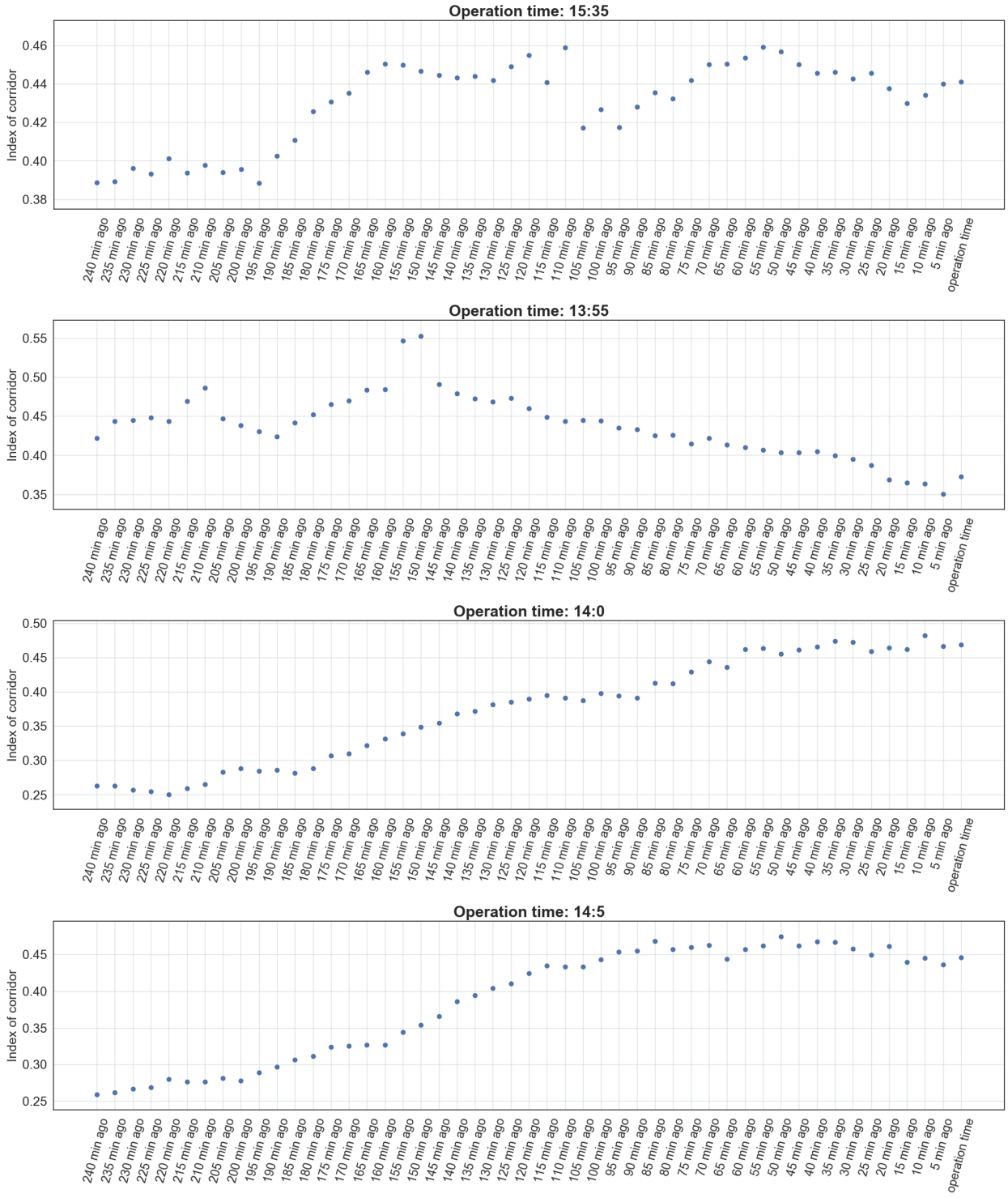

Figure 110. Graph. Sunday.


Illinois Department
of Transportation


ILLINOIS